

COMPUTATIONAL STUDY OF ETHYLENE EPOXIDATION

A THESIS SUBMITTED TO
THE GRADUATE SCHOOL OF NATURAL AND APPLIED SCIENCES
OF
MIDDLE EAST TECHNICAL UNIVERSITY

BY

MURAT OLUŞ ÖZBEK

IN PARTIAL FULFILLMENT OF THE REQUIREMENTS
FOR
THE DEGREE OF DOCTOR OF PHILOSOPHY
IN
CHEMICAL ENGINEERING

SEPTEMBER 2011

Approval of the Thesis:

COMPUTATIONAL STUDY OF ETHYLENE EPOXIDATION

submitted by **MURAT OLUŞ ÖZBEK** in partial fulfillment of the requirements for the degree of **Doctor of Philosophy in Chemical Engineering Department, Middle East Technical University** by,

Prof. Dr. Canan Özgen
Dean, **Graduate School of Natural and Applied Sciences**

Prof. Dr. Deniz Üner
Head of Department, **Chemical Engineering**

Prof. Dr. Işık Önal
Supervisor, **Chemical Engineering Dept., METU**

Prof. Dr. Rutger A. van Santen
Supervisor, **Chemical Engineering and Chemistry, TU/e**

Examining Committee Members:

Prof. Dr. İnci Eroğlu
Chemical Engineering Dept., METU

Prof. Dr. Işık Önal
Chemical Engineering Dept., METU

Prof. Dr. Rutger A. van Santen
Chemical Engineering and Chemistry, TU/e, The Netherlands

Prof. Dr. Şakir Erkoç
Physics Dept., METU

Prof. Dr. Mehmet Çakmak,
Physics Dept., Gazi University

Assist. Prof. Dr. Serkan Kıncal
Chemical Engineering Dept., METU

Assist. Prof. Dr. Görkem Külah
Chemical Engineering Dept., METU

Date:

I hereby declare that all information in this document has been obtained and presented in accordance with academic rules and ethical conduct. I also declare that, as required by these rules and conduct, I have fully cited and referenced all material and results that are not original to this work.

Name, Last name : Murat Oluş Özbek

Signature :

ABSTRACT

COMPUTATIONAL STUDY OF ETHYLENE EPOXIDATION

Özbek, Murat Oluş

Ph.D., Department of Chemical Engineering

Supervisor: Prof. Dr. Işık Önal

Supervisor: Prof. Dr. Rutger A. van Santen

September 2011, 89 Pages

This work computationally investigates the partial oxidation of ethylene (i.e. ethylene epoxidation) using periodic Density Functional Theory (DFT) on slab models that represent the catalyst surfaces. The mechanical aspects of the reaction were investigated on silver surfaces, which are industrially applied catalysts, for a wide range of surface models varying from metallic surfaces with low oxygen coverage to oxide surfaces. For comparison, the metallic and oxide phases of copper and gold were also studied. On these surfaces, the reaction paths and the transition states along these paths for the selective and non-selective reaction channels were obtained using the climbing image nudged elastic band (CI-NEB) method.

In order to answer the question “what is the relation between the surface state and the ethylene oxide selectivity?” metallic (100), (110) and (111) surfaces of Cu, Ag and Au; and, (001) surfaces of Cu₂O, Ag₂O and Au₂O oxides were studied and compared. For the studied metallic surfaces, it was found that the selective and non-selective reaction channels proceed through the oxametallacycle (OMC) intermediate, and the product selectivity depends on the relative barriers of the these channels, in agreement with the previous reports. However for the studied metallic surfaces and oxygen coverages, a surface state that favors the ethylene oxide (EO) formation was not identified. The studied Au surfaces

did not favor the oxygen adsorption and dissociation, and the Cu surfaces favored the non-selective product (acetaldehyde, AA) formation. Nevertheless, the results of Ag surfaces are in agreement with the ~50% EO selectivity of the un-promoted silver catalyst.

The catalyst surface in the oxide state was modeled by the (001) surfaces of the well defined Cu_2O , Ag_2O and Au_2O oxide phases. Among these three oxides, the Cu_2O is found not to favor EO formation whereas Au_2O is known to be unstable, however selective for epoxidation.

The major finding of this work is the identification of a direct epoxidation path that is enabled by the reaction of the surface oxygen atoms, which are in two-fold (i.e. bridge) positions and naturally exist on (001) oxide surfaces of the studied metals. Among the three oxides studied, only $\text{Ag}_2\text{O}(001)$ surface does not show a barrier for the formation of adsorbed epoxide along the direct epoxidation path. Moreover, the overall heat of reaction that is around 105 kJ/mol agrees well with the previous reports.

The single step, direct epoxidation path is a key step in explaining the high EO selectivities observed. Also for the oxide surfaces, the un-selective reaction that ends up in combustion products is found to proceed through the OMC mechanism where aldehyde formation is favored.

Another major finding of this study is that, for the studied oxide surfaces two different types of OMC intermediates are possible. The first possibility is the formation of the OMC intermediate on oxygen vacant sites, where the ethylene can interact with the surface metal atoms directly. The second possibility is the formation of a direct OMC intermediate, through the interaction of the gas phase ethylene with the non-vacant oxide surface. This occurs through the local surface reconstruction induced by the ethylene.

The effect of Cl promotion was also studied. Coadsorption of Cl is found to suppress the oxygen vacant sites and also the reconstruction effects that are induced by ethylene adsorption. Thus, by preventing the interaction of the ethylene directly with the surface metal atoms, Cl prevents the OMC formation, therefore the non-selective channel. At the same time Cl increases the electrophilicity of reacting surface oxygen. The direct epoxidation path appears to be stabilized by coadsorbed oxygen atoms.

Thus, we carry the discussions on the silver catalyzed ethylene epoxidation one step further. Herein we present that the EO selectivity will be limited in the case of metallic catalyst, whereas, the oxide surfaces enable a direct mechanism where EO is produced selectively. The role of the Cl promoter is found to be mainly steric where it blocks the sites of non-selective channel.

Keywords: silver, copper, gold, oxide, Ag₂O, Cu₂O, Au₂O, ethylene oxide, EO, DFT.

ÖZ

ETİLEN EPOKSİDASYONUNUN HESAPLAMALI ÇALIŞMASI

Özbek, Murat Oluş

Doktora, Kimya Mühendisliği Bölümü

Tez Yöneticisi: Prof. Dr. Işık Önal

Tez Yöneticisi: Prof. Dr. Rutger A. van Santen

Eylül 2011, 89 Sayfa

Bu çalışmada etilenin kısmi oksidasyonu (etilen epoksidasyonu), kataliz yüzeyini temsil eden slab modelleri üzerinde periyodik Density Functional Theory (DFT) kullanılarak çalışılmıştır. Endüstriyel kataliz olan gümüş yüzeylerde, tepkimenin mekanik özellikleri incelenmiştir. Çalışmada, az oksijen tutunumlu metalik yüzeylerden oksit yüzeylere kadar geniş bir aralıktaki yüzeyler ele alınmıştır. Gümüşün yanı sıra, karşılaştırma için metalik ve oksit bakır ve altın yüzeyleri de çalışmaya dahil edilmiştir. Bu yüzeylerde, seçici ve seçici olmayan reaksiyon kanalları ve bu kanallarda karşılaşılan geçiş halleri (transition state) Climbing Image Nudged Elastic Band (CI_NEB) metodu ile belirlenmiştir.

“Yüzeyin durumu ile etilen oksit (EO) seçiciliği arasındaki bağlantı nedir?” sorusunu cevaplayabilmek için, Cu, Ag ve Au'nun metalik (100), (110) ve (111) yüzeyleri ile, Cu₂O, Ag₂O and Au₂O oksit yapılarının (001) yüzeyleri çalışılmış ve karşılaştırılmıştır. Çalışılan metalik yüzeyler için, önceki raporlar ile uyumlu bir şekilde, seçici ve seçici olmayan reaksiyon kanallarının oxametallacycle (OMC) ara ürünü üzerinden devam ettiği, ve ürün seçiciliğinin bu kanalların karşılaştığı orantısız reaksiyon bariyerlerine bağlı olduğu bulunmuştur. Ancak, çalışılan metalik yüzeylerde ve bu yüzeylerdeki farklı oksijen tutunum oranlarında, EO oluşumunu ön plana çıkartacak bir yapıya rastlanmamıştır. Çalışılan Au yüzeyleri moleküler oksijen tutunumu ve ayrışımını mümkün kılmazken, Cu yüzeylerde

seçici olmayan asetaldehit (AA) oluşumunun tercih edilen kanal olduğu görülmüştür. Ancak, Ag yüzeylerde elde edilen sonuçlar promotör eklenmemiş gümüş katalizin ~%50 seçiciliği ile uyum göstermektedir.

Oksit fazındaki kataliz yapıları Cu_2O , Ag_2O and Au_2O oksit yapılarının (001) yüzeyleri ile modellenmiştir. Bu üç oksit yapısı içinde, Au_2O yapısının kararsız olmasına rağmen EO için seçici olduğu, ancak çok daha kararlı bir yapıya sahip olan Cu_2O 'nun EO ya karşı seçici olmadığı görülmüştür.

Bu çalışmanın en önemli buluşu, çalışılan (001) oksit yüzeylerinde doğal olarak bulunan 2-bağlı (köprü) yüzey oksijen atomlarının olası kıldığı direkt epoksidasyon kanalının tanımlanmış olmasıdır. Çalışılan üç farklı oksit yapısı içerisinde, sadece $\text{Ag}_2\text{O}(001)$ yüzeyi bu reaksiyon için bariyer göstermemektedir. Ayrıca, direkt reaksiyon kanalı için hesaplanmış olan reaksiyon ısı (~ 105 kJ/mol) önceki rapor edilmiş değerler ile örtüşmektedir.

Tek adımda gerçekleşen bu reaksiyon mekanizması, üretimde görülen yüksek EO seçiciliğinin açıklanmasında önemli bir adımdır. Metalik yüzeylerde olduğu gibi, seçici olmayan reaksiyon kanalı yine aldehit oluşumunun tercih edildiği OMC mekanizması üzerinden süregelmektedir.

Bu çalışmanın diğer önemli bir buluşu, çalışılan oksit yüzeylerinde iki farklı OMC oluşumu tanımlanmıştır. Bunlardan ilkinde, OMC, oksijen eksik sitelerde etilenin yüzey metal atomlarına tutulumu sonucu oluşmaktadır. İkincisinde, gaz fazdaki etilenin yüzeyi etkilemesi sonucu yüzeyde oluşan bölgesel yapılanma (reconstruction) direkt olarak OMC oluşumuna imkan vermektedir.

Cl promotör etkisi de incelenmiştir. Cl'nin yüzeye tutunumu yüzeydeki oksijen boşluklarını kapatarak etilen etkileşimini durdurmakta ve direkt OMC oluşumuna imkan sağlayan yüzey yapılanmasını engellemekte, bu sayede aldehit oluşumunu durdurmaktadır. Aynı zamanda aktif oksijen atomlarının komşuluğunda bulunan Cl atomları, bu oksijenlerin aktivitesini arttırmaktadır.

Bu bilgiler ışığında, gümüş katalizli etilen epoksidasyonu üzerindeki tartışmaları bir adım taşımaktayız. Bu çalışmada, metalik yüzeylerde EO seçiciliğinin sınırlı olduğunu, ancak, oksit yüzeylerde EO'nun seçici olarak üretildiği tek adımlık direkt bir mekanizmanın

olduđunu gstermekteyiz. alıřmalarda, Cl promotrn etkisinin daha ziyade yapısal olduđu ve seici olmayan kanalın gerekleřtiđi siteleri bloke ettiđi grlmřtr.

Anahtar Kelimeler: gmř, bakır, altın, oksit, Ag₂O, Cu₂O, Au₂O, etilen oksit, EO, DFT.

ACKNOWLEDGEMENTS

First of all I would like to thank my professors and mentors Prof. Dr. Işık Önal and Prof. Dr. Rutger A. van Santen for enabling this collaboration and giving me the opportunity to work under their supervision on this project. I can never express fully how much I have learned from them or how much I have enjoyed their discussions.

Secondly I would like to thank my mother Mübehher Özbek and my sister Gökçen Özbek for their support, understanding and everything else.

I would like to thank all the members of TU/e Theory Group for their support and friendship. I would like to thank Dr. Tonek Jansen for his teachings, discussions and support. I especially would like to thank Dr. Peter Vassilev, Dr. Evgeny Pidko and Dr. Cristina Popa for their invaluable friendship, supports and discussions that go well beyond science.

I would like to thank Prof. Dr. Canan Özgen, the head Graduate School of Natural And Applied Sciences in METU, for all her affords for the organization of this joint Ph.D. program. I would like to thank my colloquies and friends in GSNAS for their support and understanding throughout my thesis study. For the last, but not the least I would like to thank all my friends in Turkey and in Netherlands for their friendship. The memories of times together will always be very precious to me.

TABLE OF CONTENTS

ABSTRACT.....	iv
ÖZ.....	vii
ACKNOWLEDGEMENTS.....	x
TABLE OF CONTENTS.....	xi
LIST OF TABLES.....	xiii
LIST OF FIGURES.....	xiv
CHAPTERS	
1. INTRODUCTION.....	1
2. LITERATURE SURVEY.....	6
3. THEORY AND METHODOLOGY.....	12
3.1. Density Functional Theory.....	12
3.2. The VASP Software.....	20
3.3. Preparation of Surfaces.....	21
3.3.1. Metallic Surfaces of Copper, Silver and Gold.....	22
3.3.2. Oxide Surfaces of Copper, Silver and Gold.....	24
3.4. Computational Details.....	27
3.4.1. Atoms and Molecules in Vacuum.....	27
3.4.2. Metallic Surfaces.....	28
3.4.3. Oxide Surfaces.....	28
3.4.4. NEB method and the Determination of the Transition States.....	29
3.4.5. Vibrational Frequencies and Zero Point Energies.....	29
4. RESULTS AND DISCUSSION.....	30

4.1. Ethylene Epoxidation on Metallic Surfaces	30
4.1.1. Part I: Oxygen Coverage Dependence	31
4.1.2. Part II: Surface Structure Dependence	40
4.1.3. Conclusions	45
4.2. ETHYLENE EPOXIDATION ON SILVER OXIDE	46
4.2.1. Conclusions	55
4.3. ETHYLENE EPOXIDATION ON METAL OXIDES.....	56
4.3.1. Oxide Structures	56
4.3.2. Oxygen Adsorption	58
4.3.3. Direct Epoxidation.....	60
4.3.4. Oxygen vacancy and OMC formation	60
4.3.5. EO isomerization	61
4.3.6. Conclusion.....	66
4.4. DIRECT OMC	67
4.4.1. Conclusions	72
5. CONCLUSIONS.....	74
REFERENCES.....	77
CURRICULUM VITAE.....	88

LIST OF TABLES

TABLES

Table 3.1: Experimental and optimized bulk parameters for given metals.....	22
Table 3.2: Supercell thicknesses and surface energies of metallic surfaces.....	24
Table 3.3: Experimental and optimized bulk parameters for given metal oxides.	26
Table 3.4: Parameters of the $M_2O(001)$ supercells.....	27
Table 4.1: Adsorption energies (kJ/mol) of oxygen on (111) surfaces of Cu, Ag and Au at increasing coverages.....	33
Table 4.2: Activation energies for the formation of EO and AA through OMC intermediate.	43
Table 4.3: Calculated adsorption energies (E_{ads}), sites and charges of surface atomic oxygen; paths and the activation barriers for EO ($EEO\alpha$) and AA ($EAA\alpha$) formation for the listed surfaces and oxygen coverages (θ_o).....	48
Table 4.4: Cl effect on the reaction energies (in kJ/mol) for the reactions on $Ag_2O(001)$ surface.....	55
Table 4.5: Calculated heats of formation for bulk oxides and reference values. The energies are given in kJ/mol.	57
Table 4.6: Adsorption energies (kJ/mol) of O_2 and C_2H_4 on O-vacant surface sites.	59
Table 4.7: Computed and zero point corrected values for the activation barriers. For the considered forward and backward reactions, OMC is the starting intermediate. Energies are in kJ/mol.	63

LIST OF FIGURES

FIGURES

Figure 1.1: Triangular reaction scheme with ball-stick model.....	2
Figure 1.2: OMC geometries on metallic silver surfaces.	4
Figure 3.1: The self-consistent electronic iteration loop used in DFT computation.	19
Figure 3.2: Schematic representation for Cu, Ag and Au FCC crystals.	23
Figure 3.3: Schematic representations for the studied metallic surfaces. The light and dark shaded circles represent the surface and the sub-surface atoms, respectively.	23
Figure 3.4: Schematic for Ag ₂ O, Cu ₂ O, Au ₂ O crystals.....	25
Figure 3.5: Perspective view of M ₂ O(001) surfaces (Gray: metal atoms and, red: oxygens).	26
Figure 4.1: Relative energies of O adsorption on fcc and hcp sites of Ag(111) surface. The figures above show the oxygen distributions for given coverages. (Ag: light gray, O:red or dark gray).....	33
Figure 4.2: Ethylene adsorption on Ag(111) surface at given oxygen coverages. Charges are calculated with Bader analysis [105]. (Ag: gray, O: red or dark gray, C: black, H: cyan or light gray).	34
Figure 4.3: Relative energies of OMC paths tested for (a) fcc and (b) hcp adsorbed oxygen on Ag(111) surface at varying oxygen coverages. After OMC intermediate solid lines represent the EO path and dashed lines represent the AA path. See Scheme 4.1 for geometries of stable points and transition states.	36
Figure 4.4: Relative energies for the direct C-H activation (left side) and H-transfer to oxygen on OMC intermediate (right side), tested on Ag(111) surface for given oxygen coverages. See Scheme 4.3 for geometries of stable points and transition states.	40
Figure 4.5: Relative energies of OMC paths on (100) surfaces of metallic Cu, Ag and Au at 1/4 ML oxygen coverage. After OMC intermediate solid lines represent the EO path and dashed lines represent the AA path. See Scheme 4.4 for geometries of stable points and transition states.	44

Figure 4. 6: Relative energies of OMC paths on (110) surfaces of metallic Cu, Ag and Au at 1/4 ML oxygen coverage. After OMC intermediate solid lines represent the EO path and dashed lines represent the AA path. See Scheme 4.4 for geometries of stable points and transition states. 44

Figure 4. 7: Relative energies of OMC paths on (111) surfaces of metallic Cu, Ag and Au at 1/4 ML oxygen coverage. After OMC intermediate solid lines represent the EO path and dashed lines represent the AA path. See Scheme 4.2 for geometries of stable points and transition states. 45

Figure 4.8: Representations for the $\text{Ag}_2\text{O}(001)$ surface used in the calculations. (Ag: gray, O: red, Cl: green)..... 49

Figure 4.9: Reaction energy diagrams. The EO and AA formation path through OMC intermediate on Ag(111) surface (gray) and the direct EO formation path on $\text{Ag}_2\text{O}(001)$ surface (black line). Bottom figures represent the top views of the reaction intermediates. The energies are given with respect to $(\text{surface} + \frac{1}{2} \text{O}_{2(\text{g})} + \text{C}_2\text{H}_{4(\text{g})})$. (Ag: gray, O: red or dark gray, C: black, H: cyan or light gray)..... 51

Figure 4.10: Formation of EO (solid line) and AA (dashed line) through OMC intermediate on $\text{Ag}_2\text{O}(001)$ surface with an O-vacancy. Bottom figures represent the top views of the reaction intermediates. The energies are given with respect to $(\text{surface} + \text{C}_2\text{H}_{4(\text{g})})$. (Ag: gray, O: red or dark gray, C: black, H: cyan or light gray) 52

Figure 4.11: CH_2 rotation (black line) and AA formation (gray line) through $\text{EO}_{(\text{ads})}$ on $\text{Ag}_2\text{O}(001)$ surface. Bottom figures represent the top views of the reaction intermediates. The energies are given with respect to $(\text{surface} + \text{C}_2\text{H}_{4(\text{g})})$ 54

Figure 4.12: Oxygen adsorption energies on $\text{M}_2\text{O}(001)$ surfaces at varying coverage. The energies are calculated with respect to half of the gas phase O_2 energy ($\frac{1}{2} \text{O}_{2(\text{g})}$). 59

Figure 4.13: Energetics of direct epoxidation paths on $\text{M}_2\text{O}(001)$ surfaces. Initial points correspond to the oxygen adsorption energies on a vacant surface site that saturates the surface..... 62

Figure 4.14: (a) Energetics of the formation of the OMC intermediate on an oxygen vacancy, and (b) formation of EO and AA from OMC intermediate. Initial points correspond to oxygen adsorption that shifts the surface coverage to 75%..... 64

Figure 4.15: Comparison of the energy changes of reaction paths following EO formation. Adsorbed EO may i) desorb, ii) isomerize to ethyleneoxy intermediate, or, iii) isomerizes to AA..... 65

Figure 4.16: Un-reconstructed $M_2O(001)$ surface (left) and the local reconstruction (right). The displaced atoms are highlighted and the directions of the movements are shown with arrows. (Gray: metal atoms and, red: oxygen) 68

Figure 4.17: Relative energies of direct OMC on $M_2O(001)$ oxide surfaces. Geometries along the reaction paths are given in Scheme 4.5..... 69

Figure 4.18: Schematic representations of Cl adsorption positions studied on $Ag_2O(001)$ surface. The adsorption energies are calculated with respect to $\frac{1}{2} Cl_{2(g)}$ and $\frac{1}{2} O_{2(g)}$. (Metals: gray, O: red, C: black, H:cyan, and Cl: green) 71

Figure 4.19: EO and AA formation on Cl-adsorbed $Ag_2O(001)$ surfaces. (Metals: gray, O: red, C: black, H:cyan, and Cl: green) 72

CHAPTER 1

INTRODUCTION

Molecule-solid interactions play a key role in heterogeneous catalysis. Understanding the details of these interactions in atomic or molecular scale is an essential step for the further development. Only in recent past, detailed molecular study of catalytic systems has become possible. Starting from the late 70's, electron microscopy techniques like transmission electron microscopy (TEM), or surface probing techniques like scanning tunneling microscope (STM), in combination with the use of catalytic models as single crystal surfaces made it possible to actually "see" the solid catalyst surfaces and interacting atoms or molecules. Furthermore, theoretical simulation techniques based on quantum mechanics have made substantial progress, making it possible to understand the nature and the chemistry of these interactions. This can be recognized by the increasing importance of computational catalysis. Although systems can be identified physically now, details of many surface reactions are still waiting to be identified.

In the field of the heterogeneous catalysis understanding the interactions in atomic level is important [1]. Computational quantum chemistry makes it possible to investigate the actual systems in atomic levels. With the increase in the computational power, theoretical models of catalytic systems and simulations of catalytic reactivity close to that of experimental systems are becoming within reach. Density functional theory (DFT) has become a well developed computational quantum-chemical tool, which is also widely applied in catalytic studies. Being a successful approach to describe the ground state properties as well as transition states of condensed phase and molecular systems make it is an ideal tool to study heterogeneous surface reactions.

Previous fundamental studies mainly tested the single crystal surfaces under ultra-high vacuum conditions, at which surfaces stay essentially metallic. These studies played an important role to understand and improve the applied catalytic systems. Although their contributions are invaluable, their approach cannot represent the industrially applied high temperature and pressure conditions. Recent studies indicate that the structure and the chemical composition of the active catalysis vary from so assumed single-crystal metallic structures. Furthermore, it has been proposed that under oxygen rich conditions the active phase of the catalyst is oxide or oxide-like complexes, which can change catalytic activity considerably [2-6].

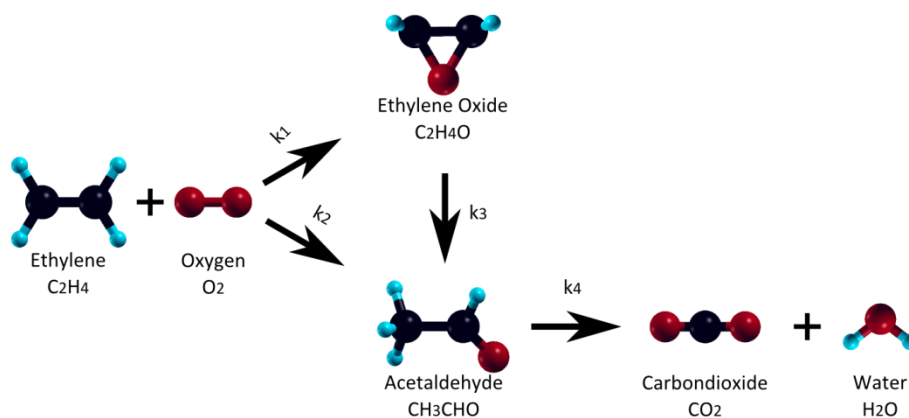


Figure 1.1: Triangular reaction scheme with ball-stick model.

The focus of this study is the silver catalyzed partial oxidation of ethylene (ethylene epoxidation) to produce ethylene oxide (EO). As illustrated in Figure 1.1, EO is a small molecule containing one oxygen and two carbon atoms, all bonded to each other in a three-member ring configuration via single bonds. EO serves as a very useful chemical intermediate from which further products such as plastics, polyester, and glycols can be derived. Industrially it is being produced at large scale, and hence reaction yield is very important for economical reasons. GIA, who announces the release of a comprehensive global report on the Ethylene Oxide markets, reported that the global market for Ethylene Oxide is projected to exceed 27 million tons by the year 2017 [7]. Thus, due to the global

capacity of this process, even slight improvements would have large scale economical benefits.

Besides its industrial importance, another attracting aspect of this reaction is that it is the “simplest example of a kinetically controlled, selective heterogeneous catalytic reaction” [8]. Although thermodynamically favored path is the complete combustion leading to CO₂ and H₂O ($\Delta H_{rxn} = -1327$ kJ/mol [9]), kinetics dictates that EO ($\Delta H_{rxn} = -105$ kJ/mol [9]) is the major product.

The industrially applied catalyst consists of silver particles dispersed on alumina (Al₂O₃). Promoters are added during catalyst preparation and during the process. The EO selectivity of un-promoted metallic silver lays around 50% [10], whereas this value is ~90% [11] for the industrial catalyst. However, these improvements on the selectivity were achieved mainly by trial-error methods [12], thus a fundamental understanding of the system is still a miss.

One of the main issues is the explanation of the high selectivity of the catalyst. The optimum state of the catalyst surface at reaction condition is not known. The role of the promoters, as alkali and chlorine that have to be added to obtain high selectivity is not well understood. It is known that in the catalytic reaction only the epoxide and total combustion products are formed. However, until recently a model for the non-selective ethylene activation processes on the silver surface was missing. For these reasons there is no conclusive answer yet why Ag is so unique in this reaction.

Fundamental studies were limited to metallic silver surfaces at low oxygen regimes [13-17]. These studies demonstrated that on metallic silver surface, both the selective and the non-selective reactions proceed through formation of the oxametallocycle (OMC) surface complex [18, 19]. The structure of this OMC intermediate is presented in Figure 1.2. Different isomerizations of OMC form EO or acetic acid (AA). Under reaction conditions AA rapidly combusts to CO₂ and H₂O, due to the high reactivity of its allylic hydrogen atoms [17, 20]. Thus the product selectivity depends on the relative barriers of EO and AA formation (E_{EO}^a and E_{AA}^a). The competitive formation of EO and AA through decomposition of the OMC intermediate agrees well with the ~50% EO selectivity of the metallic silver. However reaching high EO selectivity through OMC mechanism is still in

debate. Apart from providing an epoxidation mechanism, OMC provides the first conclusive model for the non-selective AA formation.

Being closely packed, (111) is most stable flat surface for the silver metal. Thus, many studies used Ag(111) surface to study the ethylene epoxidation. However, recent studies point to the higher EO selectivity of Ag(100) [10, 21] and Ag(110) [22] surfaces. The increased EO selectivity of these surfaces was related to the difference in the activation barriers of OMC decomposition.

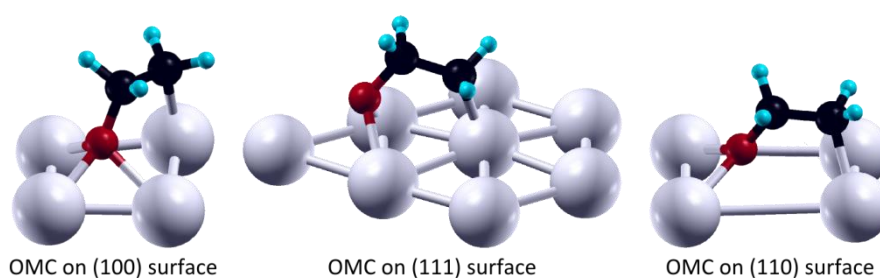


Figure 1.2: OMC geometries on metallic silver surfaces.

Early studies of the epoxidation reaction were based on the idea that adsorbed molecular oxygen was responsible for selective catalysis. Since dissociation of O_2 requires several Ag atoms to accommodate the oxygen atoms generated by dissociation, it was proposed that Cl would inhibit O_2 dissociation [14] by blocking the larger ensembles. With the demonstration that the molecular oxygen hypothesis is invalid and this role of Cl has to be rejected [8, 15, 16, 23-28]. A competitive model for the promoting effect Cl has been proposed on the hypothesis that a special type of atomically adsorbed O is responsible for selective catalysis [29-31], where Cl had a steric role. According to this model Cl suppresses the presence of vacant Ag adsorption sites that are responsible for non-selective C-H activation. The latter view will appear as a general question in this thesis.

The Sabatier's principle (i.e. volcano plots) applies to this system as well. That is, in one hand, the metal-oxygen interaction should be strong enough to dissociate O_2 molecule to form atomic oxygen species; in the other hand, not too strong to prevent desorption of the formed EO and/or cause C-H activation. The molecular oxygen dissociation can easily

be achieved on the transition metals as well as Ag and Cu but not on Au. However, strong bound surface oxygen found to act as a Lewis base that promotes C-H activation [17, 32-35]. Unlike previous studies, which investigated the mechanical effect (i.e. site blocking) of the Cl promoter, recent studies focus on the electronic effect of Cl that is neighboring the active O species, where surface and/or sub-surface Cl weakens the metal-oxygen bonds [36, 37] and makes the oxygen easier to be transferred to the ethylene [5, 6, 16, 17, 36, 38-41].

Although the concept and effect of sub-surface oxygen in ethylene epoxidation were first considered in the late 80's [16, 17, 38], the majority of the previous studies considered metal surfaces with low on-surface oxygen ratios. However, with the improvements in the experimental and theoretical methods, oxide or oxide like structures on surfaces began to gain emphasis [14, 41-48]. Furthermore, the proposal that the oxide surfaces are the active phase for the (partial) oxidation reactions finds recent support [49-51]. The presence of sub-surface oxygen has been reported to increase catalyst selectivity [52-54] even for the metallic surfaces. For the silver-oxygen systems the local formation of Ag_nO type oxide phases has been suggested [41, 43, 44, 46, 52-54], but there is not a definitive model for the overlying oxide structures yet.

In this work ethylene epoxidation on oxygenated silver and silver oxide catalyst surfaces was studied. Our approach was to perform first principles calculations for modeling the structures and reactions in periodic supercells. By determining the electronic structures of interacting atoms and molecules in finite systems, accurate descriptions of the surfaces and surface-reactions were obtained.

We attempt to answer the specific questions “what is the actual catalyst phase and the reaction path that explains the high EO selectivity?”, “why silver is the unique catalyst for ethylene epoxidation?” and “what is the role of the Cl promoter?” To answer these questions we have analyzed and evaluated both metallic and oxide systems of silver catalyst, along with previously tested candidates: copper and gold.

CHAPTER 2

LITERATURE SURVEY

Silver catalyzed ethylene epoxidation to produce ethylene oxide (EO) is an industrially applied important heterogeneous catalytic process. Following the discovery of the process in 1930's by Leford [55] extensive industrial and academic research has led to significant improvements of the industrial catalyst as well as increasing insight into reaction mechanism. Despite the fundamental studies devoted to understanding the basic factors underlying, the molecular reaction mechanism, and the roles of Ag and O in this reaction are still in debate. Furthermore, why silver is the only catalyst with a feasible selectivity for the partial oxidation of ethylene to ethylene oxide, and other common oxidation catalysts such as Pd, Pt or Ni cause complete combustion [13] is not clear.

Industrially applied catalyst consists of Ag particles dispersed on a low surface α -alumina (Al_2O_3) support. Alkali metals such as Cs are added to the solid phase to improve the dispersion of the active metal. Chlorinated hydrocarbons are added to the input gas stream in ppm amounts. Combustion of the organic part deposits Cl on the surface, where it acts as a promoter and increases the selectivity towards EO. However, throughout the operation catalyst poisoning occurs as a result of Cl accumulation. The process takes place around 550 K temperature and 1-10 atm pressure. The EO selectivity of un-promoted metallic silver lays around 50% [10], whereas this value is ~90% [11] for the industrial catalyst.

The basic kinetics of the reaction were found to consist of parallel reactions and consecutive reaction steps [56] (Figure 1.1). Later on acetaldehyde (AA) was introduced as the intermediate for total combustion. The selective (k_1) and non-selective (k_2) parallel reactions are catalyzed by silver, whereas the consecutive isomerization of EO (k_3) is found to be sensitive to the acidity of the catalyst support. For example a study, which compared

the SiO₂ and Al₂O₃ supports, related the different EO isomerization ratios for these supports to the acidity and the amount of the hydroxyl groups forming on the support [20, 57]. The acidic support causes EO isomerization to AA that is rapidly combusted in a reaction catalyzed by the Ag particle [20].

Early studies on the ethylene epoxidation had a mechanistic approach and the debates were on the nature of the active oxygen species and the role of the Cl promoter. These works generated several important proposals. Among these, the two most important are;

1. Force and Bell [29-31] proposed that surface adsorbed atomic oxygen (O_s) is the active species for selective EO formation. Co-adsorbed Cl mainly served to decrease the amount of the O_s neighboring vacancies, at which C-H activation took place. Thus the Cl promoter increased selectivity by inhibiting the non-selective path.
2. Kilty and Sachtler [14] proposed that the molecularly adsorbed O₂ (O_{2,s}) was the active species for the selective oxidation of ethylene whereas O_s caused total combustion. The interesting consequence of this proposal was that the EO selectivity should be limited to a highest value of 6/7 (85.7 %). This selectivity value was typically observed for promoted catalyst. Thus, the effect of the Cl promoter was to reduce the probability for larger Ag surface ensembles that are needed for O₂ dissociation. This effect would reduce the atomic O concentration, therefore to induce the non-selective reaction.

Soon after the 2nd proposal, EO selectivities higher than 6/7 were reported [58, 59], giving the hints of O_{2,s} was not being the active species. Key surface science type experiments leading to this conclusion were done by Lambert [15, 23, 24] and Campbell [8, 25-28]. Isotope exchange experiments performed on Ag powder [16] reported the same conclusion. Basing on these studies, the most important features of ethylene epoxidation were summarized as [38]:

1. Ethylene reacts with adsorbed atomic oxygen to epoxide.
2. Once the adsorbed atomic oxygen has been formed, the rate-limiting step for epoxidation is the insertion of this oxygen into C=C double bond. The rate limiting step for combustion is probably a C-H bond activation, although C=C bond activation cannot be definitely excluded.

3. Subsurface oxygen (or moderators, e.g., chlorine) seems to be necessary for adsorbed oxygen to react to epoxide. These subsurface species are stabilized by alkali-metal atoms, which explain why also alkali metal promoters enhance the selectivity.
4. From points 1 and 2, it follows why silver is taken as a catalyst: it has the ability to dissociate oxygen, but at the same time cannot activate C-H (or possibly C-C) bonds, since it has no open d-shell.

The works on the nature of the active oxygen species also came up with the proposal that a high local surface oxygen concentration and subsurface oxygen (O_{ss}) was needed to achieve high EO selectivity [16, 17, 38, 60, 61]. After this point, studies began to focus on the nature of the Ag/O system. Following the work of van Santen [16], the existence and the effect of the sub-surface oxygen species began to be considered and investigated.

From this point on, the studies on the ethylene epoxidation can be categorized in two groups. The first group studies the structure of the active Ag/O phase using experimental and theoretical methods [40, 41, 43, 44, 50, 62, 63]. The very first samples of this group begin with the inspection of the increasing on-surface oxygen coverage on the clean silver surface [64-67]. These studies showed that, after a relatively low surface coverage of O_s is achieved, oxygen began to diffuse into sub-surface layers [64, 65]. More recent studies of this type investigate the nature and the stability of the structures forming under high oxygen regimes, and the activity of oxygen in these structures. Comparisons for different structures, temperatures, pressures and coverage are carried out by building temperature-pressure phase diagrams to predict surface oxide concentrations as a function of oxygen chemical potential, based on ab-initio thermodynamics [12, 41, 50]. These studies reached important conclusions such as under high oxygen pressure regimes, oxide like species found to be more stable compared to the single crystal metal surfaces [5, 6], as well as confirming the formation of Ag_2O or similar oxide phases at the corrugated and the Ag(100) surfaces [50, 63].

There is now an extensive surface science literature on the oxygen over layers formed on single crystal surfaces exposed to high pressure oxygen, often accompanied with substantial metal atom restructuring [2, 41-49]. Moreover, the activity of the oxygens in 2-fold in bridge positions, which are available on oxide surfaces, were emphasized [68].

In fact, these proposals are in line with the reports of the increase in catalytic activity due to the formation of oxide (or surface-oxide [42, 46]) layers on the metallic catalyst surfaces under oxygen rich conditions, and suggest the actual catalyst as the oxide phase. For the partial oxidation of ethylene, the role and the influence of subsurface atomic oxygen (O_{ss}) on the catalytic reactivity and the selectivity patterns for the silver catalyzed ethylene epoxidation had been proposed previously [16, 38, 60, 61, 69], however it has not been involved in any of the previous mechanistic studies.

These studies investigating the Ag/O phases have not resulted in a definitive description of silver-oxide over layer structures. But, different interesting models were proposed to explore the reactivity of adsorbed oxygen atoms as a function of concentration and adsorption mode.

On the other hand, different oxygen adatoms (i.e. nucleophilic and electrophilic) with different activities towards selective and non-selective reactions were reported previously [14, 20, 25, 70-74]. Some authors relate the different activities of these surface adsorbed atomic oxygens (O_s) to different adsorption sites [16, 38, 60, 69, 71, 72]. For instance, it has been suggested that the O_s with a lower Ag coordination number, which means weaker adsorption and/or electrophilic nature, would be more reactive towards epoxidation [16, 19, 22, 38, 60, 68, 70-76]. When industrially applied high oxygen regimes are considered, previous reports on the increased activity of the oxidized surfaces towards EO, where O_{ss} is present [16, 38, 60], agree with these points. This idea also agrees with the proposals of oxide or oxide-like surfaces, where O_s occupies the bridge positions, being the active phase towards epoxidation [68].

The second group of studies focuses on the reaction kinetics and pathways of the epoxidation reaction. In the early works direct epoxidation of ethylene was proposed especially for high oxygen regimes. [17, 38, 71, 72]. However later works focused on metallic silver surfaces with low oxygen coverage. Among these works, experimental [19, 75, 77, 78] and computational [10, 19, 21, 22, 76, 79, 80] studies have concluded that oxametallocycle (OMC, Figure 1.2) is the common surface intermediate for both EO and AA formation. OMC forms on the catalyst surface through a well defined Langmuir-Hinshelwood (L-H) mechanism with the reaction of O_s and $C_2H_{4(ads)}$. It is the common precursor for both the selective and the non-selective reaction channels that produce EO and AA respectively. Thus, the product selectivity depends on the relative barriers of the

product formations (E_{EO}^a and E_{AA}^a) through the decomposition of the OMC intermediate. So far, studies on the metallic silver surfaces have reported activation barriers for EO and AA formation that are close to each other, which would explain the ~50% EO selectivity of the un-promoted metallic catalyst (i.e. model catalyst). However, an OMC model that would explain the high EO selectivity of the industrial process has not been proposed yet. On the other hand, apart from providing an epoxidation mechanism, OMC is the first conclusive model that explains the parallel non-selective AA formation.

Studies on the surface-oxide models for the Ag(111) surface [36, 81, 82], also produced similar results to those on metallic surfaces. However, recent studies point to a higher activity of Ag(100) [10, 21] and Ag(110) [22] surfaces. This increase in EO selectivity on these surfaces was related to the altered OMC decomposition barriers. On the other hand, it is known that increasing the partial pressures of ethylene and oxygen has direct and positive effects on the reaction rate and the EO selectivity [10, 20, 21, 70]. High EO selectivity of the industrial catalyst under oxygen rich conditions cannot be easily modeled with the OMC mechanism, because for all oxygen coverages on metallic surfaces, selective and non-selective paths compete.

Unlike the early studies that considered the steric effect of the Cl promoter, recent studies [36, 81] report the electronic effect of the promoters that are operational on a metallic surface. The Cl in the vicinity of the active surface oxygen weakens the Ag-O bond making the oxygen more easily transferable to ethylene. This effect changes the selectivity of OMC decomposition.

Unlike silver, the literature on the potential of the other metals for ethylene epoxidation is rather scarce. Two computational studies carried out for Cu(111) [79] and Au(111) [83] surfaces with 25% O-coverage reported that, the epoxidation reaction proceeds through the OMC intermediate as in the case of metallic silver surfaces. For the Au(111) surface it was concluded that differences of the activation energy barriers on Au and Ag are comparable. The main difference between these metallic surfaces relates to the ease of O₂ dissociation. On the other hand, the Cu(111) surface showed a lower activation barrier towards EO formation. Notwithstanding the endothermicity of the reaction of ethylene to EO with O_{ads} on Cu, it was suggested that, in theory, Cu would be a potential interesting candidate for EO catalysis. Nonetheless, there is no experimental report of selective

epoxidation catalysis of ethylene catalyzed by copper. Why other transition metals like copper and gold does not catalyze this reaction is still in debate.

Another important point that determines the EO selectivity is the size effect. Several studies concluded that the larger catalyst particles had higher EO selectivities [70, 74]. However the proposals on the size effect vary from the electronic effect (i.e. binding energies) to the amount of the surface defects and reconstructions.

CHAPTER 3

THEORY AND METHODOLOGY

The results obtained in this work were obtained by modeling the structures and reactions using quantum chemical methods. The theory behind, utilized software, models and the methodology are explained in this chapter.

3.1. Density Functional Theory

Density functional theory (DFT) has proven itself to be a successful tool for theoretical chemistry. Especially following the advances in the theory, and the computer power, realistic applications became feasible. Nowadays DFT became a popular tool in theoretical studies of chemistry and physics. This chapter aims to give a brief summary on the foundations of this method.

In 1925 Erwin Schrödinger formulated the *Schrödinger equation*, which describes how the quantum state of a physical system changes in time. For the any N-electron system that is stationary in time, or in a stationary state, the time-independent Schrödinger equation is,

$$\begin{aligned} H\Psi &= [T + V_{ext} + U]\Psi \\ &= \left[\sum_i^N -\frac{\hbar^2}{2m} \nabla_i^2 + \sum_i^N V(\vec{r}_i) + \sum_{i<j}^N U(\vec{r}_i, \vec{r}_j) \right] \Psi = E\Psi \end{aligned} \quad (3.1)$$

where, H is the Hamiltonian, E is the total energy, T is the kinetic energy, V_{ext} is the potential energy from the external field due to positively charged nuclei, and U is the electron-electron interaction energy. The operators T and U are called universal operators as they are the same for any N-electron system, while V is system dependent. This complicated many-particle equation is not separable into simpler single-particle equations because of the interaction term U . With its current form, Equation 2.1 can be considered as a force balance for a single atom. However, even for a simple di-atomic molecular system, more terms such as coulomb interaction for the nuclei should be added. Considering this, it can be seen that the solution of this equation for a molecular system is quite complicated.

There are many sophisticated methods for solving the many-body Schrödinger equation based on the expansion of the wavefunction in Slater determinants. While the simplest one is the Hartree-Fock method, more sophisticated approaches are usually categorized as post-Hartree-Fock methods. However, the problem with these methods is the computational effort required, which makes it unfeasible to apply them to larger and more complex systems.

Here DFT provides an appealing alternative, being much more versatile. It provides a way to systematically map the many-body problem, with U , onto a single-body problem without U .

In DFT the key variable is the particle density $\rho(\vec{r})$, which for a normalized wavefunction (Ψ) is given by

$$\rho(\vec{r}) = N \int d^3r_2 \int d^3r_3 \dots \int d^3r_N \Psi^*(\vec{r}, \vec{r}_2, \dots, \vec{r}_N) \Psi(\vec{r}, \vec{r}_2, \dots, \vec{r}_N) \quad (3.2)$$

DFT is nowadays a common tool for computational physicists, chemists and material scientists in the investigation of the properties of many-body systems. DFT has been shown to be quite accurate in predicting description of the ground state (electronic structure, dynamical, structural, thermochemical stability and transport) properties of materials, in bulk, at surfaces and nanostructures.

The starting point for understanding DFT is to go back to the Thomas-Fermi (TF) model which was independently put forward by Enrico Fermi and L.H. Thomas for a solution to many electron problem [84, 85].

$$E_{TF}(\rho) = A \int d^3r \rho(\mathbf{r})^{5/3} + \int d^3r V_{ext}(\mathbf{r}) \rho(\mathbf{r}) + B \int d^3r \rho(\mathbf{r})^{4/3} + \frac{1}{2} \int d^3r d^3r' \frac{\rho(\mathbf{r})\rho(\mathbf{r}')}{|\mathbf{r} - \mathbf{r}'|} \quad (3.3)$$

Where $A = \frac{3}{10} (3\pi^2)^{2/3}$, $B = -\frac{3}{4} \left(\frac{3}{\pi}\right)^{1/3}$ and $V_{ext}(\mathbf{r}) = -\sum_i \frac{Z}{|\mathbf{r} - \mathbf{r}_i|}$.

In equation 2.3, the first term is the local approximation to the kinetic energy, the third term is the local exchange and the last term is the classical electrostatic Hartree energy. To represent the exchange energy of the atom, Dirac added *exchange energy functional* to the TF model in 1928.

In 1964 Hohenberg and Kohn (HK) [86] laid the foundations of DFT with a view to systematically mapping out the many-body problem, by taking the electrons moving under an external potential. Hohenberg and Kohn gave proofs of two key theorems of DFT:

1. The ground state electron density, ρ_0 , of a many electron system in the presence of an external potential, V_{ext} , uniquely determines, except for a constant, the external potential, $V_{ext}(\mathbf{r})$. This implies that all properties are functionals of the electron density.

This theorem basically demonstrates the existence of a one-to-one mapping between the ground state electron density and the ground state wavefunction of a many-particle system, $\Psi(\mathbf{r}) \leftrightarrow \rho(\mathbf{r})$.

2. The ground state energy can be obtained variationally: the density that minimizes the total energy is the exact ground state density ρ_0 i.e. $\mathcal{E}[\rho] \geq \mathcal{E}[\rho_0]$ for every trial electron density ρ .

The electron density, $\rho(\mathbf{r})$, is given by

$$\rho(\mathbf{r}) = N \int d^3r_2 \int d^3r_3 \dots \int d^3r_N |\Psi(\vec{r}, \vec{r}_2, \vec{r}_3, \dots, \vec{r}_N)|^2 \quad (3.4)$$

Later on, in 1965 Kohn and Sham (KS) gave a prescription for obtaining the total energy of an N-electron density using one-particle formalism, by introducing the kinetic energy term. In this formalism the total ground state energy, the kinetic energy, the electron-electron interaction energy and the energy of the electrons in the external potential are all functionals of the electron density. KS considered a fictitious system of N non-interacting electrons that were subjected to a local potential $\mathbf{V}_{KS}(\mathbf{r})$, which was exactly mapped, density-wise, to a system of interacting electrons with a potential $V(\mathbf{r})$. The total electronic energy in the KS formalism is given by

$$E[\rho] = T_s[\rho] + V_{ext}[\rho] + U_{ee}[\rho] + E_{xc}[\rho] \quad (3.5)$$

$$= \int d\mathbf{r} V(\mathbf{r}) + F[\rho] \quad (3.6)$$

Where

$$F[\rho] = T[\rho] + \frac{1}{2} \int d\mathbf{r} \int d\mathbf{r}' \rho(\vec{r}) \rho'(\vec{r}') \frac{e^2}{4\pi\epsilon_i |\vec{r} - \vec{r}'|} + E_{xc}[\rho] \quad (3.7)$$

In equation (2.7), $T[\rho]$ is the kinetic energy of a non-interacting gas with density $\rho(\vec{r})$ and the second term is the classical electrostatic (Hartree) energy, $E_{xc}[\rho]$ is the exchange-correlation energy, which contains the non-classical electrostatic interaction energy and the difference between the kinetic energies of the non-interacting and interacting systems. Using equation (2.7) the variational problem of the HK density functional can be written as

$$\delta \left[F[\rho] + \int dr \mathbf{V}_{ext}(\vec{r})\rho(\vec{r}) - \mu \left(\int dr \rho(\vec{r}) - N \right) \right] = 0 \quad (3.8)$$

where μ is a Lagrange multiplier used to constrain the number of electrons to be N .
Rewriting equation (2.8) as

$$\frac{\delta T_s[\rho]}{\delta \rho(\vec{r})} + V_{KS}(\vec{r}) = \mu \quad (3.9)$$

Where the KS potential $V_{KS}(\vec{r})$ is given by

$$V_{KS}(\vec{r}) = \int dr' \frac{\rho(\vec{r}')}{|\vec{r} - \vec{r}'|} + V_{XC}(\vec{r}) + V_{ext}(\vec{r}) \quad (3.10)$$

With

$$V_{XC}(\vec{r}) = \frac{\delta E_{XC}[\rho]}{\delta \rho(\vec{r})} \quad (3.11)$$

The ground state density, ρ_0 , for this non-interacting system can be obtained by minimizing the KS energy functional:

$$\mathbf{H}_{KS}\psi_i(\vec{r}) = \left[-\frac{1}{2}\nabla^2 + V_{KS}(\vec{r}) \right] \psi_i(\vec{r}) = \epsilon_i \psi_i(\vec{r}) \quad (3.12)$$

And the electron density is given by

$$\rho(\vec{r}) = 2 \sum_{i=1}^{N/2} |\psi_i(\vec{r})|^2 \quad (3.13)$$

(the factor 2 accounts for the spin degeneracy).

The exact analytical form of the universal exchange-correlation energy, $E_{xc}[\rho]$, functional in DFT is not known and it is approximated. One of the most widely used approximations is the local density approximation (LDA). The LDA substitutes the exchange-correlation functional of an inhomogeneous system with that of an electron gas computed at the local density i.e. it assumes that the exchange-correlation interactions between electrons can be approximated by the local interactions in an electron gas. The LDA's exchange-correlation energy is given by:

$$E_{xc}[\rho] = \int \epsilon_{xc}(\rho) \rho(\vec{r}) d^3r \quad (3.14)$$

Where the exchange-energy per electron is that of the homogeneous gas is

$$\epsilon_{xc}[\rho] = \epsilon_{xc}^{hom}(\rho)|_{\rho=\rho(\vec{r})} \quad (3.15)$$

The exchange-correlation potential then takes the form

$$v_{xc}(\vec{r}) = \frac{\delta E_{xc}[\rho]}{\delta \rho(\vec{r})} = \epsilon_{xc}(\rho(\vec{r})) + \rho(\vec{r}) \frac{d\epsilon_{xc}}{d\rho} |_{\rho=\rho(\vec{r})} \quad (3.16)$$

The values of exchange-correlation energy of homogeneous electron gases of varying densities have been calculated by Ceperley and Alder [87] using Monte Carlo methods. In

the limit of slowly varying densities the LDA is exact. However, most physically interesting systems have rapidly varying densities thereby rendering the LDA to be a very crude approximation. Surprisingly, even in these cases the LDA gives very good results! Part of this success can be attributed to the fact that it obeys the sum rule for the exchange-correlation hole [88]. A spin polarized form of the LDA is the local spin density approximation (LSDA), which takes the electron spin into account as follows:

$$\mathbf{E}_{XC}[\rho \uparrow, \rho \downarrow] = \int \epsilon_{XC}(\rho \uparrow, \rho \downarrow) \boldsymbol{\rho}(\vec{r}) d^3r \quad (3.16)$$

An improvement of the LDA is the generalized gradient approximations (GGA), which not only takes into account the local density but also includes the density fluctuations (inhomogeneities) via the gradient of the density at the same coordinate:

$$\mathbf{E}_{XC}[\rho] = \int \epsilon_{XC}(\rho, \nabla\rho) \boldsymbol{\rho}(\vec{r}) d^3r \quad (3.17)$$

The GGA functional gives very good results for crystalline properties, ground state energies and molecular properties. Two of the most common analytic representation in use for ϵ_{XC}^{hom} are that of Perdew and Zunger [89] and that due to Perdew and Wang [90]. In this work we have mostly used the Perdew and Wang parameterization of the GGA (PW91).

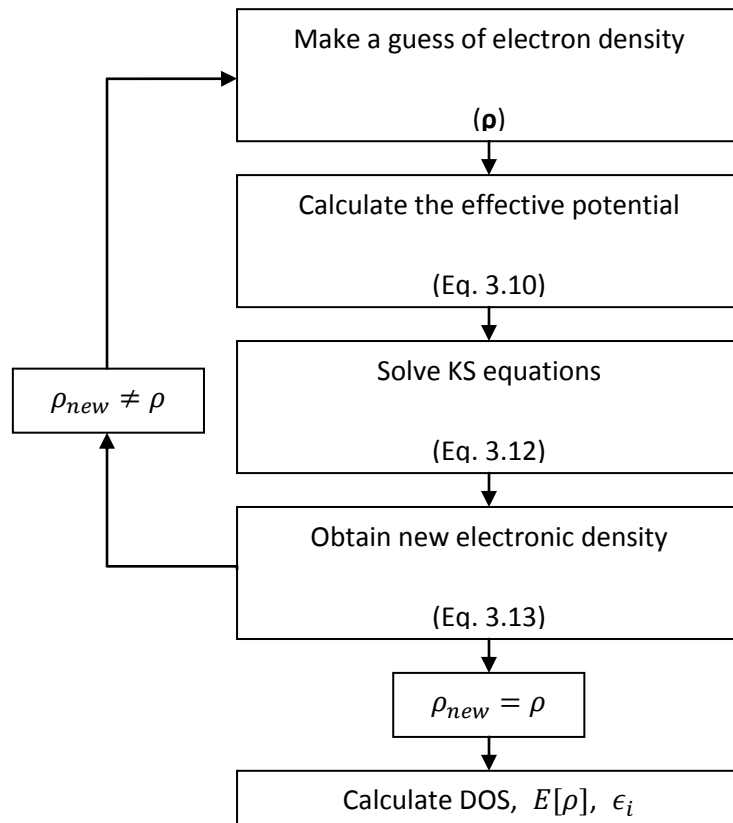


Figure 3.1: The self-consistent electronic iteration loop used in DFT computation.

In DFT computation, one makes an initial guess of the electron density, $\rho(r)$, (**Error! eference source not found.**). This electron density is used to calculate the effective potential using either the LDA or the GGA functional. The effective potential is then used to solve the KS equation after which the electronic density is computed. This process is repeated iteratively until self-consistency is achieved. Once the self-consistent loop is converged one can then calculate properties such as total energy, band structure and density of states (DOS).

Although the GGA has done much better than the LDA but there are cases where the LDA has also given very good results. This is evident in the 5d transition metals[91] and in alumina structural predictions [92, 93] where the LDA has scored favorably relative to the GGA. Well known deficiencies of LDA include overestimation of bulk modulus and

cohesive energy, underestimation of lattice constant and thus cell volume. Thus, the LDA gives a lower bound to the pressure for a given volume. The GGA's shortcoming, on the other hand, include: underestimation of the bulk modulus and cohesive energy, overestimation of lattice constant and thus cell volume. It thus gives an upper bound to the pressure for a given volume.

An improvement of the GGA are the hybrid functionals. The hybrid functional incorporate a portion of the exact exchange from Hartree-Fock with that from DFT's exchange-correlation form. For instance, the B3PW91 uses the Becke-3 exchange blended with the PW91 correlation. The B3LYP functional has a fraction of exact (Hartree-Fock) exchange and a correlation-energy functional from the LDA. It combines Becke's 3-parameter exchange functional [94] and the non-local correlation potential of Lee, Yang and Parr [95] as shown in equation (2.18).

$$\begin{aligned} \mathbf{E}_{XC}^{B3LYP} = \mathbf{E}_{XC}^{LDA} + a_0(\mathbf{E}_X^{HF} - \mathbf{E}_X^{LDA}) + a_X(\mathbf{E}_X^{GGA} - \mathbf{E}_X^{LDA}) \\ + a_C(\mathbf{E}_C^{GGA} - \mathbf{E}_C^{LDA}) \end{aligned} \quad (3.18)$$

Where the coefficients a_i are adjustable parameters, which are determined from a fit to atomization energies, ionization energies, atomic charges and proton affinities from a set of molecules.

3.2. The VASP Software

All the DFT calculations presented in this work were performed using the Vienna Ab-initio Simulation Package (VASP) [96, 97], which was developed by G. Kresse, J. Furthmuller and their colleagues in the University of Vienna. The software was developed for solid state systems with periodic boundary conditions. It is developed as an DFT algorithm to solve the many body electronic problem via the Kohn-Sham equations. Plane wave basis sets are used to express the electronic properties such as charge density and orbitals. The interactions between the electrons and the ions are described by using projector-

augmented wave (PAW) method. To determine the electronic ground state, VASP carries out two types of numerical iterations: i) the inner (electronic) loop and ii) the outer (ionic) loop. The inner loop is essentially an implementation of a self-consistent algorithm for solving the Kohn–Sham equations. The total energy and the forces are also evaluated. The outer loop is concerned with the ionic movement and supports geometry optimization and molecular dynamics algorithms. More detailed information is available at:

<http://cms.mpi.univie.ac.at/vasp/vasp/vasp.html>.

The results were mostly produced and analyzed using standard methods, such as the density of states analysis and charge analysis. However, a non-standard method was implemented to study the reaction coordinates. The reaction paths and the transition states (TS) along these reaction paths were produced using the nudged elastic band (NEB) method, with the implementation of climbing image method (CI-NEB) [98]. In the standard NEB application, N number of images are produced between the two stable points corresponding to the reactants and the products. During the optimization procedure each image is relaxed separately. However, these images are bound to each other via spring forces, and also to the potential energy surface (PES) with the tangent forces. Thus, a continuous path on the PES between the reactants and products is kept. In the standard implementation of NEB, the images are not allowed to move on the PES along the created path. However, on CI-NEB implementation, movement of the images along this path is possible. Thus, it is possible to obtain the exact TS only using the NEB run. More detailed information on this implementation can be found at:

<http://theory.cm.utexas.edu/vtsttools/neb>

3.3. Preparation of Surfaces

The first step in this theoretical study was to prepare the model surfaces to be studied. Three transition state metals Cu, Ag and Au were studied for their metallic and M_2O oxide phases. To obtain the surface models, first the metallic and oxide crystals were optimized for their bulk parameters. Once the optimum parameters for the bulk crystals were

determined construction and optimization of the surface models (slab) to be studied were carried out.

The studied model surfaces are,

- p(2x2), p(3x3) and p(4x4) Ag (111) metallic surfaces,
- p(3x3) Cu(111) and Au(111) metallic surfaces,
- p(2x2) (100) and (110) metallic surfaces of Cu, Ag and Au, and,
- p(2x2) Ag₂O(001), Cu₂O(001) and Au₂O(001) oxide surfaces.

Later on, reaction paths and energetics were studied on these surfaces for ethylene epoxidation. The model preparation process is explained below.

3.3.1. Metallic Surfaces of Copper, Silver and Gold

Metallic Cu, Ag and Au crystals have face centered cubic (FCC) structure with a Fm-3m (#225) symmetry [99]. FCC crystal for these elements is schematically presented in Figure 3.2. A comparison of the experimentally measured and optimized cell parameters for these elements are listed in Table 3.1.

Table 3.1: Experimental and optimized bulk parameters for given metals.

Element	Experimental Value [99]	Optimized Value
Cu	4.049	3.635
Ag	4.086	4.155
Au	4.078	4.168

*For the optimization of the lattice parameter (15x15x15) k-points and 500 eV cut-off energy was used.

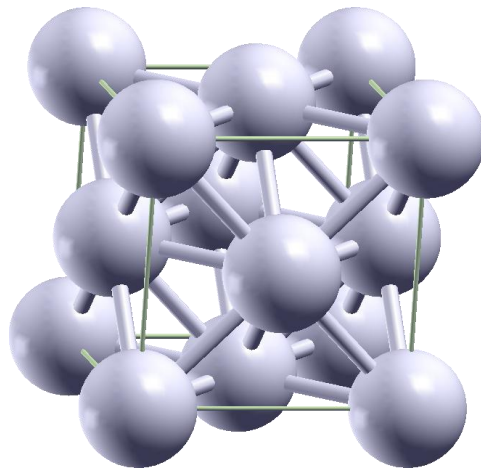


Figure 3.2: Schematic representation for Cu, Ag and Au FCC crystals.

Once the crystal cells were optimized, $M(hkl)$ surfaces were prepared by cutting the bulk structures along each respective plane. Then periodic supercells are prepared by placing a vacuum region above each surface. The minimum height of the vacuum region used was 15 Å. Each surface model (supercell) was relaxed to observe surface relaxation. At this step, by relaxing several slabs of different thicknesses, the surface energies were also calculated as described in [100]. By determining the point where the surface energies were converged, the optimum thicknesses of the slabs were also determined. The calculated surface energies and the parameters of the slabs are listed in Table 3.2. Schematic representation for the metallic surfaces can be seen in Figure 3.3.

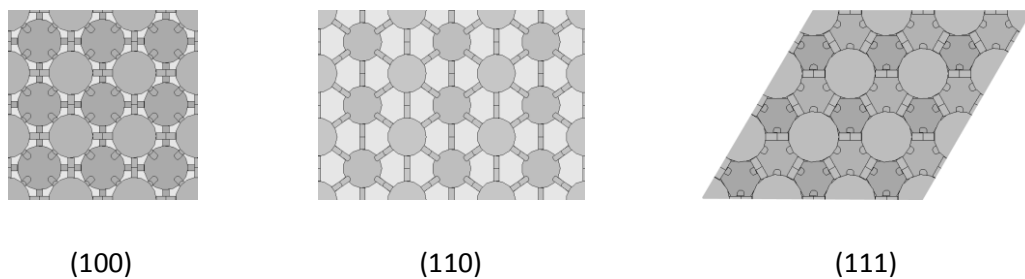


Figure 3.3: Schematic representations for the studied metallic surfaces. The light and dark shaded circles represent the surface and the sub-surface atoms, respectively.

Table 3.2: Supercell thicknesses and surface energies of metallic surfaces.

Surface	Slab Thickness (\AA)	Slab Thickness (Atomic Layers)	Vacuum Thickness (\AA)	Calculated E_{surf} (J/m^2)	Reference E_{surf} (J/m^2)[101]
Cu(111)	6.213	4	15	1.95	1.82
Cu(100)	8.063	6	15	2.15	2.16
Cu(110)	8.84	6	15	2.29	2.23
Ag(111)	7.188	4	15	1.01	1.24
Ag(100)	9.197	6	15	1.18	1.20
Ag(110)	10.119	6	15	1.35	1.23
Au(111)	7.277	4	15	1.32	1.50
Au(100)	9.191	6	15	1.72	1.62
Au(110)	10.150	6	15	1.85	1.70

3.3.2. Oxide Surfaces of Copper, Silver and Gold

Figure 3.4 shows a schematic for the unitcells of the Cu_2O , Ag_2O and Au_2O crystals. All these three crystal have FCC structure with a Fm-3m (#225) symmetry [35, 102]. The FCC metal atoms, and O atoms occupy 2 tetrahedral sites on the volume diagonal of the cube. A comparison of the experimentally measured and optimized cell parameters for these elements are listed in Table 3.3.

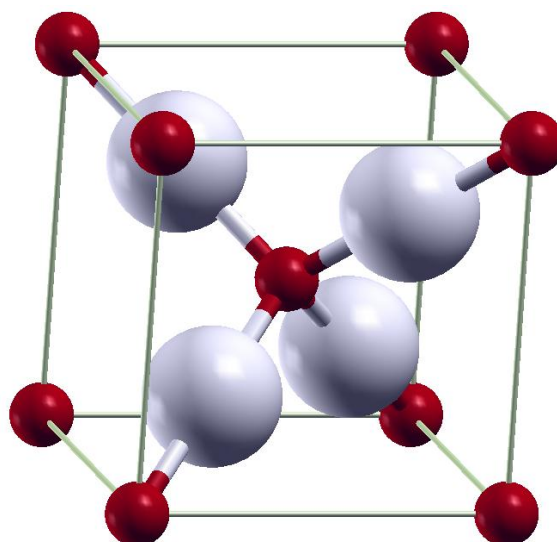


Figure 3.4: Schematic for Ag_2O , Cu_2O , Au_2O crystals.

Once the crystal cells were optimized, $\text{M}_2\text{O}(001)$ surfaces were prepared by cutting the bulk structures along each respective plane. Then periodic supercells were prepared by placing a vacuum region above each surface. The minimum height of the vacuum region used for the oxide surfaces is 15 Å. Each surface model (supercell) was relaxed to observe surface relaxation. At this step, by relaxing several slabs of different thicknesses, the surface energies are also calculated as described in [100]. The surface energy is calculated only for the $\text{Ag}_2\text{O}(001)$ surface as 1.324 J/m^2 . The parameters of the $\text{M}_2\text{O}(001)$ supercells are listed in Table 3.4. The $\text{M}_2\text{O}(001)$ surfaces used in the calculations consist of 4 layers of M_2O chains, that is 8 atomic layers counting each metal and oxide layer. Schematic representation for the oxide surfaces can be seen in Figure 3.5.

Table 3.3: Experimental and optimized bulk parameters for given metal oxides.

Element	Experimental Value (Å)	Optimized Value (Å)	Formation Energy (kJ/mol)
Cu ₂ O	4.26	4.30	-134 -169 [99]
Ag ₂ O	4.72	4.82	-39 -31 [99]
Au ₂ O	4.81	4.79	+21 +22 [35]

*For the optimization of the lattice parameter (15x15x15) k-points and 500 eV cut-off energy was used.

** Formation energies calculated with the formula: $2xM_{(bulk)} + \frac{1}{2} O_{2(gas)} \rightarrow M_2O_{(bulk)}$

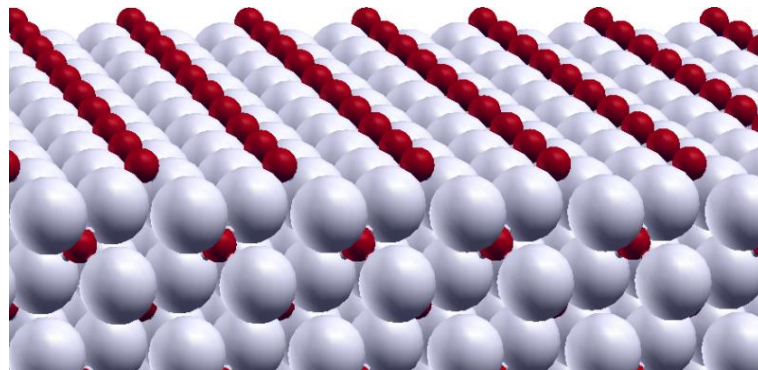


Figure 3.5: Perspective view of M₂O(001) surfaces (Gray: metal atoms and, red: oxygens).

Table 3.4: Parameters of the $M_2O(001)$ supercells.

	Slab Thickness	Vacuum Thickness
Surface	(Å)	(Å)
$Cu_2O(001)$	7.31	15
$Ag_2O(001)$	8.36	15
$Au_2O(001)$	8.34	15

3.4. Computational Details

The results presented in this work were obtained with the the periodic DFT computations that were performed with the VASP package [96, 97], using PW basis sets with GGA [103, 104]. For all the computations presented within this work, 500 eV cut-off energy was used. Necessary dipole corrections due to the asymmetric usage of slabs were included into the computations. All the results presented were obtained by relaxing the structures until the net force acting on the ions was ≤ 0.015 eV/Å. The reaction paths were generated using the climbing image (CI-NEB) method [98]. Spin polarized computations were carried out for the necessary systems such as those involving molecular oxygen, or those involve gold, and the corresponding energies were reported.

3.4.1. Atoms and Molecules in Vacuum

The total energies of gas phase atoms and molecules (i.e. in vacuum and non-interacting) were calculated by placing them in a supercell, where the periodic atoms/molecules were separated with a minimum of 10 Å vacuum distances in all Cartesian directions. These computations were performed using a single k-point (gamma point) K-points mesh.

3.4.2. Metallic Surfaces

The (100), (110) and (111) metallic surfaces of d-block metals Cu, Ag and Au were studied and compared for the reaction paths and intermediates along the ethylene epoxidation reaction. The M(100) and M(110) surface models of these metals (M: Cu, Ag and Au), were constructed using 6 layers thick p(2x2) slabs. In the computations the K-points sampling was generated using the Monkhorst Pack procedure with a (4x4x1) mesh for all the computations involving these slabs.

The M(111) surfaces for these metals were modeled using 6 layers thick slabs. For the Ag(111) surface, slabs of 2 different sizes were prepared to study the coverage effect. Thus, in the following sections results were presented for p(3x3) and p(4x4) Ag(111) surfaces, whereas only for p(3x3) Cu(111) and Au(111) surfaces. During the computations involving these models, the k-point sampling was produced using a (3x3x1) mesh for the p(4x4) Ag(111) and using a (4x4x1) mesh for all the remaining p(3x3) M(111) slabs. For all the metal surfaces studied, periodic the structures were separated with 15 Å vacuum distances.

3.4.3. Oxide Surfaces

As explained in the previous sections, the M₂O(001) surfaces (M: Cu, Ag, Au) were constructed from their respective crystals [35, 102] upon optimizing lattice parameters. Each M₂O(001) slab consists of 8 atomic layers (for example 4 Ag₂O layers, 8.5 Å) with a p(2x2) square surface. The supercells were constructed with a minimum vacuum height of 15 Å. In the calculations the bottom layer was kept fixed for all the slabs, where all the remaining atoms were relaxed. The k-points sampling was generated by the Monkhorst Pack procedure with a (4x4x1) mesh for all the slabs.

3.4.4. NEB method and the Determination of the Transition States

Once the geometries for the reactants and the products were obtained, the candidate reaction paths were studied between these two geometries using CNEB method. Using a script, a series of equally separated images (usually 4 or 8) were produced between the reactant and the product geometries. The script produced N number of images by linearly dividing the distance between initial and the final position of each atom. During a NEB run, each image was relaxed on the potential energy surface (PES), while still being kept tied to each other.

At the end of the NEB run, the geometry with the highest energy is taken as a candidate for transition state (TS), and further relaxed using Newton-Raphson algorithm. The resulting geometry was then tested to see if it is the exact TS, using the vibrational analysis. Once a single imaginary (or negative) vibrational frequency along the reaction coordinate was observed, the geometry was taken as the TS geometry and the corresponding energy as the TS energy.

3.4.5. Vibrational Frequencies and Zero Point Energies

The vibrational frequencies of adsorbed surface species and transition states were calculated by calculating the Hessian matrix based on a finite difference approach with a step size of 0.02 Å for the displacements of the individual atoms along each Cartesian coordinate. During the frequency calculations symmetry was excluded explicitly. The frequencies of the surface ions were excluded basing on the frozen phonon approximation.

Zero-point energy (ZPE) corrections were calculated using the harmonic approximation; and the positive modes of the vibrational data. The half of the sum of the normal mode frequencies produced the zero point energy difference ($\hbar\nu/2$), and thus could be calculated directly from the computational output. Within this work, in the following chapters, for the reported values of zero point energy corrected activation energy barriers, ZPE correction was included for both the reactant and the transition state.

CHAPTER 4

RESULTS AND DISCUSSION

Ethylene epoxidation reaction was investigated for its reaction mechanisms on various surfaces of silver as well as two more candidates copper and gold. On the possible catalyst surfaces the reaction paths, transition states along these paths and the reaction energies were studied and compared at varying surface oxygen ratios. The effect of the oxygen coverage was also studied by using different surface models varying from metallic to oxide surfaces. This chapter presents these studies by giving the results obtained with discussions. In the first section the ethylene epoxidation reaction is investigated for different metallic surfaces of Ag, Cu and Au, and at varying oxygen coverages. The second section presents the direct epoxidation mechanism on $\text{Ag}_2\text{O}(001)$ surface identified in this work. The third section makes a comparison between silver oxide, copper oxide and gold oxide surfaces. The last section opens a discussion for the surface stability and the effect of the Cl promoter.

4.1. Ethylene Epoxidation on Metallic Surfaces

This section aims to address the following points. First of all, a clear separation between the oxygen adsorption sites (i.e. fcc v.s. hcp sites of (111) surfaces) and the corresponding activity of the surface oxygen on epoxidation has not always been done consistently. Although the difference between adsorption energy of oxygen on fcc and hcp sites is not large, the extra stability of surface oxygen may play a role on the EO selectivity. Secondly, as it will be demonstrated, high oxygen coverage prevents the on surface ethylene adsorption, and changes the OMC formation mechanism from Langmuir-Hinshellwood (L-

H) to Eiley-Rideal (E-R). This change in the mechanism of surface complex formation may change the rate limiting step of overall reaction. And finally, the ethylene epoxidation on the metallic surfaces of Ag, Cu and Au has been studied by many different groups with different approaches. Therefore, a comparison of these different results is not always readily possible. Since we apply the same approach to the study of the different systems, such a comparison can now be more reliably made.

The ethylene epoxidation on metallic surfaces was handled in two parts. In the first part the effect of the oxygen coverage on the epoxidation mechanism was studied for Ag(111) surface. In the second part, the epoxidation mechanism was investigated for the metallic (100), (110) and (111) surfaces of Cu, Ag and Au. The results are presented below with discussions.

4.1.1. Part I: Oxygen Coverage Dependence

Effect of oxygen coverage on ethylene epoxidation was investigated on the Ag(111) surface for the 1/9, 4/16 and 3/9 ML oxygen coverages. The results are presented below with discussions.

4.1.1.1. Oxygen and Ethylene Adsorption

Figure 4.1 shows the adsorption energies of oxygen and oxygen distribution on the Ag(111) . The adsorption energies were calculated for the simultaneous dissociative adsorption of $n/2$ gas phase molecular oxygen ($O_{2(g)}$). An example calculation is given below for the p(4x4) surface where the oxygen coverage increases from 0 to 4/16 ML.

$$E_{ads} = \frac{1}{4} \left[E(\text{slab with 4 oxygen}) - E(\text{clean slab}) - 4x\left(\frac{1}{2}O_{2(g)}\right) \right]$$

As expected, the adsorption energy is higher for the low coverages and decrease with the increasing coverage. There is a constant energy difference of ~ 10 kJ/mol between the fcc and hcp adsorption of oxygen.

The experimental value for oxygen adsorption (0.41 ML) on silver surface is approximately 40 kJ/mol for per adsorbed oxygen atom [64]. The fcc adsorption energies in this work are very close to this experimental value. In a previous work that studied Ag-O interaction theoretically [62] the adsorption energies of oxygen are listed as -46 and -29 kJ/mol for fcc and hcp sites respectively at $1/9$ ML coverage, and, -14 and -3 kJ/mol fcc and hcp sites respectively at $3/9$ ML coverage. Similarly, the oxygen adsorption energies were reported for Cu(111) surface at $1/4$ ML coverage [80] are -151 and -158 kJ/mol for fcc and hcp sites respectively, whereas for the Au(111) surface at the same coverage reported to be 7 kJ/mol, without explicit definition of the adsorption site. Apart from the differences in the methods and computation details, our results agree with previous reports.

Table 4.1 compares the oxygen adsorption energies for the (111) surfaces of Cu, Ag and Au, at $1/9$, $2/9$ and $3/9$ ML oxygen coverages. The energy difference separating the fcc and hcp adsorption for the Ag(111) surface was not observed for the Cu(111) surface. However, this difference is almost 20 kJ/mol for the Au(111) case. Moreover, while adsorption is exothermic for all the coverages for Ag(111) and Cu(111) surfaces, feasible O adsorption is only possible for the very low concentrations on the Au(111) surface.

Figure 4.2 shows the ethylene adsorption positions and energies on clean and oxygenated Ag(111) surfaces. As the schematics show, the preferred ethylene adsorption position is the on top site with a hexagonal empty space around. As can be seen in the schematics of Figure 4.1, this adsorption site is only available for the coverages up to $3/9$ ML (33%). For 33% and higher coverages ethylene adsorption site is occupied. However, as will be discussed in the following section, OMC formation is still exothermic for high coverages. Thus a change in the OMC formation mechanism is proposed.

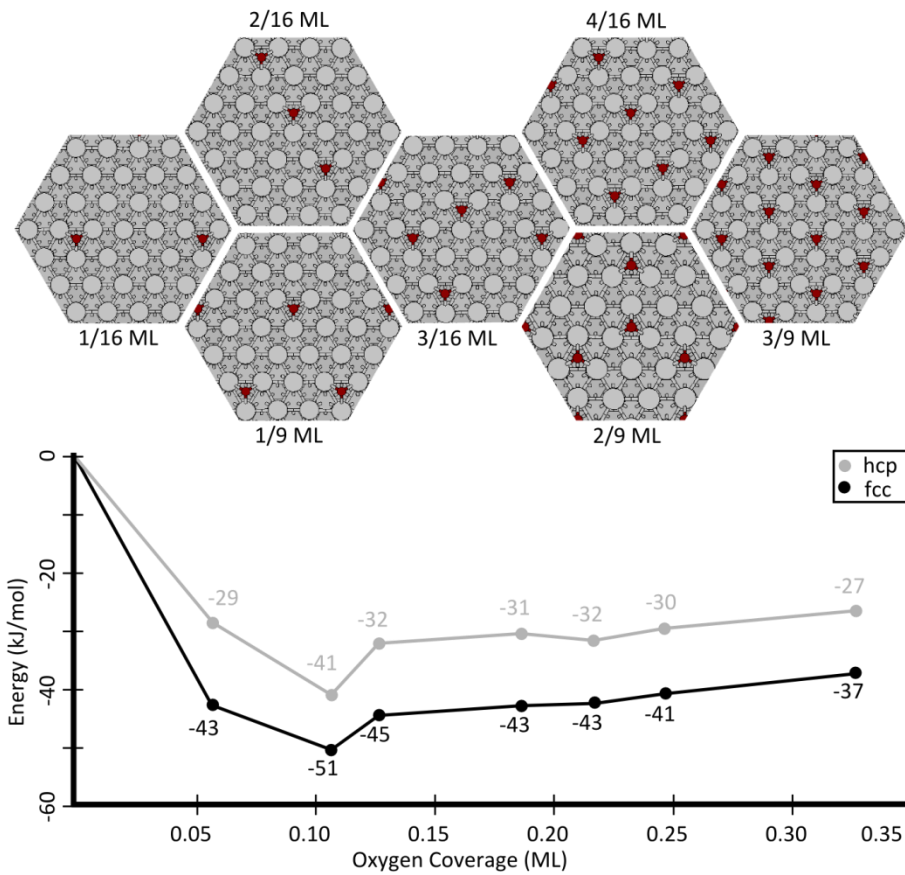


Figure 4.1: Relative energies of O adsorption on fcc and hcp sites of Ag(111) surface. The figures above show the oxygen distributions for given coverages. (Ag: light gray, O:red or dark gray).

Table 4.1: Adsorption energies (kJ/mol) of oxygen on (111) surfaces of Cu, Ag and Au at increasing coverages.

	1/9 ML		2/9 ML		3/9 ML	
	fcc	hcp	fcc	hcp	fcc	hcp
Cu(111)	-168	-167	-161	-161	-154	-156
Ag(111)	-51	-41	-43	-31	-37	-27
Au(111)	-8	13	-6	18	6	30

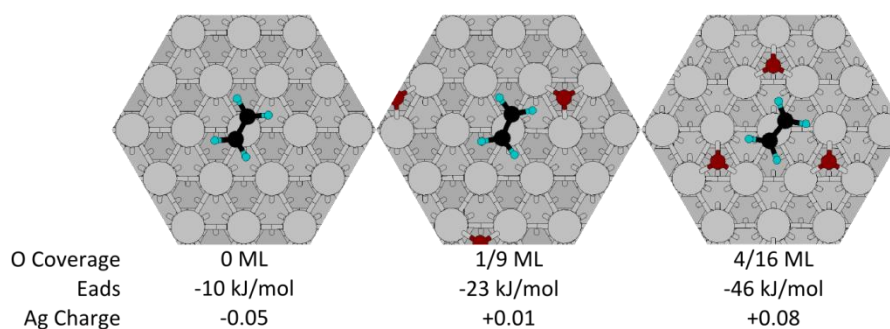


Figure 4.2: Ethylene adsorption on Ag(111) surface at given oxygen coverages. Charges are calculated with Bader analysis [105]. (Ag: gray, O: red or dark gray, C: black, H: cyan or light gray).

As Figure 4.2 shows, the interaction of ethylene becomes more exothermic with increasing oxygen coverage. This is a result of the higher (+) charge on the surface Ag atom, which is induced by the increasing number of oxygen neighbors. The increasing (+) charge on the metal cause stronger interaction with the C=C double bond. The extreme point for this interaction is the di-sigma adsorption of ethylene on the metal surface [106]. However, only pi-adsorption is observed in this study. It can be commented that both the adsorption site and the strong enough (+) charge on the metal atoms cannot be satisfied with the monolayer on-surface oxygen adsorption.

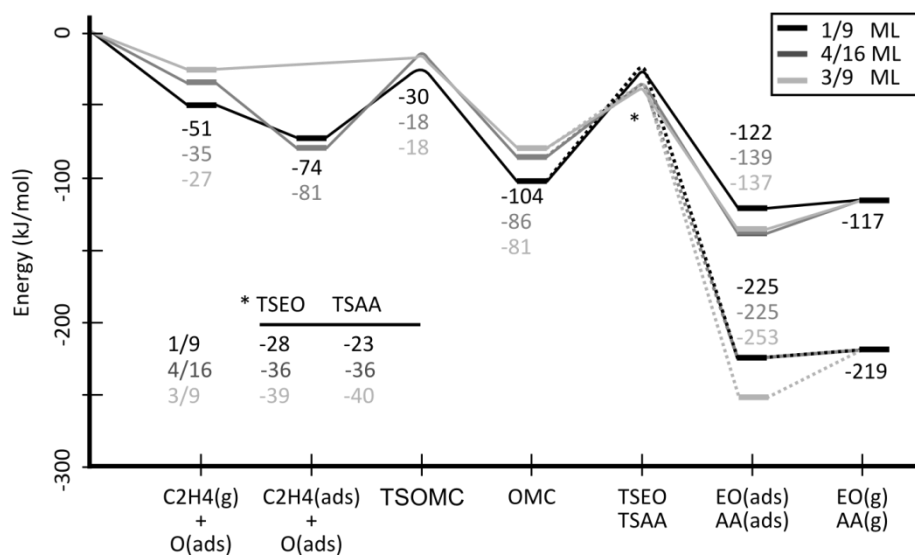
4.1.1.2. Formation of EO and AA through OMC

Figure 4.3 shows the effect of oxygen coverage on the relative energies along the selective and non-selective reaction path of OMC mechanism on Ag(111) surface. The geometries corresponding to stable points and transition states can be seen in Scheme 4.1. When Figure 4.3.a and Figure 4.3.b are compared, the main energy difference for the reaction paths on O(fcc) and O(hcp) is due to the extra oxygen stability in fcc positions (i.e. ~10 kJ/mol difference). Thus, although the absolute values of the transition states does not differ, the activation barriers are higher in case of O(fcc).

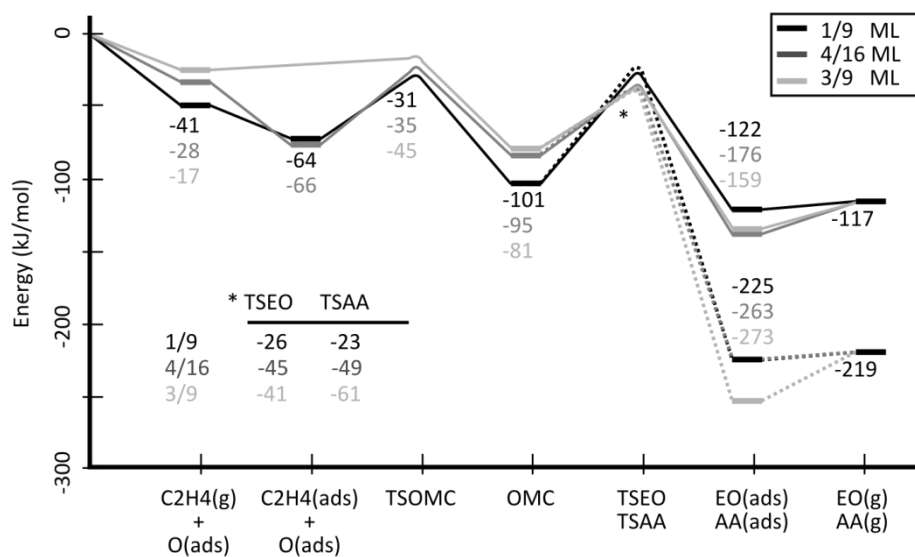
When the L-H formations of OMC are compared for the 1/9 and 4/16 ML coverages, it can be seen that the E_{OMC}^a is higher for 4/16 ML coverage, where ethylene adsorption is

more stable. However, as discussed in previous section, ethylene adsorption at 3/9 ML is not possible. Nonetheless, calculations show that the formation of OMC is still exothermic for this coverage. Thus, formation of OMC through E-R mechanism is considered. This time, when gas phase ethylene interacts with O_s to form OMC directly, a much smaller barrier is faced. Change of OMC formation mechanism from L-H to E-R may be playing an important role. As Figure 4.3 shows, when the mechanism is L-H, the barriers for the OMC formation are larger than the products formations. Thus, when the mechanism changes to E-R, the rate limiting step changes to the product formations.

With the increasing oxygen coverage, $EO_{(ads)}$ and $AA_{(ads)}$ formations get more exothermic while the E_{EO}^a and E_{AA}^a decreases with the increasing oxygen coverage. Both of these effects can be attributed to the weakening of Ag-O bonds. However, for none of the coverages studied a change in the selectivity was observed. That is, a distinct separation between E_{EO}^a and E_{AA}^a does not occur. Although the smaller activation barriers point to faster reaction, the expected EO selectivity still would be around 50%, as reported for the un-promoted metallic catalyst.



(a)

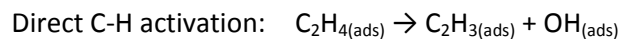


(b)

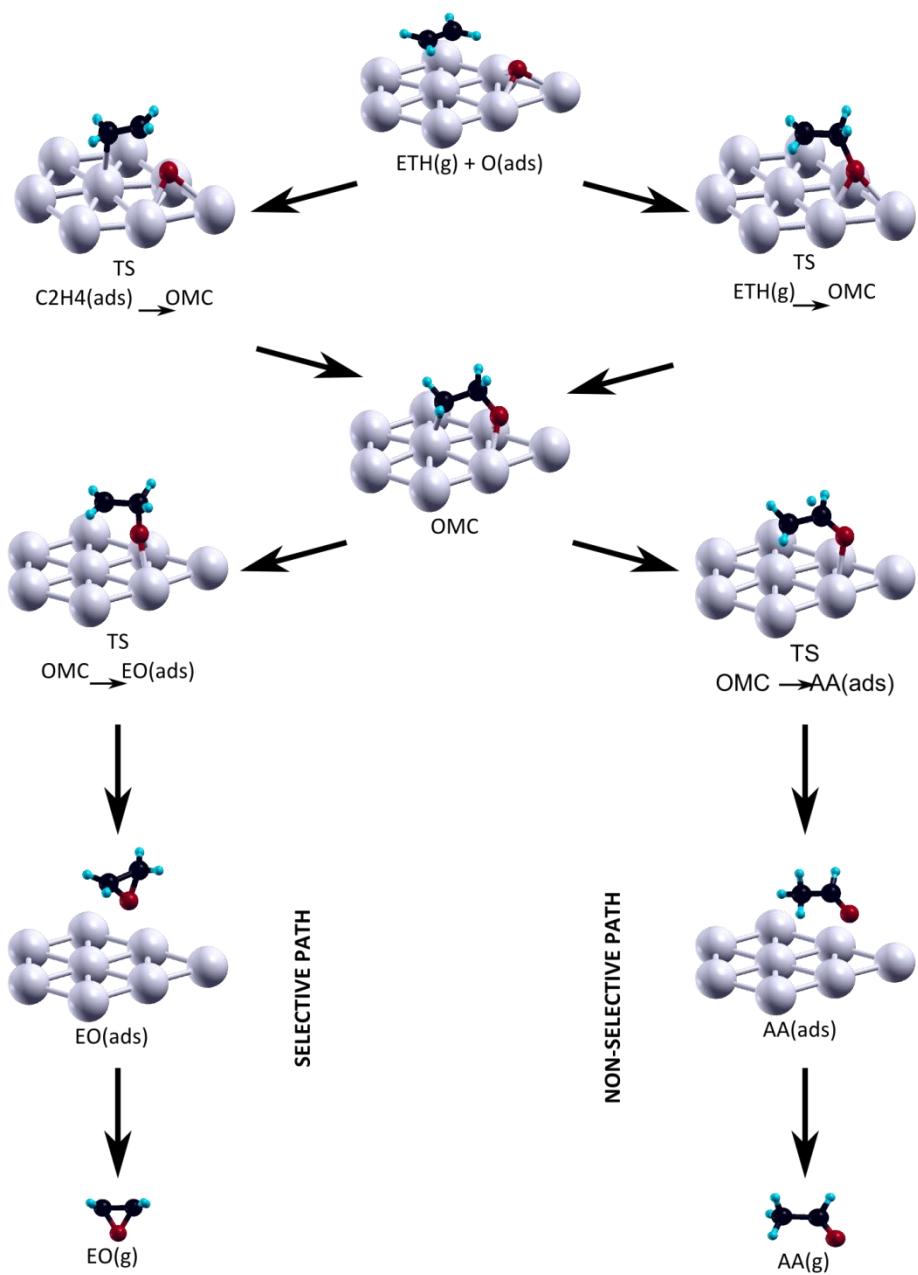
Figure 4.3: Relative energies of OMC paths tested for (a) fcc and (b) hcp adsorbed oxygen on Ag(111) surface at varying oxygen coverages. After OMC intermediate solid lines represent the EO path and dashed lines represent the AA path. See Scheme 4.1 for geometries of stable points and transition states.

4.1.1.3. Alternate Paths

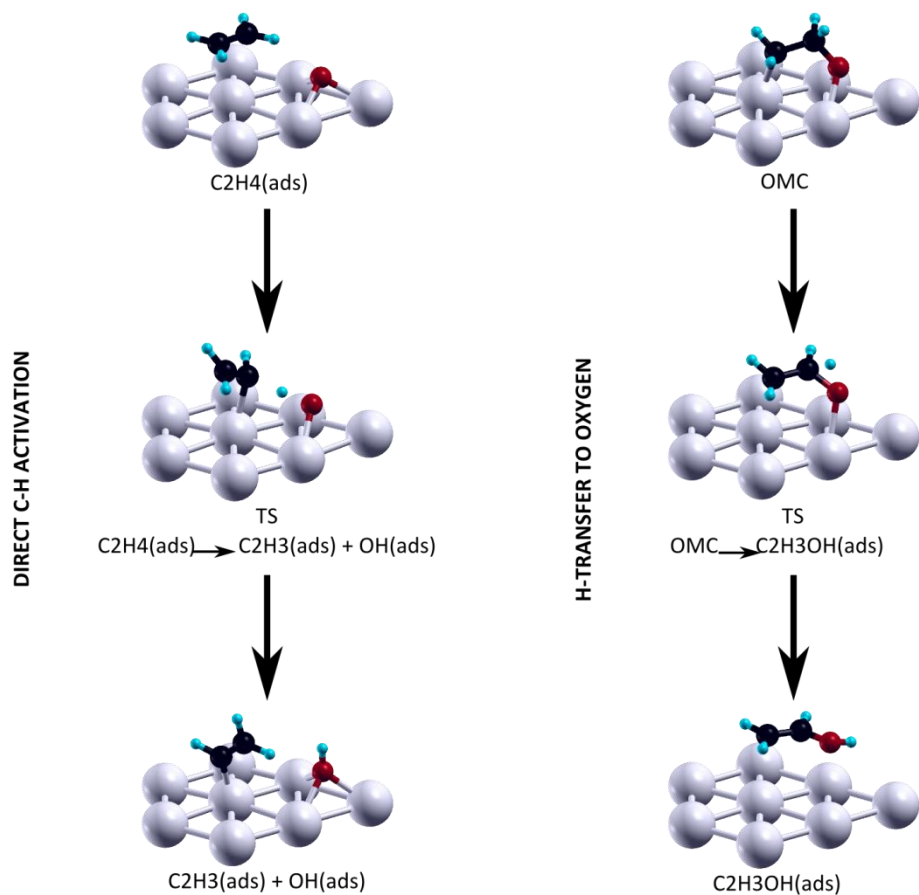
Along with the well defined selective and non-selective reaction channels of OMC, two more alternate paths were evaluated. Formations of vinyl type of intermediates were considered with the reactions:



The geometries of stable points and transition states are given in Scheme 4.2. The energies corresponding to these points are given in Figure 4.4. The left side of Figure 4.4 shows the energies of the direct C-H activation reaction. The right side shows the formation of vinyl alcohol (CH_2CHOH) through OMC intermediate. Both of these reactions have higher activation barriers, compared to that of OMC formation and/or EO/AA formation through OMC. Thus, formation of OMC and its decomposition to produce EO or AA are the reaction paths followed.



Scheme 4.1: Geometries along OMC mechanism on (111) surface. (M: light gray, O: red or dark gray, C: black, H: cyan or gray).



Scheme 4.2: Geometries along C-H activation paths on Ag(111) surface. (M: light gray, O:red or dark gray, C: Black, H:cyan or gray).

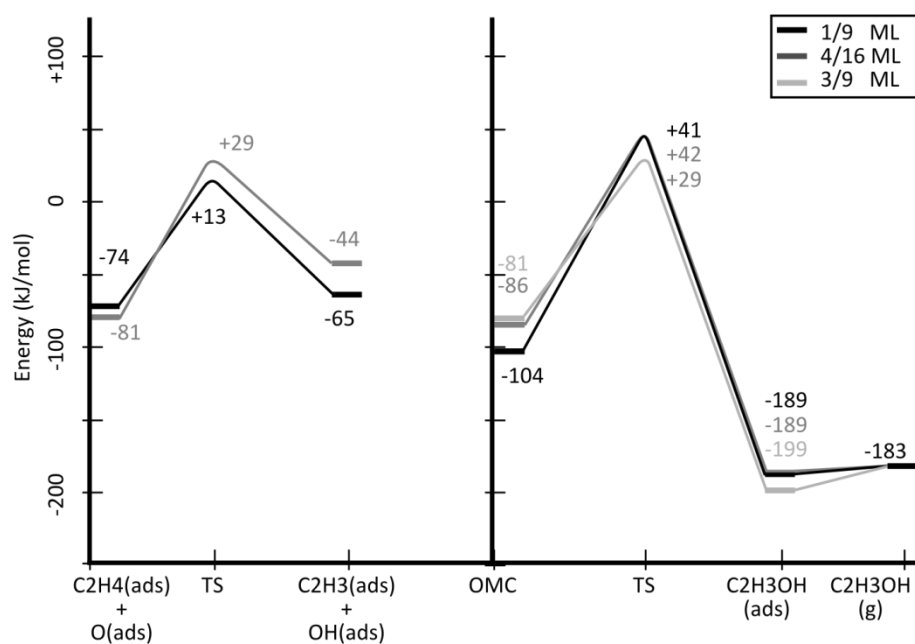


Figure 4.4: Relative energies for the direct C-H activation (left side) and H-transfer to oxygen on OMC intermediate (right side), tested on Ag(111) surface for given oxygen coverages. See Scheme 4.3 for geometries of stable points and transition states.

4.1.2. Part II: Surface Structure Dependence

Apart from the commonly studied Ag(111) surface, different studies computationally tested the Ag(100) and Ag(110) surfaces, and also Cu(111) and Au(111) surfaces for their activities towards ethylene epoxidation. The Ag(100), Ag(110) and Cu(111) surfaces were reported to be more selective towards EO, whereas the Au(111) surface was reported to behave similar to Ag(111) surface. However because of the different computational approaches followed, a direct comparison of these different works is not possible. Thus, we tested the (100), (110) and (111) surfaces of Cu, Ag and Au for their activities towards ethylene epoxidation and compared the results.

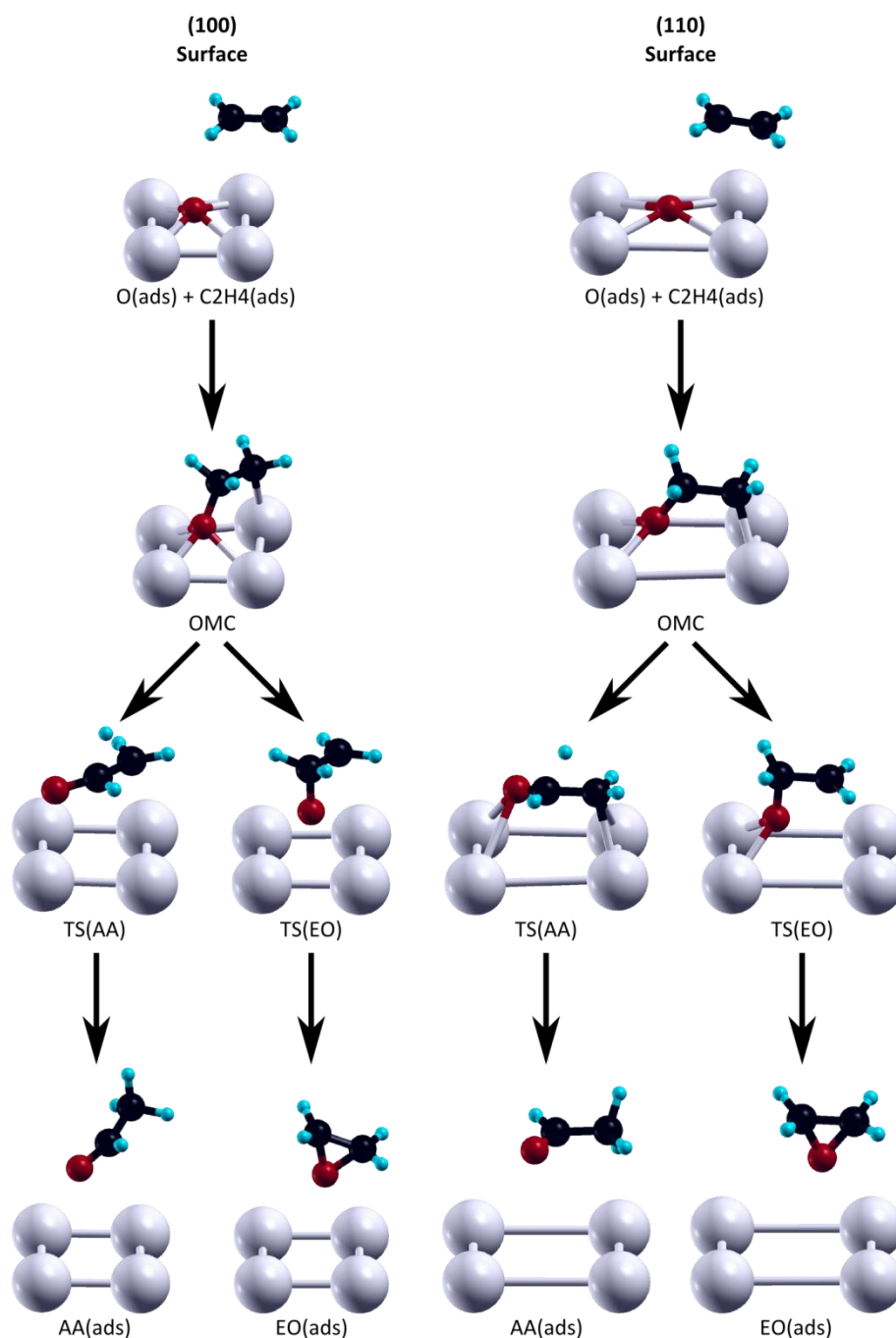
Previous studies of the Ag(100) [10] and Ag(110) [22] surfaces reported an increase in EO selectivity due to changes in E_{EO}^a and E_{AA}^a . In these studies, E_{EO}^a was reported to be lower than E_{AA}^a by ~ 10 kJ/mol for Ag(100) surface and ~ 5 kJ/mol for Ag(110) surface. However, as Figure 4.5 and Table 4.2 show, the lowering of the E_{EO}^a on Ag(100) surface

was not observed in this work. As Table 4.2 shows, the E_{EO}^a values are close to each other for Ag(111) and Ag(100) surfaces. The difference between these surfaces is in E_{AA}^a . On the other hand, we find E_{EO}^a to be ~ 5 kJ/mol lower than E_{AA}^a on Ag(110) surface (Figure 4.6). However, it should also be noted that, in the previous study, the OMC intermediate was constructed on a 2-fold oxygen species assuming reconstructed (110) surface using a non-periodic cluster method. In this work, a more strongly adsorbed O (4-fold) was used for the same purpose because of the instability of 2-fold oxygen on such a surface.

A previous study on Cu(111) surface [79] concluded that Cu(111) surface would be more selective towards EO compared to Ag(111) surface with a ~ 25 kJ/mol lower E_{EO}^a than E_{AA}^a . We also confirm this finding on Cu(111) surface, where our difference is ~ 10 kJ/mol, which is still larger than the differences for Ag surfaces. However, other Cu surfaces do not favor the EO formation. An important point for Cu surfaces is that, EO formation is endothermic with respect to the oxygenated surface, whereas AA formation is exothermic, which shows that AA would be the preferred product.

Figure 4.7 shows that, Au(111) behaves similarly to Ag(111) as has also been concluded by [83]. However, Au(111) shows lower activation barriers compared to Ag(111) and Cu(111) surfaces. This is due to the less stable OMC intermediate. Although the gold surface produce lower E_{EO}^a than E_{AA}^a compared to the other metals, gold is still not selective for EO.

Among the studied silver surfaces, the Ag(111) and Ag(110) surfaces showed lower barriers for EO formation than that of AA. However, the differences between the activation barriers of the competing paths are rather small and within the DFT error range. For all the silver surfaces studied, E_{EO}^a and E_{AA}^a values being close to each other, agrees with the $\sim 50\%$ EO selectivity of un-promoted silver catalyst.



Scheme 4.3: Geometries along OMC mechanism on (100) and (110) surfaces.
(M: light gray, O:red or dark gray, C: Black, H:cyan or gray).

For the different metals and surfaces studied in this work, the energy levels of the transition states are generally close to each other. However, the different stabilities of the precursor surface species cause the differences in the activation barriers of product

formations. For instance, the high stability of the OMC intermediate on copper surfaces results in very high barriers for EO and AA formations. On the contrary, less feasible OMC formation on gold surfaces results in the smallest barrier. However, on gold surfaces the dissociative oxygen adsorption is not feasible. These two effects make Cu and Au unsuitable catalysts for ethylene epoxidation. Since Ag is able to dissociate the oxygen molecule, and forms reaction intermediates with moderate energy levels silver is an optimum catalyst for ethylene epoxidation. Although slight shifts in selectivities are found, no conclusive result to relate the high EO selectivity to the metallic surface.

Table 4.2: Activation energies for the formation of EO and AA through OMC intermediate.

	E_{EO}^a	E_{AA}^a
	(kJ/mol)	(kJ/mol)
Cu(100)	154	144
Ag(100)	72	66
Au(100)	89	56
Cu(110)	198	171
Ag(110)	91	97
Au(110)	93	68
Cu(111)	142	157
Ag(111)	76	81
Au(111)	30	18

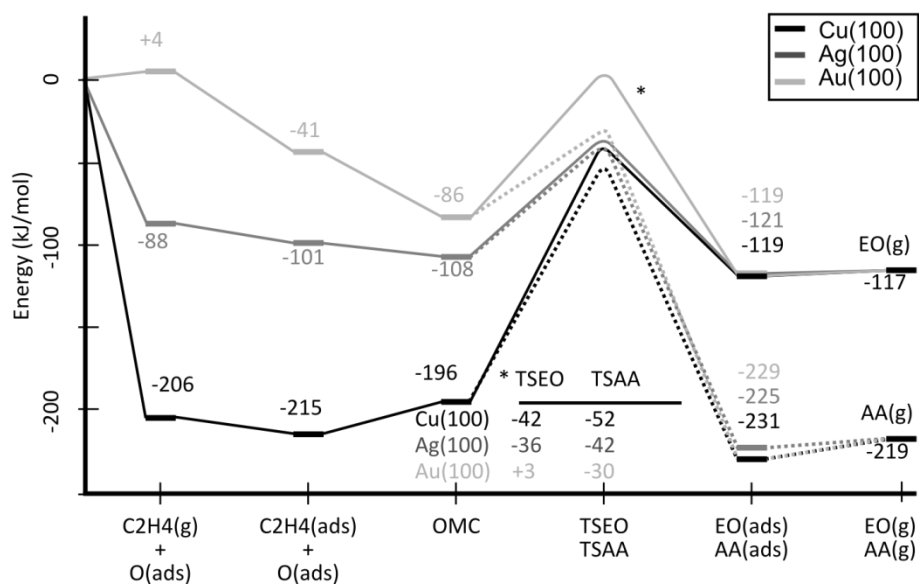


Figure 4.5: Relative energies of OMC paths on (100) surfaces of metallic Cu, Ag and Au at 1/4 ML oxygen coverage. After OMC intermediate solid lines represent the EO path and dashed lines represent the AA path. See Scheme 4.4 for geometries of stable points and transition states.

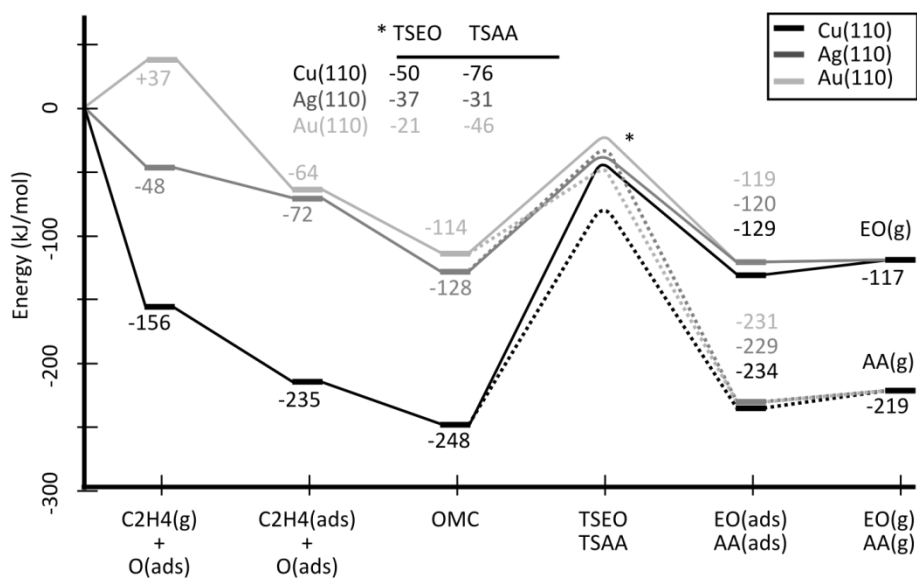


Figure 4.6: Relative energies of OMC paths on (110) surfaces of metallic Cu, Ag and Au at 1/4 ML oxygen coverage. After OMC intermediate solid lines represent the EO path and dashed lines represent the AA path. See Scheme 4.4 for geometries of stable points and transition states.

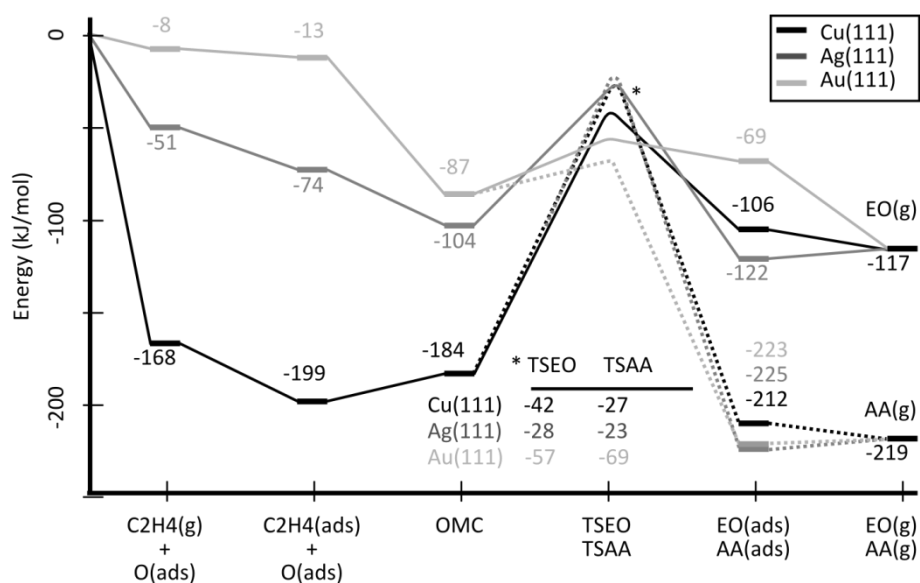


Figure 4. 7: Relative energies of OMC paths on (111) surfaces of metallic Cu, Ag and Au at 1/4 ML oxygen coverage. After OMC intermediate solid lines represent the EO path and dashed lines represent the AA path. See Scheme 4.2 for geometries of stable points and transition states.

4.1.3. Conclusions

This part of the study which focused on the formation of EO through the OMC mechanism for 11%, 25% and 33% oxygen coverages on the Ag(111) surface, and also compared the reactivities of the (100), (110) and (111) surfaces of metallic Cu, Ag and Au.

For the Ag(111) surface, oxygen adsorption on fcc sites were ~10 kJ/mol more exothermic than on the hcp site independent of oxygen coverage. For coverages of 33% and higher, ethylene adsorption on the metallic part of the Ag(111) surface cannot occur. For all the metallic surfaces and coverages, OMC formation occurs exothermically. For the different oxygen coverages on Ag(111) surface, the EO selectivity does not change.

When the (100), (110) and (111) surfaces of Cu, Ag and Au are compared, in general, the relative energies of the transition states for EO and AA formation are generally close to each other. For the different metals the activation barriers differ because of the different

stabilities of precursor OMC intermediate. Among these three metals, Cu gave the most stable surface intermediates, thus the highest activation barriers. On the contrary Au gave the least stable surface intermediates, thus the smallest activation barriers. In agreement with the conclusions of previous authors for the Ag surfaces, computational results predict ~50% EO selectivity in agreement with experimental observations for the un-promoted metallic silver [17, 21]. With the exception of the Cu(111) surface the Cu and Au surfaces have a lower selectivity than the Ag surfaces.

4.2. ETHYLENE EPOXIDATION ON SILVER OXIDE

The activity of the atomic surface oxygen, therefore, the nature of the surface has an important role on the selectivity. In the previous section it was shown that, for the metallic silver surfaces with low oxygen coverage, O_s prefers maximum coordination. As given in Table 4.3, threefold and fourfold hollow sites (i.e. triangular or rectangular surface lattice, respectively) are the preferred and most stable adsorption sites, depending on the surface lattice, whereas the adsorption energy of O_s is inversely proportional with surface coverage. Similar observations have been made in previous studies as well.

A relative comparison between the O_s charges is also given in Table 4.3. Compared to the $Ag_2O(001)$ surface, O_s on the metallic surfaces have a nucleophilic nature. This, and the strong adsorption of O_s on the metallic surface can explain why the minimum energy path of epoxidation follows initial adsorption of the ethylene and consequent formation of the OMC, through a Langmuir-Hinshelwood (L-H) mechanism, as reported in previous studies [10, 19, 21, 22, 75, 76, 79, 80].

For the metallic surfaces, as long as the oxygen coverage is kept monolayer, E_{EO}^a and E_{AA}^a are affected in a parallel and similar manner from the oxygen coverage. In other words, if the surface is kept metallic, increasing the coverage does not affect the selectivity of the products, nor the reaction channel. However, reduced activation barriers point towards an increase in the reaction rate.

Figure 4.8 shows the $\text{Ag}_2\text{O}(001)$ oxide surface studied in this work, where 2-fold (bridge) sites are the natural adsorption sites for the O_s , due to the O_{ss} in tetragonal positions. The low interaction energy of O_s that occupies bridge positions on the oxide surface suggests high reactivity towards epoxidation as a result of weak binding energy and electrophilic nature.

Bridging O_s on the oxide surface causes a totally different epoxidation path from the two-step OMC mechanism. As Figure 4.9 shows, O_s interacts directly with the $\text{C}=\text{C}$ double bond, resulting in the non-activated formation of EO through a Mars-van Krevelen [107] mechanism. This direct reaction path does not include an intermediate such as OMC. Gas phase ethylene directly reacts with O_s where $\text{EO}_{(\text{ads})}$ forms directly releasing 174 kJ/mol energy. Consequent desorption of $\text{EO}_{(\text{ads})}$ requires 73 kJ/mol, which gives the overall heat of the epoxidation reaction as -101 kJ/mol.

From Figure 4.9 it can be seen that, the activation energies of the rate controlling steps in both reaction mechanisms (i.e OMC vs. direct) are similar and agree with experimentally reported values that are around 70 kJ/mol [9, 108, 109]. However, it should be stressed that the corresponding reaction steps that go through a barrier are different (i.e. OMC activation versus EO desorption). It should also be noted that, on the oxygen covered oxide surface ethylene cannot directly interact with the silver surface ions, thus no OMC intermediate forms. This prevents C-H bond activation, therefore AA formation.

Table 4.3: Calculated adsorption energies (E_{ads}), sites and charges of surface atomic oxygen; paths and the activation barriers for EO (E_{EO}^a) and AA (E_{AA}^a) formation for the listed surfaces and oxygen coverages (θ_o)

Surface	θ_o (ML)	E_{ads}^a (kJ/mol)	Ads. site (n-fold)	Charge ^a		Path	E_{EO}^a	E_{AA}^a
				O	Ag			
Ag(111) ^b	0.11	-50.7	3	-0.9	+0.2	OMC	74	79
Ag(111) ^b	0.25	-42.0	3	-0.9	+0.2	OMC	57	56
Ag(111) ^b	0.33	-37.4	3	-0.8	+0.3	OMC	48	47
Ag(111)[10]	0.25	-62.7	3	-	-	OMC	77	70
Ag(111) [10]	-	-	-	-	-	OMC	70	72
Ag(111)[19]	0.25	-31	3	-	-	OMC	63	-
Ag(100)	0.25	-88.0	4	-0.9	+0.2	-	-	-
Ag(100)	0.50	-73.6	4	-0.9	+0.4	-	-	-
Ag(100)[19]	-	-	-	-	-	OMC	88	98
Ag(110)	0.25	-63.0	4	-0.9	+0.1	-	-	-
Ag(110)[22]	0.5	-	2	-	-	OMC	76	-
Ag ₂ O(001)	0.50	-15	2	-0.7	+0.6	Direct	73 ^c	-
Ag ₂ O Bulk	-	-	-	-1.0	+0.5	-	-	-

^a Charge calculated by Bader analysis [105]. For supercells with more than one oxygen, average charge is reported. Average charge of Ag atoms neighboring the surface oxygen is reported.

^b For Ag(111) surface only 3-fold fcc sites are considered.

^c This E_a actually shows the desorption energy of EO from the surface.

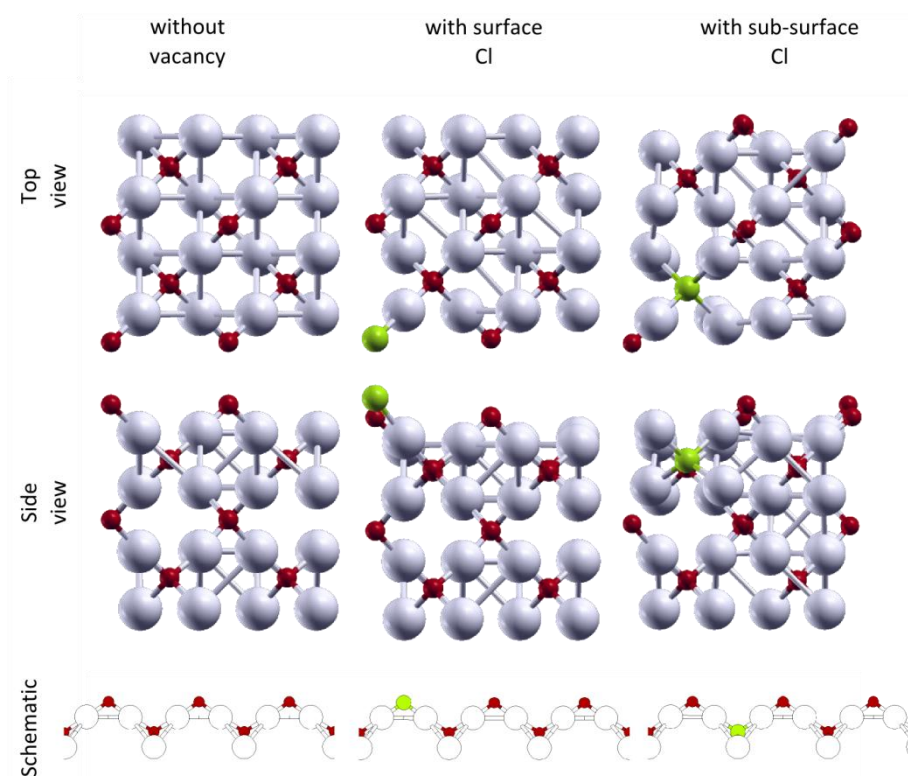


Figure 4.8: Representations for the $\text{Ag}_2\text{O}(001)$ surface used in the calculations. (Ag: gray, O: red, Cl: green)

However, when there is an oxygen vacancy on the oxide surface, the two $\text{Ag}^{\delta+}$ ions are exposed to the vacuum. These Ag ions hold larger (+) charge compared to those of the metallic surface (Table 4.3). O_{ss} causes this relatively strong charge on the Ag ions of the oxide surface. Ethylene interacts easily with these $\text{Ag}^{\delta+}$ ions, which results in the exothermic adsorption of ethylene (-85 kJ/mol) on this oxygen vacancy.

As shown in Figure 4.10, following its adsorption, ethylene interacts with a neighboring O_s through a non-activated process. This interaction results in an OMC formation, releasing 75 kJ/mol. The OMC formed on the oxide surface is significantly more stable compared to the OMC formed on the metallic surface (i.e. -160 kJ/mol v.s. -52 kJ/mol). Here again, decomposition of the OMC produces EO as well as AA, this time with a lower barrier towards AA formation. The significantly lower activation barrier for non-selective path shows that once OMC is formed, the EO selectivity will be lower compared to the metallic surface.

These results agree with the previous experimental reports [51] where initial and selective production of EO is followed by AA production as the O_s are consumed. The initial and highly selective production of EO removes the surface oxygens, which causes O-vacancy formation on the surface. Ethylene adsorption on the oxygen vacant surface sites opens the non-selective reaction path. In order to maintain high EO selectivity rapid silver oxidation should occur, while the O-vacancies are being blocked or suppressed.

Formation of non-selective product, acetaldehyde, through OMC mechanism also explains the increase in the EO selectivity when deuterated ethylene is used [15]. Substitution of hydrogen with deuterium has a rate-decreasing effect on the non-selective path during H-transfer reaction, as explained in a previous work [82].

The dependence of the EO selectivity on particle shape [10, 21] and its decrease with particle size [70] can be explained with the O-vacancy concentration as well. In the smaller particles, the lower selectivity can be explained by the presence of higher fraction of edge and corner sites where bridging O_s does not exist. Furthermore, the increased vacancy concentration would favor the OMC formation and reduce the selectivity. The shape dependence on the other hand, may stem from the ease of oxygen diffusion to sub-surface layers, therefore ease of surface oxidation that would supply bridging oxygens.

Previous studies [42, 46, 110] testing oxide like surfaces (i.e. $Ag_{1.83}O$ surface oxide) used the oxidized Ag(111) surface models. Apart from the validity of the models (different models have been proposed for the Ag(111) surface oxide) the common point in these models was the O_s occupying the 3-fold sites on the surface. Due to these strongly adsorbed O_s , and available Ag atoms on the surface, the studies resulted in the EO/AA formation through OMC intermediate.

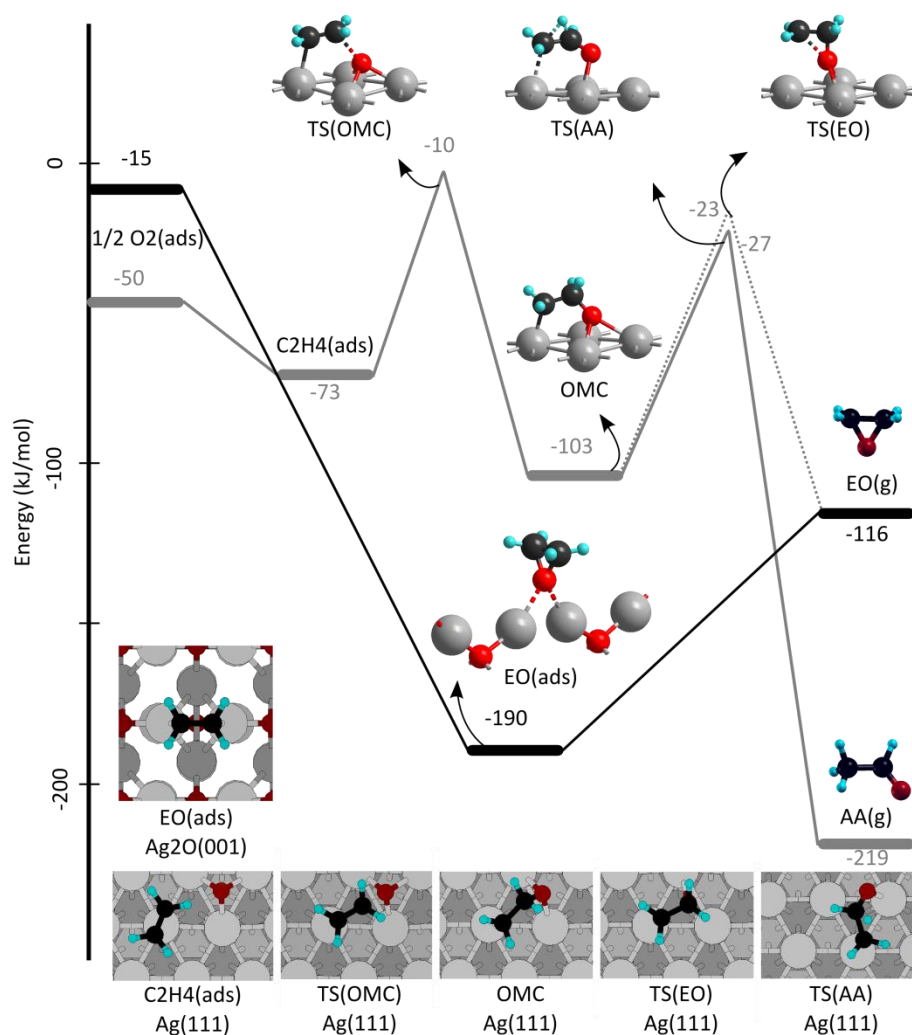


Figure 4.9: Reaction energy diagrams. The EO and AA formation path through OMC intermediate on Ag(111) surface (gray) and the direct EO formation path on Ag₂O(001) surface (black line). Bottom figures represent the top views of the reaction intermediates. The energies are given with respect to (surface + ½ O_{2(g)} + C₂H_{4(g)}). (Ag: gray, O: red or dark gray, C: black, H: cyan or light gray)

Figure 4.11 compares the possible paths following the EO formation on the surface. Considered paths are the desorption of the EO_(ads) to gas phase, EO isomerization to AA (i.e. H-transfer), and the cleavage of O-C bond.

Among these paths, EO isomerization to AA requires a very high barrier (~ 150 kJ/mol), which is substantially higher than the energy requirement for desorption. However, the

energy required for the O-C bond activation is comparable with the desorption energy. Moreover, this ethylenoxy type intermediate is identified as a stable geometry. This intermediate enables rotation of the CH₂ group and explains the cis-trans isomerization, as observed in experimental studies [111, 112]. The formation of this surface species is exothermic by 88 kJ/mol with respect to C₂H_{4(g)} and hence of comparable energy to the EO desorption energy. The competing energies of desorption v.s. isomerization is in agreement with the equal distributions of cis and trans isomers.

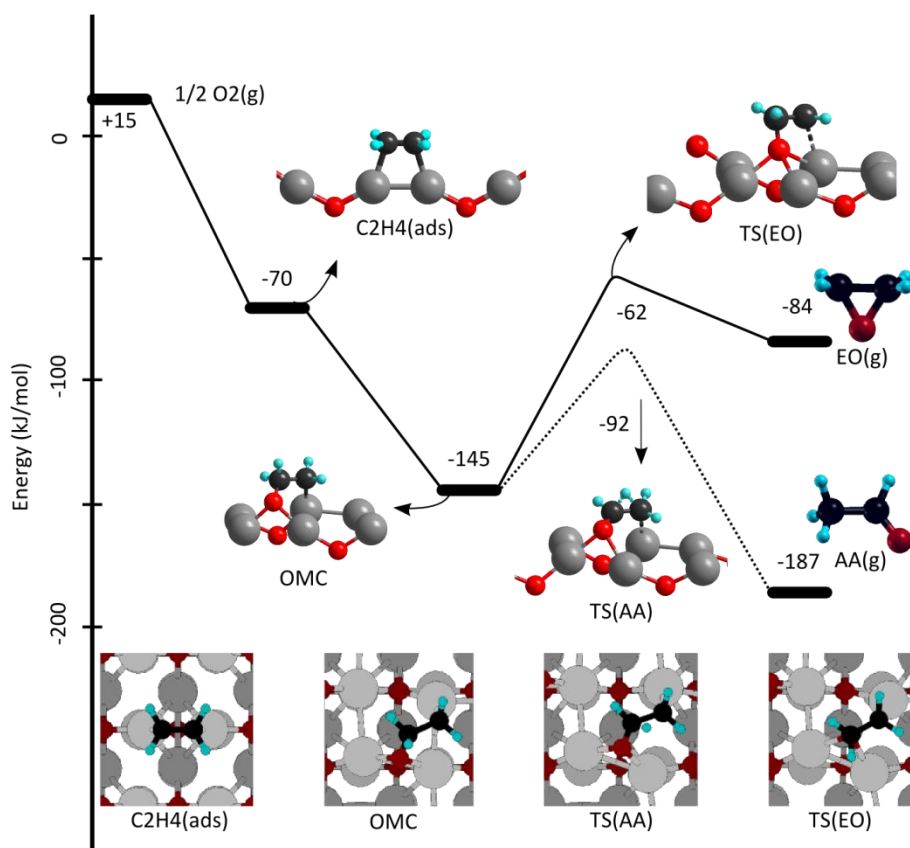


Figure 4.10: Formation of EO (solid line) and AA (dashed line) through OMC intermediate on Ag₂O(001) surface with an O-vacancy. Bottom figures represent the top views of the reaction intermediates. The energies are given with respect to (surface + C₂H_{4(g)}). (Ag: gray, O: red or dark gray, C: black, H: cyan or light gray)

These results show that the key to high EO selectivity is the necessity of O_s in bridge positions and absence or the suppression of the vacant sites, where C-H activation (i.e. AA formation) occurs.

Molecular adsorption of O_2 and C_2H_4 on this vacancy is both exothermic for both by -20 and -85 kJ/mol respectively. The dissociative adsorption of O_2 on the O-vacant surface depends on the existing O_s coverage. For example, when the θ_O increases from 0.25 to 0.50, the value is -32 kJ/mol, whereas it is -62 kJ/mol when the θ_O increases from 0 to 0.25, which is comparable with the metal case [40].

The adsorption of Cl atom on the same vacancy is highly exothermic by -185 kJ/mol, when calculated with respect to $Cl_{2(g)}$. Hence the most likely role of Cl in the epoxidation reaction is to block the vacant sites next to reactive oxygen, as proposed in an early study [29-31]. On oxide surfaces the stronger Cl-Ag, interaction, compared to O-Ag and/or C_2H_4 -Ag, will reduce the concentration of surface vacancies and suppress OMC formation, resulting in the inhibition of the non-selective path.

When a surface O-vacancy is blocked by a Cl atom, it does not change the reaction channels of ethylene and has small effect on the energies. These energies are listed in Table 4.4. In the presence of a Cl atom, the change in the energies of direct EO formation, and EO desorption are less than 5 kJ/mol. However, when a subsurface O atom is replaced by a Cl atom (as in the case of sub-surface Cl diffusion [113]) the change in energies is significant. In this case, the reactive surface oxygen and sub-surface chlorine atom share a common silver atom (Figure 4.8). This configuration weakens O_s interaction energy, and increases the energy of the EO formation on the surface. However, the weak Ag- O_s interaction energy in case subsurface Cl present indicates that, diffusion of Cl into the sub-surface layers (i.e. replacement of O_{ss} with Cl) is a probable scenario for catalyst poisoning. In this scenario subsurface Cl would prevent O_s regeneration, and result in oxygen vacant sites on the surface. The energy changes in the presence of surface and subsurface Cl atom are listed in Table 4.4.

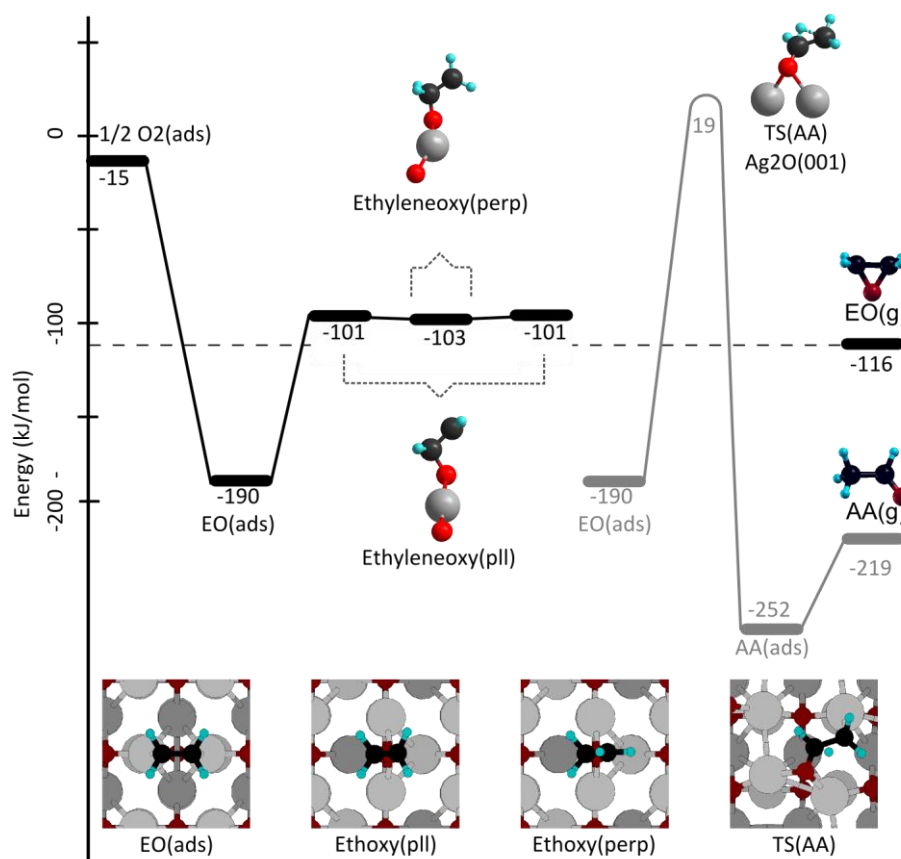


Figure 4.11: CH₂ rotation (black line) and AA formation (gray line) through EO_(ads) on Ag₂O(001) surface. Bottom figures represent the top views of the reaction intermediates. The energies are given with respect to (surface + C₂H_{4(g)}).

For an O-vacancy on the Ag₂O(001) surface, the exothermicity of the adsorptions follows the order Cl>>C₂H₄>O₂. However, if O₂ adsorbs molecularly, ethylene may interact with O_{2(ads)} to form an unstable surface complex in the form of Ag-O-CH₂-CH₂-O-Ag. In order to form this unstable complex, the intermolecular bonds of O₂ open to form two O-CH₂ bonds. This unstable intermediate directly decomposes without facing a barrier. The resulting species are two adsorbed formaldehydes (Ag-O-CH₂). When calculated with respect to O_{2(ads)} and C₂H_{4(g)}, the formation of the formaldehydes is quite exothermic by -867 kJ/mol. However, the unfeasible initial adsorption of O₂ prevents this path; on the other hand, this path explains the small amounts of formaldehyde formation observed [114].

Table 4.4: Cl effect on the reaction energies (in kJ/mol) for the reactions on Ag₂O(001) surface.

	Without Cl	Surface Cl	Sub-surface Cl
O _s adsorption (w.r.t. ½ O _{2(g)})	-15	-10	+32
EO formation	-174	-179	-207
EO desorption	+73	+68	+59

4.2.1. Conclusions

This part of the study demonstrated the existence of a possible reaction mechanism for EO formation that is different from the OMC path. The demonstrated path occurs on an oxide phase as a result of weakly bound 2-fold surface oxygens. As long as no surface vacancies are present, EO is produced selectively. In this direct reaction path, there is no competitive formation of AA. Oxygen vacancies favor the non-selective path through OMC formation. The effect of the Cl-promoter is to block these vacancies and prevent non-selective path.

Experimentally observed cis-trans isomerization during ethylene epoxidation is also explained by the defined stable ethyleneoxy intermediates

4.3. ETHYLENE EPOXIDATION ON METAL OXIDES

The previous sections have shown that the electrophilic nature of bridging oxygen atoms on the Ag₂O(001) surface makes them very selective for the epoxidation reaction, and demonstrated the possibility of a direct epoxidation pathway that proceeds through a low activation energy. This is different from the OMC mechanism that takes place on three or four coordinated oxygen atoms with nucleophilic nature adsorbed on the metallic Ag surfaces.

This section presents a comparison between the reactivities of the Cu₂O, Ag₂O and Au₂O oxide surfaces. Having the same crystal structure, herein studied (001) surfaces contain oxygen atoms in bridge positions. The reaction paths that were previously identified for Ag₂O(001) surface are tested for Cu₂O(001) and Au₂O(001) surfaces and compared. Among these three oxide structures Au₂O is known to be unstable. Yet, it presents an interesting case for the comparison.

4.3.1. Oxide Structures

The formation energies of the bulk oxides from their respective bulk metals are listed in Table 4.5. The energies are calculated with respect to the reaction:

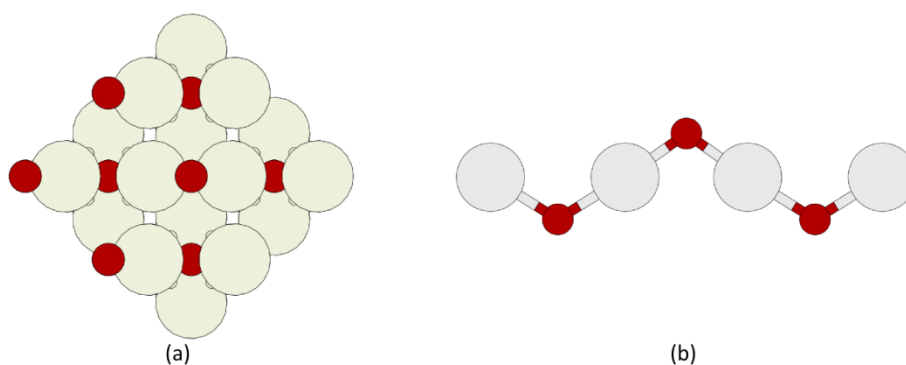


As Table 4.5 shows, the formation of the oxides gets less favorable downwards the periodic table. Formation of Au₂O structure is endothermic. However, since it has the same crystal structure as Ag₂O and Cu₂O, the Au₂O(001) surface was evaluated for comparison as well.

Table 4.5: Calculated heats of formation for bulk oxides and reference values. The energies are given in kJ/mol.

Oxide	ΔH_f	ΔH_f^0 (ref)
Cu ₂ O	-134	-169 [99]
Ag ₂ O	-39	-31 [99]
Au ₂ O	+21	+22 [35]

A schematic representation of the studied M₂O(001) surfaces is given in Scheme 4.4: Schematic representation of the studied M₂O(001) surfaces. (a) Top view, and (b) side view of M₂O chain. Gray (light) and red (dark) colored circles represent the metal and oxygen atoms respectively.. As can be seen, each surface model (i.e. slab) has four O_s in 2-fold bridge positions. Removal of these oxygens creates oxygen vacancies on the surface where metal atoms are exposed to vacuum. As explained in previous section, because of the subsurface oxygen atoms, these surface metal atoms are more positively charged (M^{δ+}) compared to their respective metal surfaces. Thus, this oxygen vacancy is a suitable site for O₂ and C₂H₄ adsorption.



Scheme 4.4: Schematic representation of the studied M₂O(001) surfaces. (a) Top view, and (b) side view of M₂O chain. Gray (light) and red (dark) colored circles represent the metal and oxygen atoms respectively.

4.3.2. Oxygen Adsorption

Figure 4.12 compares the adsorption energies of oxygen on the respective oxide surface following the complete removal of the surface oxygen layer (i.e. 4 O_s). When all O_s are removed, the surface shifts to a more metallic nature. At 25% coverage the oxygen adsorption energy is the highest and rapidly converges as the full coverage is achieved. As shown in section 4.1, for the metallic surfaces, the adsorption energies decrease downward the periodic table. The reported oxygen adsorption energies are ~ 150 kJ/mol for Cu [79], ~ 50 kJ/mol for Ag [79], and ~ 10 kJ/mol for Au [83]. As **Table 4.6** shows, this trend can only be seen for the adsorption energies of the molecular oxygen, however, not for dissociative adsorption. An interesting result is that, the atomic (single O-vacant) and dissociative (2 O-vacant) oxygen adsorption on Au_2O surface is more exothermic than adsorption on Ag_2O surface. This finding can be considered to be parallel with a previous study [14], which concluded that the existence of pre-adsorbed atomic oxygen on Au surface favors O_2 dissociation. Furthermore, in case of Au_2O , the larger separation between the metal atoms induces chemical interactions comparable to that of the isolated atoms more than for the metal surface. For instance atomic covalent bonds to a Au atom tend to be stronger than to Cu or Ag (for ex. [115]).

The third column of Table 4.6 lists the adsorption energies of C_2H_4 molecule on an oxygen vacancy (see Figure 4.14). When a single O-vacancy is considered, it can be seen that ethylene adsorption will be favored over molecular O_2 adsorption on Ag_2O and Au_2O surfaces. Previously we reported that the reaction of adsorbed ethylene with surface oxygen leads to formation of OMC on the vacant Ag_2O surface and competes with the direct epoxidation. Decomposition of OMC has then also a lower barrier for AA formation (non-selective path) (Figure 4.14). The direct selective epoxidation path on Ag_2O has been found to only occur, because OMC formation is prevented. Thus, the absence of surface oxygen vacancies is important to have high EO selectivity. Therefore, rapid generation of the surface oxygens or the site blocking effect of a promoter (i.e. Cl) are essential for the sake of EO selectivity [116].

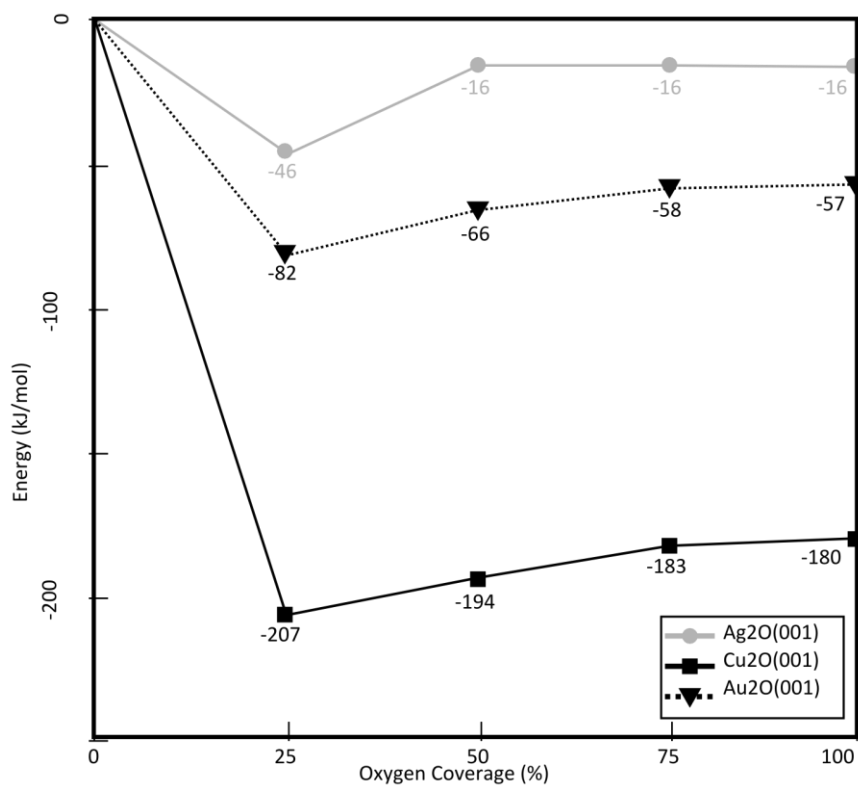


Figure 4.12: Oxygen adsorption energies on M₂O(001) surfaces at varying coverage. The energies are calculated with respect to half of the gas phase O₂ energy ($\frac{1}{2}$ O_{2(g)}).

Table 4.6: Adsorption energies (kJ/mol) of O₂ and C₂H₄ on O-vacant surface sites.

	Molecular O ₂ adsorption*	Dissociative O ₂ adsorption**	C ₂ H ₄ adsorption
	(-Ag-O-O-Ag-)	2x(-Ag-O-Ag-)	(-Ag-CH ₂ -CH ₂ -Ag-)
Cu ₂ O	-122	-363	-123
Ag ₂ O	-20	-32	-86
Au ₂ O	-11	-116	-106

* O_{2(g)} + V* --> O_{2(ads)}

** O_{2(g)} + 2V* --> 2O_s

4.3.3. Direct Epoxidation

When ethylene is prevented to interact with the surface metal atoms ($M^{\delta+}$) (i.e. no O-vacancy, or site blocker), reaction of the $C_2H_{4(g)}$ and O_s results in the direct formation of EO through a Mars van Krevelen [107] type mechanism as shown in Figure 4.13. When $C_2H_{4(g)}$ approaches the surface, it interacts with the O_s to form $EO_{(ads)}$ through a single step reaction. There is no intermediate OMC formation. Among the three oxide surfaces considered, only on Ag_2O reaction proceeds without a barrier. Other two surfaces show small barriers for the interaction of $C_2H_{4(g)}$ and O_s . The $Au_2O(001)$ surface appears to have the highest reactivity for EO formation. In essence, because of the weaker interaction energy of EO with the single O vacant Au_2O surface. On the other hand, formation of EO on $Cu_2O(001)$ surface is endothermic. This finding for Cu is in parallel with a previous report for metallic Cu surface[79], which was also confirmed in this study.

When the OMC mechanism, as reported for metallic surfaces, and the direct mechanism on $Ag_2O(001)$ surface are compared, it can be seen that the activation energies of the rate controlling steps in both reaction mechanisms (i.e. OMC vs. direct mechanism) are similar and agree with experimentally reported values that are around 70 kJ/mol [108, 109]. However, the corresponding reaction steps are different (i.e. OMC activation vs. EO desorption). The rate controlling step of the direct mechanism is the EO desorption. The order of EO desorption energies follow the relative stability of the oxides (i.e. oxygen binding energies). Desorption of the epoxide to be rate limiting is consistent with the observed low reaction order in ethylene but a high reaction order in oxygen [117]. Furthermore, the reported [118] increase of the EO selectivity with the increasing oxygen coverage, is also consistent with the preference for EO formation on an oxidized Ag surface in this manner.

4.3.4. Oxygen vacancy and OMC formation

In the case of an O-vacancy, ethylene interacts with the surface metal atoms and adsorbs on this O-vacant site. Figure 4.14 compares the elementary reactions that follow ethylene adsorption. Once adsorbed, the ethylene molecule may interact with a neighboring O_s and form the OMC intermediate. This reaction proceeds through small barriers on Cu_2O and

Au₂O; and without a barrier on Ag₂O. Once this OMC intermediate is formed, the reaction may proceed through selective or non-selective channels, as reported for metallic surfaces. However, for all the oxides studied, the formation of AA through the OMC intermediate has lower barrier compared to that of EO. Thus, following the ethylene adsorption, the OMC mechanism predicts preferred formation of AA, which gives a rapid total combustion.

Table 4.7 compares the activation energies along the OMC path. Starting from OMC intermediate, both forward and backward reactions are considered. Forward reactions produce EO and AA through selective and non-selective channels. In the backward reactions OMC decomposes to produce ethylene and surface oxygen.

Figure 4.14 and Table 4.7 show that, only on Ag₂O and Au₂O forward reactions are more feasible than backward reaction. On Cu₂O surface, besides being highly stable on the surface, OMC would probably go back to adsorbed ethylene due to lower activation barrier in the backward direction. On Ag₂O and Au₂O, once formed OMC would either produce EO or AA.

4.3.5. EO isomerization

In order to successfully obtain EO as the product, it has to desorb unreacted from the surface. Upon its formation on the oxide surface, three possible follow up paths are considered. These are, i) desorption, ii) ring opening, and iii) isomerization to AA. The relative energies of these paths are compared in Figure 4.15.

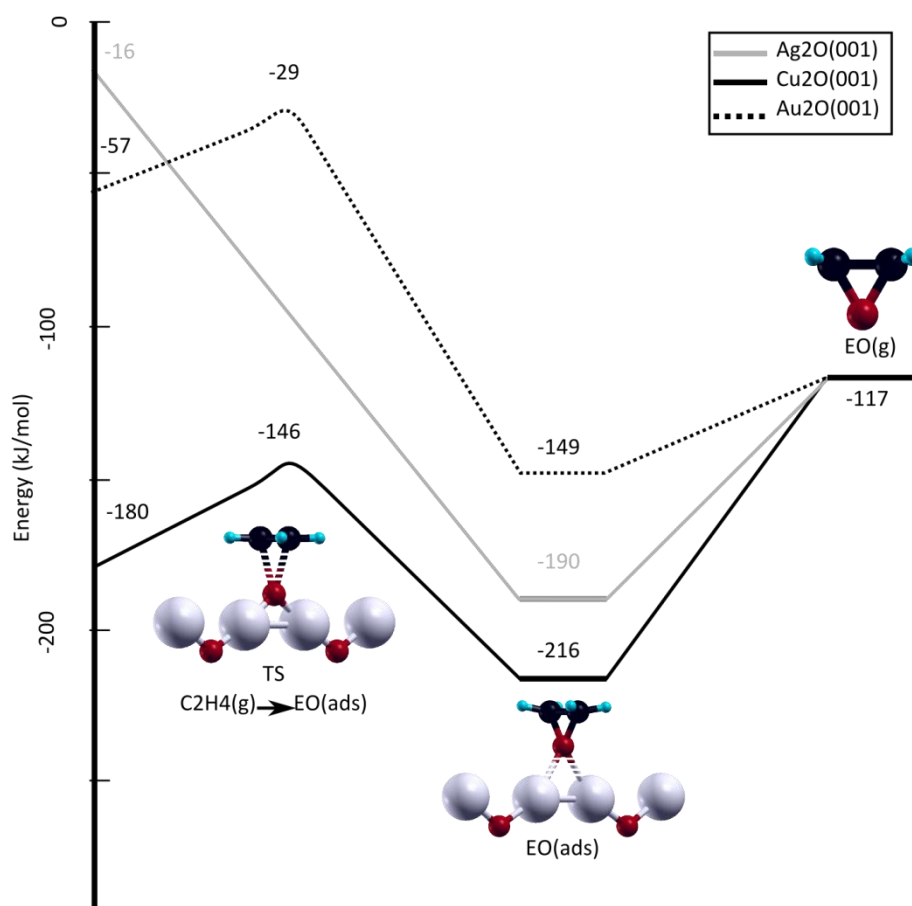


Figure 4.13: Energetics of direct epoxidation paths on $M_2O(001)$ surfaces. Initial points correspond to the oxygen adsorption energies on a vacant surface site that saturates the surface¹.

¹ In Figure 6.3, the transition states (TS) reported for the direct epoxidation paths could not be verified with frequency calculations, thus they should be considered as approximate. However, to get the most precise value all the images along the reaction path were relaxed until the convergence criteria ($F_{net} \leq 0.015 \text{ eV/\AA}$) was strictly reached. For the geometries corresponding to these peaks C_2H_4 is not completely surface bound. Thus, frequency calculations do not produce single imaginary frequency as it should be for a TS geometry. In these results, two more imaginary frequencies exist for translation and rotation.

Table 4.7: Computed and zero point corrected values for the activation barriers. For the considered forward and backward reactions, OMC is the starting intermediate. Energies are in kJ/mol.

	E^a_{OMC}		E^a_{EO}		E^a_{AA}	
	Comp.	ZPC	Comp.	ZPC	Comp.	ZPC
Cu ₂ O	63	57	206	203	158	146
Ag ₂ O	75*	75*	83	82	53	46
Au ₂ O	140	133	75	68	102	89

* E^a_{OMC} for Ag₂O(001) corresponds to the energy required to desorb ethylene from the surface. See Figure 4.14.

The horizontal line in Figure 4.15 (117 kJ/mol) shows the energy level of desorbed EO. The left part of the figure shows the formation of ethyleneoxy intermediate through ring opening of adsorbed EO. Starting from EO_(ads), when one of the O-C bonds activate, first ethyleneoxy_(pll) intermediate forms where the H atoms of the free CH₂ group stays parallel to the surface plane, and then they become perpendicular to the surface with the rotation. This kind of a ring opening and rotation of CH₂ group explains the cis-trans isomerization observed in experimental studies [111, 112]. Ethyleneoxy_(perp) intermediate would go back to EO_(ads) following the same path backwards. The similar energies required for EO isomerization and desorption on Ag₂O(001) surface can explain the equal distributions of cis and trans isomers as observed in experimental studies.

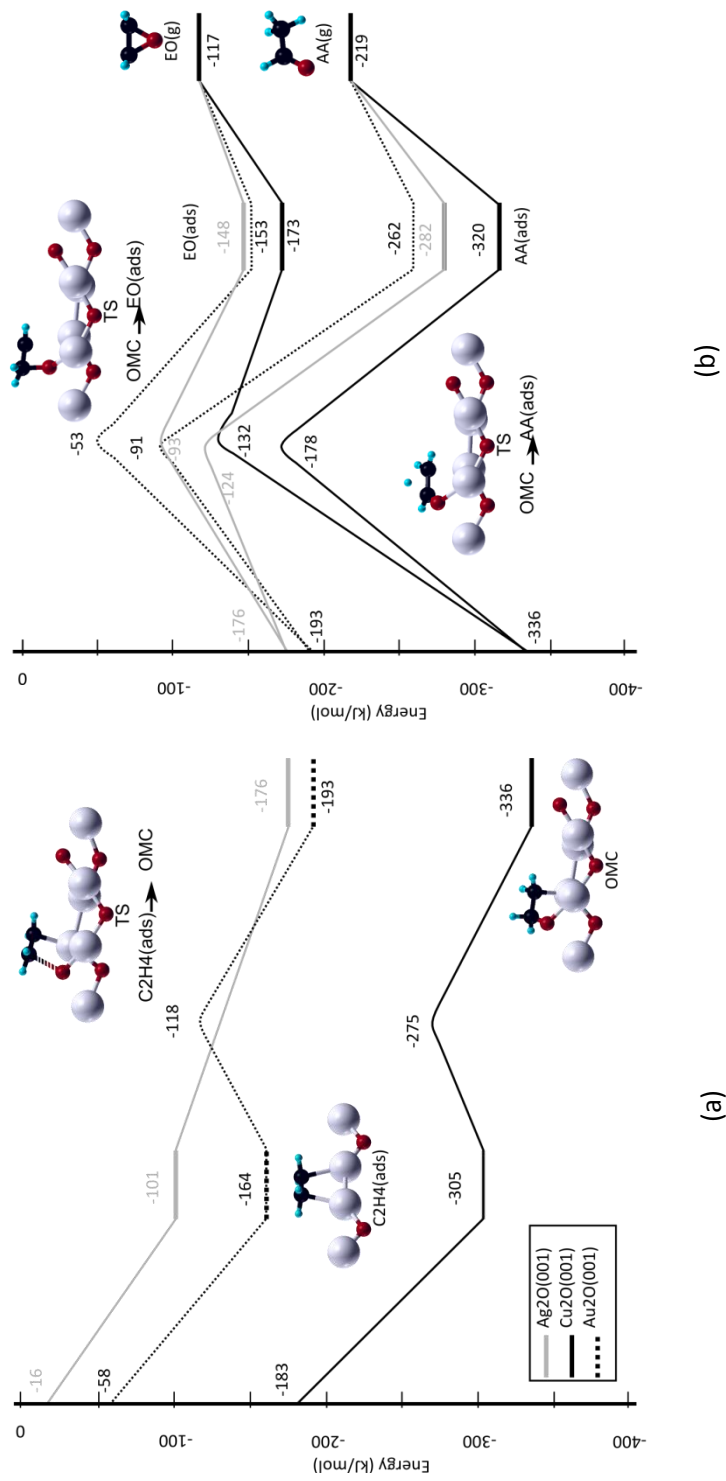


Figure 4.14: (a) Energetics of the formation of the OMC intermediate on an oxygen vacancy, and (b) formation of EO and AA from OMC intermediate. Initial points correspond to oxygen adsorption that shifts the surface coverage to 75%.

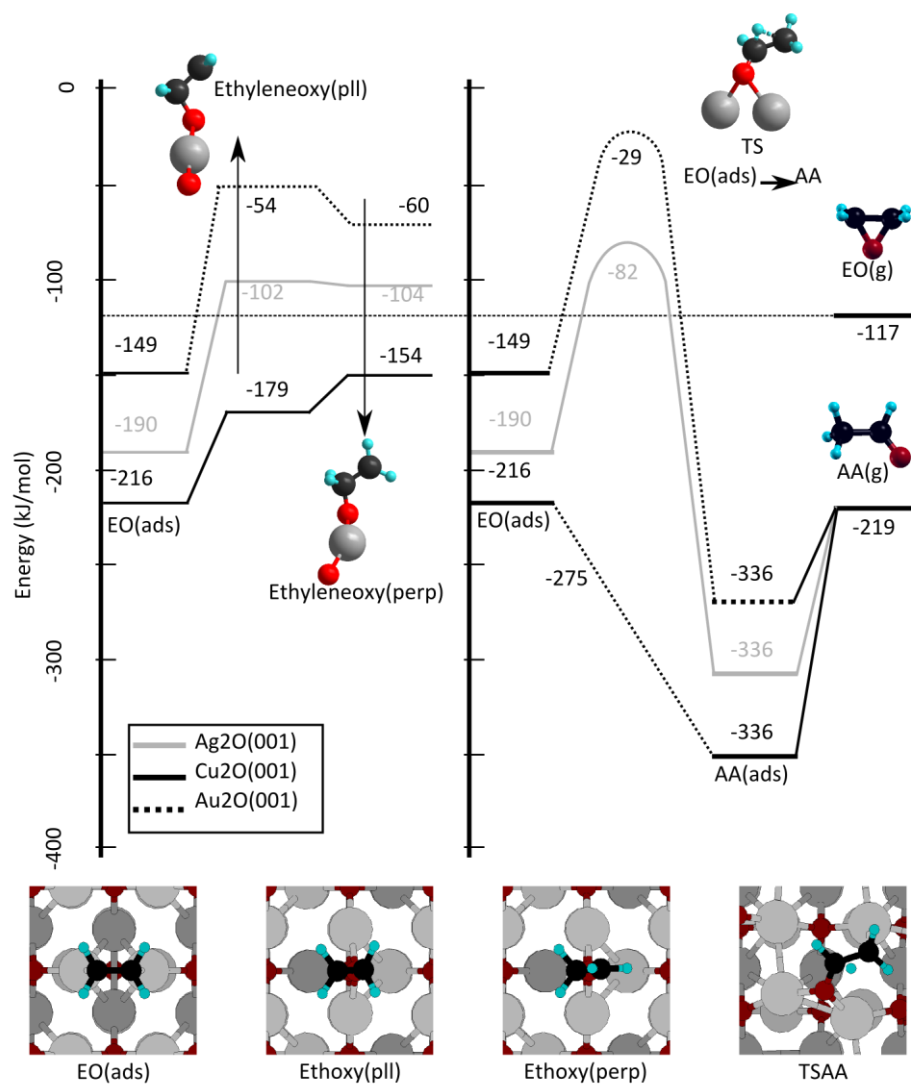


Figure 4.15: Comparison of the energy changes of reaction paths following EO formation. Adsorbed EO may i) desorb, ii) isomerize to ethyleneoxy intermediate, or, iii) isomerizes to AA.

Right part of Figure 4.15 shows the EO isomerization to AA starting from EO_(ads). On Ag₂O and Au₂O surfaces, this isomerization goes through respective activation barriers, which are substantially higher than EO desorption. This indicates that EO desorption will be the preferred path instead of AA formation. On Cu₂O however, isomerization of EO to AA is quite exothermic and does not have a barrier. Thus, although direct formation of adsorbed EO on Cu₂O surface is more exothermic compared to other surfaces, the overall

reaction is non-selective because of rapid EO isomerization to AA makes. Also, giving the most exothermic EO formation, Cu₂O surface has the highest EO desorption energy.

4.3.6. Conclusion

This section aimed to computationally analyze the epoxidation selectivity of ethylene on highly oxygenated metal surfaces. For ethylene epoxidation, highly oxidized catalyst surface has been suggested to be selective, however a conclusive model of the Ag surface at the epoxidation conditions does not exist. Thus, in this study the reactivities of well defined Cu₂O(001), Ag₂O(001) and Au₂O(001) oxide surfaces were explored towards ethylene epoxidation. The relative stabilities and the oxygen binding energies of these compounds decrease downwards the periodic table. The Au₂O structure is not a stable oxide structure, but having the same crystal structure with Ag₂O and Cu₂O it presents an interesting case for comparison. For the three M₂O(001) surfaces studied, a direct epoxidation channel has been found to exist with a low or no barrier.

Non-selective AA formation is only found to compete with EO formation on the Cu₂O surface. This is essentially due to the relatively weak O-C bond interaction and the high desorption energy of EO.

The OMC intermediate is formed on O-vacant surface sites. For all three surfaces studied, the barrier for AA formation through the OMC intermediate was found to be lower than that of EO formation. The Cu₂O(001) surface gave the most exothermic OMC formation and the highest consequent EO and AA barriers. The Ag₂O(001) and Au₂O(001) surfaces show more moderate energy values along the OMC mechanism.

Au₂O(001) is not a stable structure, and, Cu₂O(001) does not favor the EO formation. The intermediate value of Ag₂O's stability and its oxygen bond strength between Au₂O and Cu₂O relate the uniqueness of the silver catalyst for ethylene epoxidation. The interaction of Ag₂O(001) surface with O₂ is strong enough to re-oxidize the Ag surface to the oxide, and also weak enough to prevent the ring opening of EO as well as to prevent the activation of the CH bonds.

An additional prerequisite for high selectivity is the absence of O-vacancies that enable OMC formation. Most likely this is the moderating role of Cl that is added to the catalyst as promoter.

The ethyleneoxy intermediate is found to be possible for all studied oxides. However, the cis-trans isomerization of EO is only feasible on $\text{Ag}_2\text{O}(001)$ surface. On the other hand, the $\text{Cu}_2\text{O}(001)$ surface is found to isomerize the formed EO to AA.

4.4. DIRECT OMC

As it is shown in the previous section, direct EO formation is a feasible path for the unreconstructed $\text{M}_2\text{O}(001)$ type surfaces. EO forms on the surface through a single step reaction, with the symmetric attack of the electrophilic oxygen to the electron rich C=C double bond. On the other hand, ethylene interaction with an O-vacant surface site results in the ethylene adsorption with a geometry that resembles di-sigma adsorption ($\text{M}-\text{CH}_2-\text{CH}_2-\text{M}$). The adsorbed ethylene on the surface interacts with neighboring oxygen to form the OMC intermediate, which has a lower barrier for AA formation.

However, our simulations show that ethylene interaction with the surface may induce a local reconstruction on the $\text{M}_2\text{O}(001)$ surface that creates a surface metal atom that is available for OMC formation. The adsorption of ethylene in this manner creates a possibility of *direct OMC* formation through a single step non-activated process.

Formation of direct OMC is possible with the prerequisite of reconstruction. As Figure 4.16 shows, this reconstruction causes the displacement of one oxygen and two metal atoms (highlighted area). As arrows indicate in Figure 4.16, these three atoms that are initially located at the parallel M-O-M rows get closer to form a site where the oxygen adsorption becomes three-fold. This configuration resembles the metallic (111) surfaces or surface oxide structures [44, 46, 119] of metal surfaces highly covered by atomic oxygen. For the $\text{Ag}_2\text{O}(001)$ surface, this configuration destabilizes the surface by 18 kJ/mol, but makes highly exothermic direct OMC formation possible.

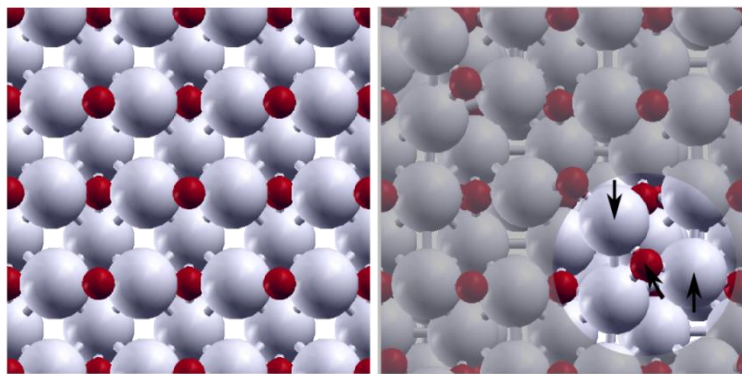


Figure 4.16: Un-reconstructed $M_2O(001)$ surface (left) and the local reconstruction (right). The displaced atoms are highlighted and the directions of the movements are shown with arrows. (Gray: metal atoms and, red: oxygen)

Unlike the direct EO path that requires a single Ag-O-Ag row, formation of the direct OMC intermediate requires a larger ensemble of surface atoms, and an endothermic surface reconstruction. However the nature of the electrophilic surface oxygen that is included into the OMC ring does not change. Thus, what makes this OMC configuration possible is the change of the surface metal atoms.

As Figure 4.17 shows, the reactive adsorption of ethylene to form OMC on the reconstructed site is exothermic for all studied $M_2O(001)$ surfaces. When compared with the direct EO formation on $Ag_2O(001)$ surface ($\Delta H_{rxn} = -190$ kJ/mol), OMC formation is ~ 50 kJ/mol more exothermic.

Once formed on the surface, the OMC forms EO and AA competitively, as in the case of metal surfaces and/or O-vacant oxide surfaces. However, for the direct OMC formed on the $Ag_2O(001)$ surface, the difference in E_{EO}^a and E_{AA}^a activation energies points to a more favored EO production. For $Cu_2O(001)$ and $Au_2O(001)$ surfaces, this is not observed. The increased EO selectivity of OMC intermediate on $Ag_2O(001)$ surface agrees with the suggestions that the higher epoxidation selectivity relates to the presence more weakly bound (electrophilic) oxygen [36, 37, 68, 72]

The difference in the activation barriers is caused by the fact that ethylene is less activated. That is, in the *direct OMC* configuration ethylene does not give the exact di-

sigma adsorption geometry. Rotation of the CH₂ groups around the single-bond axis is less, compared to other OMC structures, where C atoms have tetragonal configurations. Thus the planar ethylene geometry is less deformed. Since the geometry stays more similar to EO and/or ethylene, H-transfer becomes harder, which causes the increase in the activation barrier for AA formation, and EO formation becomes easier.

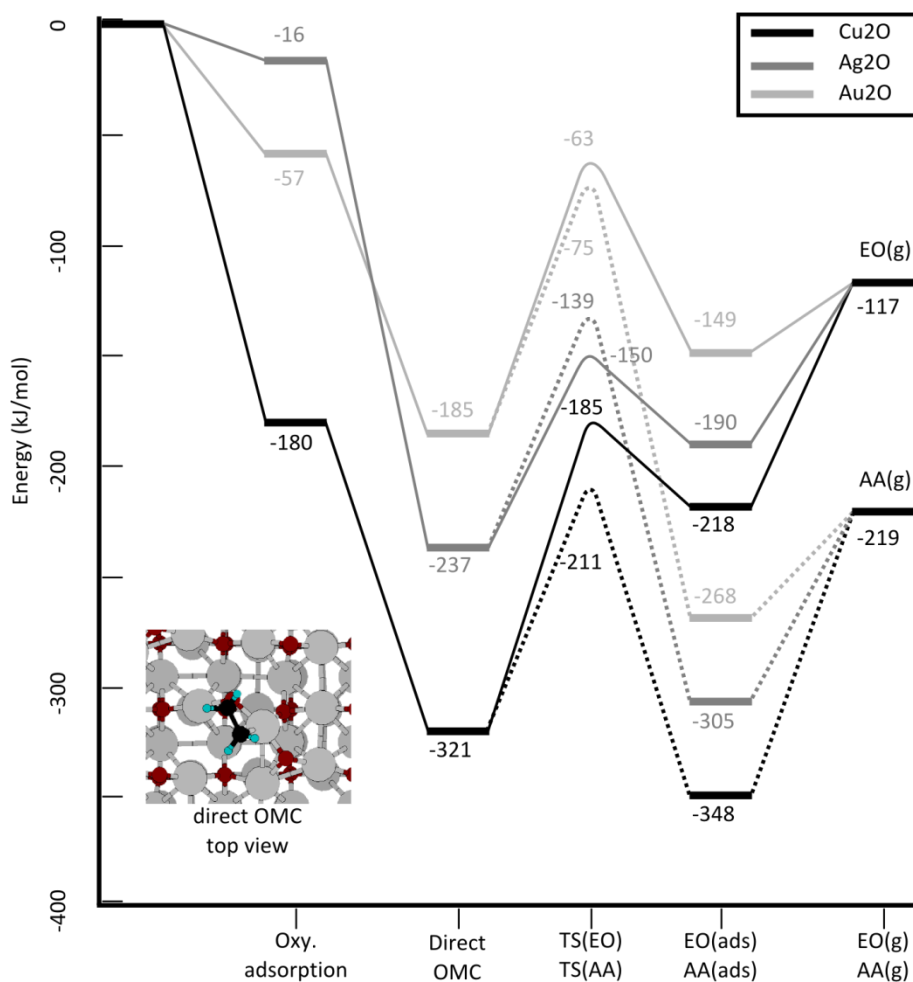
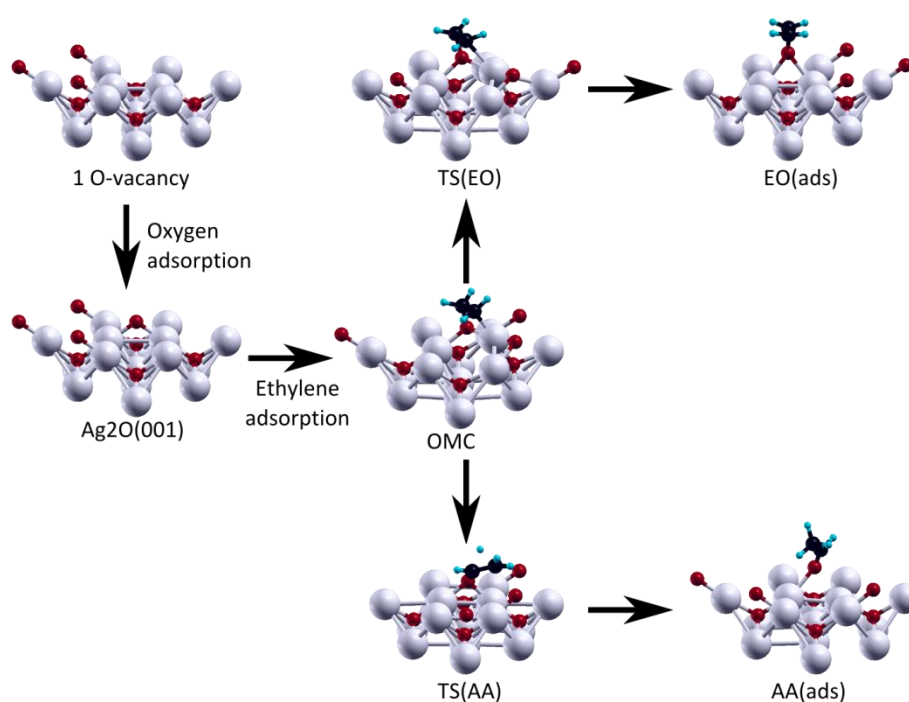


Figure 4.17: Relative energies of direct OMC on M₂O(001) oxide surfaces. Geometries along the reaction paths are given in Scheme 4.5.

In order to test the effect of Cl on direct OMC formation a set of simulations were carried out where surface and/or first sub-surface layer oxygen atoms of the Ag₂O(001) oxide surface are replaced with Cl, and/or extra Cl atoms are introduced to the system. These geometries are schematically presented in Figure 4.18 with their corresponding energies.

These simulations showed that Cl addition had two major effects. The first effect is completely blocking the surface sites where reconstruction occurs. This way, the ethylene cannot interact with the surface metal atoms to induce reconstruction. Thus reconstruction and the direct OMC formation are prevented. Second effect is, when Cl exists in surface or sub-surface positions, it weakens the metal-oxygen bonds, increasing the activity of the surface oxygens. This way the EO formation becomes more exothermic and can compete with the thermodynamically favored direct OMC path that may take place in un-chlorinated surface sites. .



Scheme 4.5: Geometries along the direct OMC path on $M_2O(001)$ surfaces.
(Metals: gray, O: red, C: black, and H: cyan)

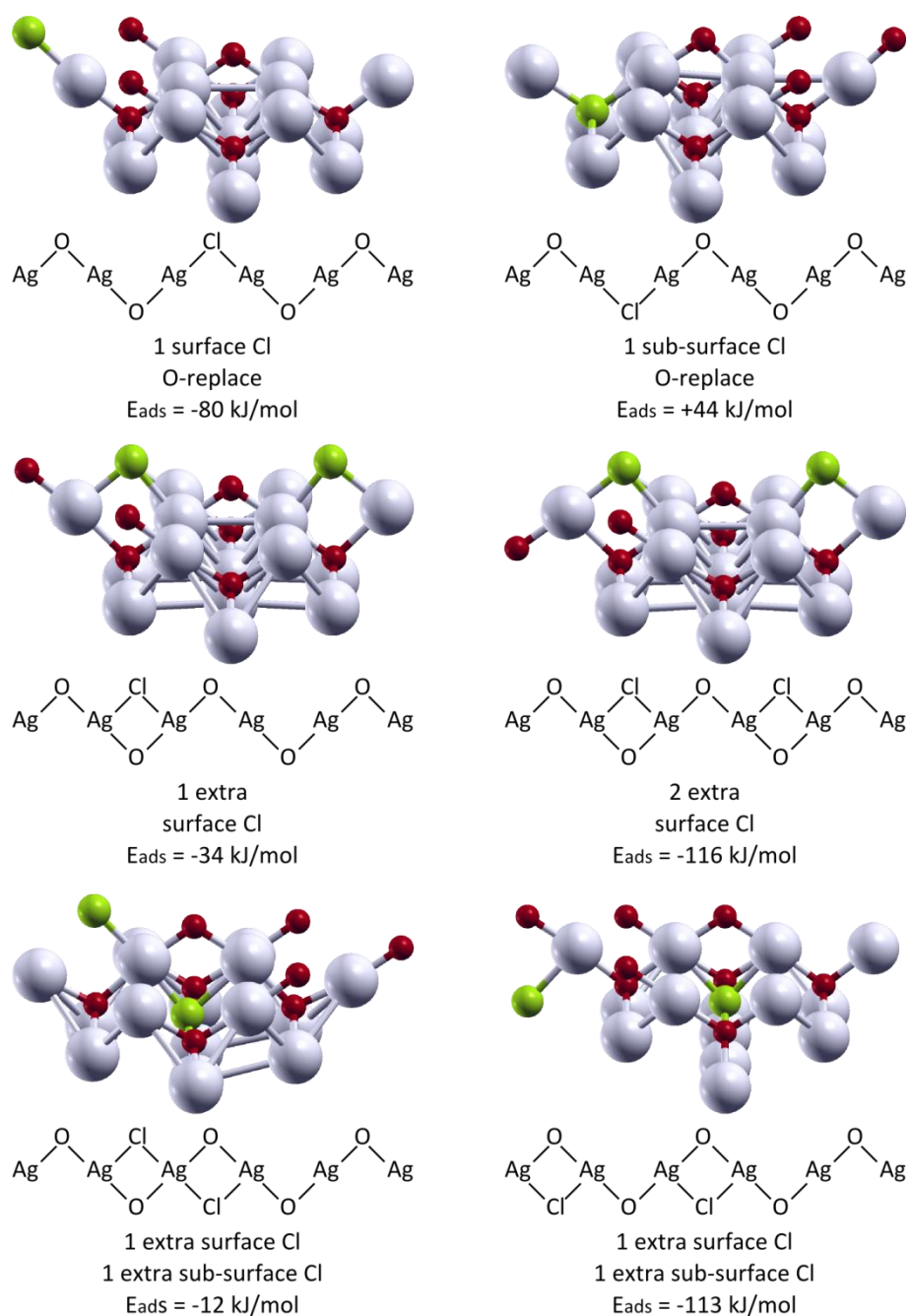


Figure 4.18: Schematic representations of Cl adsorption positions studied on $\text{Ag}_2\text{O}(001)$ surface. The adsorption energies are calculated with respect to $\frac{1}{2} \text{Cl}_2(\text{g})$ and $\frac{1}{2} \text{O}_2(\text{g})$. (Metals: gray, O: red, C: black, H: cyan, and Cl: green)

As described in Sections 4.2 and 4.3, isomerization of adsorbed EO to AA is also tested for the $\text{Ag}_2\text{O}(001)$ surface, where the active surface oxygen has two surface Cl neighbors. These EO and AA geometries are presented in Figure 4.19. The activation energy for this

isomerization reaction is found to be 215 kJ/mol. This value for the reaction barrier is ~ 100 kJ/mol higher compared to the surface without Cl. It is also ~ 70 kJ/mol higher than the energy required for the EO desorption showing that EO desorption is still the preferred path over isomerization.

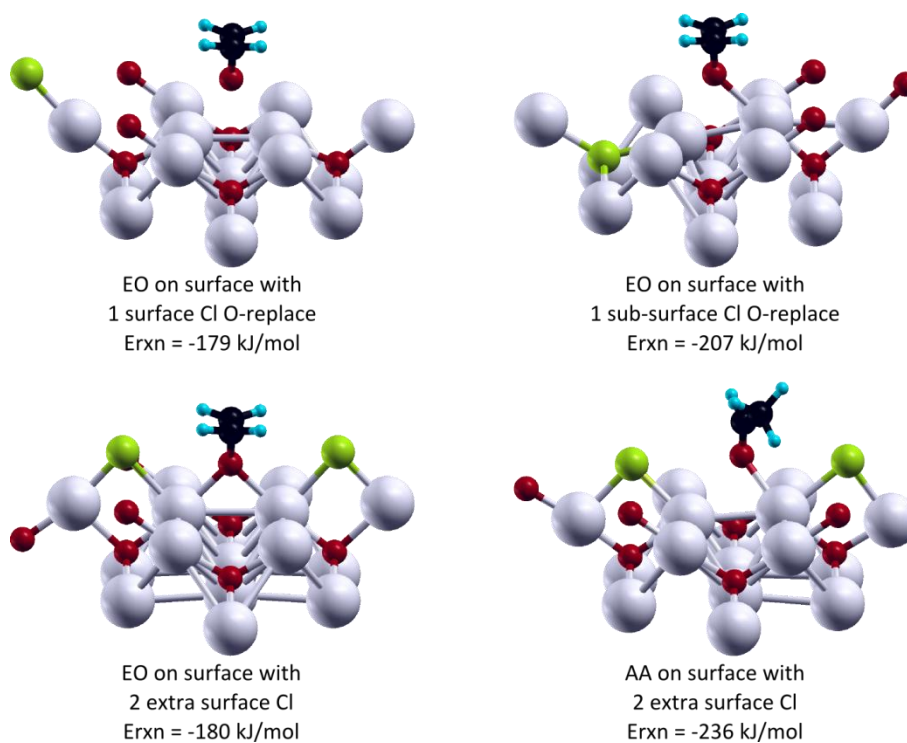


Figure 4.19: EO and AA formation on Cl-adsorbed $\text{Ag}_2\text{O}(001)$ surfaces. (Metals: gray, O: red, C: black, H: cyan, and Cl: green)

4.4.1. Conclusions

The mechanism of ethylene epoxidation strongly depends on the state of the surface and the nature of the active oxygen. Along with the OMC intermediate that was already identified on the metallic surfaces, two more OMC intermediates exist for the oxide surfaces. In the cases of metallic surface, and the oxygen vacant sites of oxide surfaces OMC preferably produces the non-selective product AA. The third OMC, *direct OMC*, forms on the reconstructed sites of the oxides through a non-activated reaction. Having a higher activation barrier for AA, it preferably produces EO. The increased EO selectivity of OMC with the electrophilic nature of oxygen is consistent with the reports of recent

experimental works. On the other hand, the direct epoxidation path does not have competing path and produces EO selectively, which is necessary for the high EO selectivity.

Based on these observations we propose a new model for the role of the Cl promoter. Within this model Cl acts in two ways. Cl adsorption on the surface blocks the sites where the ethylene interacts with the surface metal atoms, and hence, prevents the reconstruction required to form the OMC intermediate that is responsible for the non-selective reaction. Furthermore, surface or sub-surface Cl weakens the metal-oxygen bonds, increasing the reactivity of the surface oxygen.

CHAPTER 5

CONCLUSIONS

Following its discovery in 1930's, the silver catalyzed ethylene epoxidation has been investigated extensively for almost a decade. Ethylene oxide (EO) is an important intermediate for the chemical industry. Its main use is for the production of glycol that is widely used as antifreeze component. Due to its large scale production worldwide, even small improvements have large scale benefits for the environment and the economy.

This thesis focuses on the mechanistic aspects of this reaction. Most important is the question "how the selectivity of the reaction depends on the state of the Ag surface during reaction?" Since many experimental studies agree that the surface should be in an oxidized state, in this thesis the reactivity of the silver oxide surface is studied. This complements many computational studies that focus on the surfaces, which exist in the metallic state.

In this study the mechanism of silver catalyzed ethylene epoxidation was theoretically investigated using periodic DFT calculations on slab models that represent the metal or oxide Ag catalyst surfaces. The reaction paths and the transition states along these paths were obtained using the climbing image nudged elastic band (CI-NEB) method. As a reference to the study of the oxide surface, different metallic surface models were tested with oxygen coverages varying from low coverage oxygen to that of the oxide surface.

For comparison, the metallic phases of copper and gold were also revisited. It is found that the epoxidation reaction proceeds through the oxametallacycle (OMC) intermediate, regardless of the surface oxygen ratio on the metallic surfaces.

In practice Au cannot be applied since the oxygen dissociation is not feasible on the gold surface, whereas on the copper surface endothermic epoxide formation cannot compete

with the exothermic aldehyde formation. Results on metallic silver surfaces are consistent with a prediction of ~50% EO selectivity of the un-promoted silver catalyst. However, metallic surfaces fail to explain the high EO selectivity of the order of 90% that can be obtained in the industrial process.

The catalyst surface in the oxidic state was modeled by the (001) surfaces of the well defined Cu_2O , Ag_2O and Au_2O oxide phases. Among these three oxides, the Cu_2O is found not to favor EO formation whereas Au_2O is known to be unstable, however selective for epoxidation.

A major discovery is the identification of a direct epoxidation path by the reaction of the two-fold oxygen atoms in bridge positions, which naturally exist on (001) oxide surfaces of the studied metals. Among three oxides studied, only $\text{Ag}_2\text{O}(001)$ surface does not show a barrier for formation of adsorbed epoxide following the direct epoxidation path.

The single step, direct epoxidation path is a key step in explaining the high EO selectivities observed. Unlike OMC mechanism that produces epoxide and aldehyde competitively, the direct reaction channel produces only EO, without a competing parallel un-selective reaction. The un-selective reaction that ends up in combustion products is found to proceed through the OMC mechanism where aldehyde formation is favored.

Another major finding of this study is that, for the studied oxide surfaces, two different types of OMC intermediates are possible. The first possibility is the formation of the OMC intermediate on oxygen vacant sites. Because of the possibility of interaction of the ethylene molecule with the metal atoms that are exposed to vacuum, OMC formation becomes possible. This OMC formation is always non-selective towards EO, regardless of the oxide structure. The second possibility is the formation of a direct OMC intermediate, through the interaction of the gas phase ethylene with the non-vacant oxide surface. This occurs through the local surface reconstruction induced by the ethylene. This reconstruction enables a surface metal atom to interact with the ethylene. On the $\text{Ag}_2\text{O}(001)$ surface, the direct OMC path has a higher EO selectivity compared to that is formed on an oxygen vacancy.

In this study we also studied the effect of Cl promotion of the catalyst. Co-adsorption of Cl is found to suppress the reconstruction effects induced by ethylene adsorption. At the

same time Cl increases the electrophilicity of reacting surface oxygen. The direct epoxidation path appears to be stabilized by coadsorbed oxygen atoms.

The necessary condition for high EO selectivity is a surface modification that prevents direct contact of the surface Ag cations with the carbon atoms of ethylene. However since surface metal atoms may become destabilized by ethylene coadsorption, Cl is needed to “overcrowd” the surface so that Lewis acidic Ag cations do not become exposed. An important discovery on this side is the steric effect of the chlorine. The investigated cases of surface and sub-surface Cl adsorption showed that, Cl inhibits the interaction of the ethylene and the surface metal atoms, and hence, prevents the OMC formation. That is, adsorption of Cl on O-vacant sites prevents the ethylene adsorption on this position. Also, existence of the surface and sub-surface Cl atoms is found to prevent the surface reconstruction where the direct OMC forms. In any case, when OMC formation is prevented, the non-selective reaction channel does not occur, hence the EO selectivity is kept high. Furthermore, Cl in the neighboring of reactive oxygen is found to weaken the metal oxygen bond, favoring the EO formation.

Thus, we carry the discussions on the silver catalyzed ethylene epoxidation one step further. Herein we present that the EO selectivity will be limited in the case of metallic catalyst, whereas, the oxide surfaces enable a direct mechanism where EO is produced selectively. The role of the Cl promoter is found to be mainly steric where it blocks the sites of non-selective channel.

REFERENCES

1. Goodman, D.W., *Model catalysts: from imagining to imaging a working surface*. Journal of Catalysis. **216**(1-2): p. 213-222.
2. Reuter, K. and M. Scheffler, *Composition, structure, and stability of RuO₂(110) as a function of oxygen pressure*. Physical Review B, 2001. **65**(3): p. 035406.
3. Over, H., et al., *Atomic-Scale Structure and Catalytic Reactivity of the RuO₂(110) Surface*. Science, 2000. **287**(5457): p. 1474-1476.
4. Hendriksen, B.L.M. and J.W.M. Frenken, *CO Oxidation on Pt(110): Scanning Tunneling Microscopy Inside a High-Pressure Flow Reactor*. Physical Review Letters, 2002. **89**(4): p. 046101.
5. Nagy, A.J., et al., *The Correlation of Subsurface Oxygen Diffusion with Variations of Silver Morphology in the Silver-Oxygen System*. Journal of Catalysis, 1999. **182**(2): p. 417-429.
6. Savinova, E.R., et al., *On the mechanism of Ag(111) sub-monolayer oxidation: a combined electrochemical, in situ SERS and ex situ XPS study*. Electrochimica Acta, 2000. **46**(2-3): p. 175-183.
7. Inc, G.I.A., *ETHYLENE OXIDE (EO) (Complete Report)*, in *A Global Strategic Business Report 2011*, Global Industry Analysts Inc. p. 346.
8. Campbell, C.T., *Surface science study of selective ethylene epoxidation catalyzed by the Ag(110) surface: Structural sensitivity*. Journal of Vacuum Science & Technology A: Vacuum, Surfaces, and Films, 1984. **2**(2): p. 1024-1027.
9. Kestenbaum, H., et al., *Silver-Catalyzed Oxidation of Ethylene to Ethylene Oxide in a Microreaction System*. Industrial & Engineering Chemistry Research, 2002. **41**(4): p. 710-719.

10. Christopher, P. and S. Linic, *Engineering Selectivity in Heterogeneous Catalysis: Ag Nanowires as Selective Ethylene Epoxidation Catalysts*. Journal of the American Chemical Society, 2008. **130**(34): p. 11264-11265.
11. SHELL. *Ethylene oxide/ethylene glycol (EO/EG) processes*. [web page] 2010 [cited 2011 April 2011]; Available from: http://www.shell.com/home/content/global_solutions/products_services/licensed_technologies/petrochemical_technology/ethylene_oxide_processes/.
12. Michaelides, M.-L.B.a.A., *Exploring the Catalytic Activity of a Noble Metal: The Ag Catalyzed Ethylene Epoxidation Reaction*, in "Physics of Single Molecules on Crystal Surfaces, P.G.e.W.H. F. Rosei, Editor. 2006, Imperial College Press. p. 389-424.
13. Mavrikakis, M., D.J. Doren, and M.A. Barteau, *Density Functional Theory Calculations for Simple Oxametallacycles: Trends across the Periodic Table*. The Journal of Physical Chemistry B, 1998. **102**(2): p. 394-399.
14. Kilty, P.A. and W.M.H. Sachtler, *THE MECHANISM OF THE SELECTIVE OXIDATION OF ETHYLENE TO ETHYLENE OXIDE*. Catalysis Reviews: Science and Engineering, 1974. **10**(1): p. 1 - 16.
15. Grant, R.B. and R.M. Lambert, *A single crystal study of the silver-catalysed selective oxidation and total oxidation of ethylene*. Journal of Catalysis, 1985. **92**(2): p. 364-375.
16. van Santen, R.A. and C.P.M. de Groot, *The mechanism of ethylene epoxidation*. Journal of Catalysis, 1986. **98**(2): p. 530-539.
17. Van Santen, R.A. and H.P.C.E. Kuipers, *The Mechanism of Ethylene Epoxidation*, in *Advances in Catalysis*, H.P. D.D. Eley and B.W. Paul, Editors. 1987, Academic Press. p. 265-321.
18. Linic, S. and M.A. Barteau, *Formation of a Stable Surface Oxametallacycle that Produces Ethylene Oxide*. Journal of the American Chemical Society, 2001. **124**(2): p. 310-317.
19. Linic, S. and M.A. Barteau, *Construction of a reaction coordinate and a microkinetic model for ethylene epoxidation on silver from DFT calculations and surface science experiments*. Journal of Catalysis, 2003. **214**(2): p. 200-212.

20. Bulushev, D.A., et al., *Transient response and infrared studies of ethylene oxide reactions on silver catalysts and supports*. Applied Catalysis A: General, 1995. **123**(2): p. 301-322.
21. Christopher, P. and S. Linic, *Shape- and Size-Specific Chemistry of Ag Nanostructures in Catalytic Ethylene Epoxidation*. ChemCatChem, 2010. **2**(1): p. 78-83.
22. Lukaski, A. and M. Barteau, *Investigation of Ethylene Oxide on Clean and Oxygen-Covered Ag(110) Surfaces*. Catalysis Letters, 2009. **128**(1): p. 9-17.
23. Grant, R.B. and R.M. Lambert, *Mechanism of the silver-catalysed heterogeneous epoxidation of ethylene*. Journal of the Chemical Society, Chemical Communications, 1983(12): p. 662-663.
24. Grant, R.B. and R.M. Lambert, *Basic studies of the oxygen surface chemistry of silver: Chemisorbed atomic and molecular species on pure Ag(111)*. Surface Science, 1984. **146**(1): p. 256-268.
25. Campbell, C.T., *Chlorine promoters in selective ethylene epoxidation over Ag(111): A comparison with Ag(110)*. Journal of Catalysis, 1986. **99**(1): p. 28-38.
26. Campbell, C.T., *The selective epoxidation of ethylene catalyzed by Ag(111): A comparison with Ag(110)*. Journal of Catalysis, 1985. **94**(2): p. 436-444.
27. Campbell, C.T. and K.A. Daube, *The structure of alkali promoters on catalysts prepared by traditional versus surface science methods: A case study with Cs on Ag(111)*. Journal of Catalysis, 1987. **106**(1): p. 301-306.
28. Campbell, C.T. and B.E. Koel, *Chlorine promotion of selective ethylene oxidation over Ag(110): Kinetics and mechanism*. Journal of Catalysis, 1985. **92**(2): p. 272-283.
29. Force, E.L. and A.T. Bell, *Infrared spectra of adsorbed species present during the oxidation of ethylene over silver*. Journal of Catalysis, 1975. **38**(1-3): p. 440-460.
30. Force, E.L. and A.T. Bell, *The effect of dichloroethane moderation on the adsorbed species present during the oxidation of ethylene over silver*. Journal of Catalysis, 1976. **44**(2): p. 175-182.

31. Force, E.L. and A.T. Bell, *The relationship of adsorbed species observed by infrared spectroscopy to the mechanism of ethylene oxidation over silver*. Journal of Catalysis, 1975. **40**(3): p. 356-371.
32. Stuve, E.M. and R.J. Madix, *Bonding and dehydrogenation of ethylene on palladium metal. Vibrational spectra and temperature-programed reaction studies on palladium(100)*. The Journal of Physical Chemistry, 1985. **89**(1): p. 105-112.
33. Friend, C.M. and X. Xu, *Reactions on Transition-metal Surfaces*. Annual Review of Physical Chemistry, 1991. **42**: p. 251-278.
34. Frank, M., et al. *Adsorption and reaction of ethene on oxide-supported Pd, Rh, and Ir particles*. 2001. Boston, Massachusetts (USA): AVS.
35. Shi, H., R. Asahi, and C. Stampfl, *Properties of the gold oxides Au₂O₃ and Au₂O : First-principles investigation*. Physical Review B, 2007. **75**(20): p. 205125.
36. Torres, D., F. Illas, and R.M. Lambert, *Towards an understanding of promoter action in heterogeneously catalyzed ethene epoxidation: Why chlorine is the best halogen*. Journal of Catalysis, 2008. **260**(2): p. 380-383.
37. Waugh, K.C. and M. Hague, *The detailed kinetics and mechanism of ethylene epoxidation on an oxidised Ag/[alpha]-Al₂O₃ catalyst*. Catalysis Today, 2010. **157**(1-4): p. 44-48.
38. Van den Hoek, P.J., E.J. Baerends, and R.A. Van Santen, *Ethylene epoxidation on silver(110): the role of subsurface oxygen*. The Journal of Physical Chemistry, 1989. **93**(17): p. 6469-6475.
39. Saravanan, C., et al., *Oxametallacycle Intermediates on Clean and Cs-Promoted Ag(111) Surfaces*. The Journal of Physical Chemistry B, 2000. **104**(36): p. 8685-8691.
40. Li, W.-X., C. Stampfl, and M. Scheffler, *Subsurface oxygen and surface oxide formation at Ag(111): A density-functional theory investigation*. Physical Review B, 2003. **67**(4): p. 045408.
41. Michaelides, A., K. Reuter, and M. Scheffler, *When seeing is not believing: Oxygen on Ag(111), a simple adsorption system?* Journal of Vacuum Science & Technology A: Vacuum, Surfaces, and Films, 2005. **23**(6): p. 1487-1497.

42. Bocquet, M.-L., et al., *Specific Ethene Surface Activation on Silver Oxide Covered Ag{111} from the Interplay of STM Experiment and Theory*. Journal of the American Chemical Society, 2003. **125**(10): p. 3119-3125.
43. Schmid, M., et al., *Structure of Ag(111)-p(4x4)-O: No Silver Oxide*. Physical Review Letters, 2006. **96**(14): p. 146102.
44. Schnadt, J., et al., *Revisiting the Structure of the p(4x4) Surface Oxide on Ag(111)*. Physical Review Letters, 2006. **96**(14): p. 146101.
45. Bocquet, M.L., et al., *Initial stages in the oxidation and reduction of the 4x4 surface oxide phase on Ag{111}: A combined density-functional theory and STM simulation study*. Physical Review B, 2003. **68**(7): p. 075413.
46. Bocquet, M.-L., et al., *New Insights into Ethene Epoxidation on Two Oxidized Ag{111} Surfaces*. Journal of the American Chemical Society, 2003. **125**(19): p. 5620-5621.
47. Carlisle, C.I., et al., *Imaging the Surface and the Interface Atoms of an Oxide Film on Ag{111} by Scanning Tunneling Microscopy: Experiment and Theory*. Physical Review Letters, 2000. **84**(17): p. 3899.
48. Michaelides, A., et al., *Structures and thermodynamic phase transitions for oxygen and silver oxide phases on Ag{1 1 1}*. Chemical Physics Letters, 2003. **367**(3-4): p. 344-350.
49. Reuter, K. and M. Scheffler, *Oxide formation at the surface of late 4d transition metals: insights from first-principles atomistic thermodynamics*. Applied Physics A: Materials Science & Processing, 2004. **78**(6): p. 793-798.
50. Gajdos, M., A. Eichler, and J. Hafner, *Ab initio density functional study of O on the Ag(0 0 1) surface*. Surface Science, 2003. **531**(3): p. 272-286.
51. Frondelius, P., H. Häkkinen, and K. Honkala, *Formation of Gold(I) Edge Oxide at Flat Gold Nanoclusters on an Ultrathin MgO Film under Ambient Conditions*. Angewandte Chemie International Edition, 2010. **49**(43): p. 7913-7916.
52. Kibis, L.S., et al., *The investigation of oxidized silver nanoparticles prepared by thermal evaporation and radio-frequency sputtering of metallic silver under oxygen*. Applied Surface Science, 2010. **257**(2): p. 404-413.

53. Su, H.-Y., et al., *First-Principles Study of Carbon Monoxide Oxidation on Ag(111) in Presence of Subsurface Oxygen and Stepped Ag(221)*. The Journal of Physical Chemistry C, 2009. **113**(19): p. 8266-8272.
54. Xu, Y., J. Greeley, and M. Mavrikakis, *Effect of Subsurface Oxygen on the Reactivity of the Ag(111) Surface*. Journal of the American Chemical Society, 2005. **127**(37): p. 12823-12827.
55. Lefort, E.T., *Process for the production of ethylene oxide*. 1935, Catalyse, Generalisee FR. DE. SA.: United States.
56. Voge, H.H. and C.R. Adams, *Catalytic Oxidation of Olefins*, in *Advances in Catalysis*, H.P. D.D. Eley and B.W. Paul, Editors. 1967, Academic Press. p. 151-221.
57. I. Bukhtiyarov, V., et al., *XPS study of the size effect in ethene epoxidation on supported silver catalysts*. Journal of the Chemical Society, Faraday Transactions, 1997. **93**(13): p. 2323-2329.
58. Bryce-Smith D., B.E.T., Griffe de Martinez B. , *Chemistry and Industry*, 1983. **18**.
59. Park, D.M., S. Ghazali, and G. Gau, *A cyclic reactor study of ethylene epoxidation*. Applied Catalysis, 1983. **6**(2): p. 175-193.
60. Backx, C., et al., *Reactivity of oxygen adsorbed on silver powder in the epoxidation of ethylene*. Journal of Catalysis, 1981. **72**(2): p. 364-368.
61. Su, D.S., et al., *Surface Chemistry of Ag Particles: Identification of Oxide Species by Aberration-Corrected TEM and by DFT Calculations*. Angewandte Chemie, 2008. **120**(27): p. 5083-5086.
62. Li, W.-X., C. Stampfl, and M. Scheffler, *Oxygen adsorption on Ag(111): A density-functional theory investigation*. Physical Review B, 2002. **65**(7): p. 075407.
63. Buatier de Mongeot, F., et al., *Sub-surface incorporation of oxygen on Ag(001) during molecular dissociation*. Chemical Physics Letters, 1999. **302**(3-4): p. 302-306.
64. Campbell, C.T., *Atomic and molecular oxygen adsorption on Ag(111)*. Surface Science, 1985. **157**(1): p. 43-60.

65. Campbell, C.T. and M.T. Paffett, *The interactions of O₂, CO and CO₂ with Ag(110)*. Surface Science, 1984. **143**(2-3): p. 517-535.
66. Goddard, P.J. and R.M. Lambert, *Basic studies of the oxygen surface chemistry of silver: Oxygen, dioxygen, oxide and superoxide on rubidium-dosed Ag(111)*. Surface Science, 1981. **107**(2-3): p. 519-532.
67. Kitson, M. and R.M. Lambert, *Basic studies of the oxygen chemistry of silver: Oxygen, dioxygen and superoxide on potassium-dosed Ag(100)*. Surface Science, 1981. **109**(1): p. 60-74.
68. Wang, C.-B., G. Deo, and I.E. Wachs, *Interaction of Polycrystalline Silver with Oxygen, Water, Carbon Dioxide, Ethylene, and Methanol: In Situ Raman and Catalytic Studies*. The Journal of Physical Chemistry B, 1999. **103**(27): p. 5645-5656.
69. Santen, R.A.v., *epoxidation catalysis using heterogeneous catalysis*. Handbook of Heterogeneous Catalysis, ed. G. Ertl, H. Knözinger, and J. Weitkamp. Vol. 5. 1997, Weinheim: Wiley-VCH.
70. Goncharova, S.N., E.A. Paukshtis, and B.S. Bal'zhinimaev, *Size effects in ethylene oxidation on silver catalysts. Influence of support and Cs promoter*. Applied Catalysis A: General, 1995. **126**(1): p. 67-84.
71. Carter, E.A. and W.A. Goddard III, *Chemisorption of oxygen, chlorine, hydrogen, hydroxide, and ethylene on silver clusters: A model for the olefin epoxidation reaction*. Surface Science, 1989. **209**(1-2): p. 243-289.
72. Carter, E.A. and W.A. Goddard, *The surface atomic oxyradical mechanism for Ag-catalyzed olefin epoxidation*. Journal of Catalysis, 1988. **112**(1): p. 80-92.
73. Bal'zhinimaev, B.S., et al., *Catalytic and structural properties of ultradispersed silver powder, prepared by a wire explosion technique*. Mendeleev Communications, 1998. **8**(3): p. 100-101.
74. Bukhtiyarov, V.I., et al., *XPS study of oxygen adsorption on supported silver: effect of particle size*. Surface Science, 1997. **381**(2-3): p. L605-L608.
75. Linic, S. and M.A. Barteau, *Heterogeneous Catalysis of Alkene Epoxidation*, in *Handbook of Heterogeneous Catalysis*, G. Ertl, et al., Editors. 2008, Wiley-VCH

76. Medlin, J.W. and M.A. Barteau, *The Formation of Epoxides from Reactions of Oxametallacycles on Ag(110): A Density Functional Theory Study*. The Journal of Physical Chemistry B, 2001. **105**(41): p. 10054-10061.
77. Jones, G.S., et al., *First Synthesis, Experimental and Theoretical Vibrational Spectra of an Oxametallacycle on a Metal Surface*. Journal of the American Chemical Society, 1998. **120**(13): p. 3196-3204.
78. Linic, S., J.W. Medlin, and M.A. Barteau, *Synthesis of Oxametallacycles from 2-Iodoethanol on Ag(111) and the Structure Dependence of Their Reactivity*. Langmuir, 2002. **18**(13): p. 5197-5204.
79. Torres, D., et al., *Why Copper Is Intrinsically More Selective than Silver in Alkene Epoxidation: Ethylene Oxidation on Cu(111) versus Ag(111)*. Journal of the American Chemical Society, 2005. **127**(31): p. 10774-10775.
80. Torres, D., N. Lopez, and F. Illas, *A theoretical study of coverage effects for ethylene epoxidation on Cu(111) under low oxygen pressure*. Journal of Catalysis, 2006. **243**(2): p. 404-409.
81. Linic, S. and M.A. Barteau, *On the Mechanism of Cs Promotion in Ethylene Epoxidation on Ag*. Journal of the American Chemical Society, 2004. **126**(26): p. 8086-8087.
82. Linic, S. and M.A. Barteau, *Control of Ethylene Epoxidation Selectivity by Surface Oxametallacycles*. Journal of the American Chemical Society, 2003. **125**(14): p. 4034-4035.
83. Torres, D. and F. Illas, *On the Performance of Au(111) for Ethylene Epoxidation: A Density Functional Study*. The Journal of Physical Chemistry B, 2006. **110**(27): p. 13310-13313.
84. Fermi, E., *Eine statistische Methode zur Bestimmung einiger Eigenschaften des Atoms und ihre Anwendung auf die Theorie des periodischen Systems der Elemente*. Zeitschrift für Physik A Hadrons and Nuclei, 1928. **48**(1): p. 73-79.
85. Thomas, L.H., *The calculation of atomic fields*. Mathematical Proceedings of the Cambridge Philosophical Society, 1927. **23**(05): p. 542-548.
86. Hohenberg, P. and W. Kohn, *Inhomogeneous Electron Gas*. Physical Review, 1964. **136**(3B): p. B864.

87. Ceperley, D.M. and B.J. Alder, *Ground State of the Electron Gas by a Stochastic Method*. Physical Review Letters, 1980. **45**(7): p. 566.
88. Jones, R.O. and O. Gunnarsson, *The density functional formalism, its applications and prospects*. Reviews of Modern Physics, 1989. **61**(3): p. 689.
89. Perdew, J.P. and A. Zunger, *Self-interaction correction to density-functional approximations for many-electron systems*. Physical Review B, 1981. **23**(10): p. 5048.
90. Perdew, J.P. and Y. Wang, *Pair-distribution function and its coupling-constant average for the spin-polarized electron gas*. Physical Review B, 1992. **46**(20): p. 12947.
91. M. Körling and J. Häglund, *Cohesive and electronic properties of transition metals: The generalized gradient approximation*. Physical Review B, 1992. **45**(23): p. 13293.
92. Verdozzi, C., et al., *Sapphire (0001) Surface, Clean and with d-Metal Overlayers*. Physical Review Letters, 1999. **82**(4): p. 799.
93. Yourdshahyan, Y., et al., *Theoretical investigation of the structure of kappa -Al2O3*. Physical Review B, 1997. **55**(14): p. 8721.
94. Becke, A.D., *Density-functional thermochemistry. III. The role of exact exchange*. The Journal of Chemical Physics, 1993. **98**(7): p. 5648-5652.
95. Lee, C., W. Yang, and R.G. Parr, *Development of the Colle-Salvetti correlation-energy formula into a functional of the electron density*. Physical Review B, 1988. **37**(2): p. 785.
96. Kresse, G. and J. Furthmüller, *Efficiency of ab-initio total energy calculations for metals and semiconductors using a plane-wave basis set*. Computational Materials Science, 1996. **6**(1): p. 15-50.
97. Kresse, G. and J. Hafner, *Ab initio molecular-dynamics simulation of the liquid-metal–amorphous-semiconductor transition in germanium*. Physical Review B, 1994. **49**(20): p. 14251.

98. Henkelman, G. and H. Jonsson, *Improved tangent estimate in the nudged elastic band method for finding minimum energy paths and saddle points*. The Journal of Chemical Physics, 2000. **113**(22): p. 9978-9985.
99. *Handbook of Chemistry & Physics Online*. 2011 [cited 2011 April]; 91:[Available from: <http://www.hbcnetbase.com/>].
100. Vincenzo, F. and M. Methfessel, *Extracting convergent surface energies from slab calculations*. Journal of Physics: Condensed Matter, 1996. **8**(36): p. 6525.
101. Vitos, L., et al., *The surface energy of metals*. Surface Science, 1998. **411**(1-2): p. 186-202.
102. Suzuki, T., *X-Ray Study on the Binding Properties of Cu₂O and Ag₂O Crystals*. Journal of the Physical Society of Japan. **15**(Copyright (C) 1960 The Physical Society of Japan): p. 2018.
103. E., B.P., *Projector augmented-wave method*. Physical Review B, 1994. **50**(24): p. 17953.
104. Perdew, J.P., et al., *Erratum: Atoms, molecules, solids, and surfaces: Applications of the generalized gradient approximation for exchange and correlation*. Physical Review B, 1993. **48**(7): p. 4978.
105. Tang, W. and et al., *A grid-based Bader analysis algorithm without lattice bias*. Journal of Physics: Condensed Matter, 2009. **21**(8): p. 084204.
106. Simonetti, S., G. Brizuela, and A. Juan, *Study of the adsorption, electronic structure and bonding of C₂H₄ on the FeNi(1 1 1) surface*. Applied Surface Science, 2010. **256**(21): p. 6459-6465.
107. Mars, P. and D.W. van Krevelen, *Oxidations carried out by means of vanadium oxide catalysts*. Chemical Engineering Science, 1954. **3**(Supplement 1): p. 41-59.
108. Larrabee, A.L. and R.L. Kuczkowski, *The oxidation of ethylene-1,2-d₂ over a silver catalyst studied by microwave spectroscopy*. Journal of Catalysis, 1978. **52**(1): p. 72-80.
109. Kanoh, H., T. Nishimura, and A. Ayame, *Supported silver catalysts for the oxidation of ethylene: The effects of thermal treatment of alumina as catalyst support*. Journal of Catalysis, 1979. **57**(3): p. 372-379.

110. Gao, W., M. Zhao, and Q. Jiang, *A DFT Study on Electronic Structures and Catalysis of Ag₁₂O₆/Ag(111) for Ethylene Epoxidation*. *The Journal of Physical Chemistry C*, 2007. **111**(10): p. 4042-4046.
111. Cant, N.W. and W.K. Hall, *Catalytic oxidation : VI. Oxidation of labeled olefins over silver*. *Journal of Catalysis*, 1978. **52**(1): p. 81-94.
112. Richey, W.F., *Stereochemistry of the silver-catalyzed epoxidation of olefins*. *The Journal of Physical Chemistry*, 1972. **76**(2): p. 213-216.
113. Roldán, A., et al., *The chemistry of chlorine on Ag(1 1 1) over the sub-monolayer range: A density functional theory investigation*. *Surface Science*, 2008. **602**(15): p. 2639-2642.
114. Berndt, T. and O. Böge, *Gas-Phase Epoxidation of Propylene and Ethylene*. *Industrial & Engineering Chemistry Research*, 2005. **44**(4): p. 645-650.
115. Barrio, L., et al., *Effects of Hydrogen on the Reactivity of O₂ toward Gold Nanoparticles and Surfaces*. *The Journal of Physical Chemistry C*, 2007. **111**(51): p. 19001-19008.
116. Özbek, M.O., I. Önal, and R.A.v. Santen, *Ethylene Epoxidation Catalyzed By Chlorine Promoted Silver Oxide*. *Journal of Physics: Condensed Matter*, 2011. **Accepted for publication**.
117. Klugherz, P.D. and P. Harriott, *Kinetics of ethylene oxidation on a supported silver catalyst*. *AIChE Journal*, 1971. **17**(4): p. 856-866.
118. Akella, L.M. and H.H. Lee, *Selectivity characterization of ethylene oxidation reactions: Oxygen chemisorption*. *Journal of Catalysis*, 1984. **86**(2): p. 465-472.
119. Bocquet, M.-L. and D. Loffreda, *Ethene Epoxidation Selectivity Inhibited by Twisted Oxametallacycle: A DFT Study on Ag Surface-Oxide*. *Journal of the American Chemical Society*, 2005. **127**(49): p. 17207-17215.

CURRICULUM VITAE

M. Oluş Özbek was born in November 26th 1978 in Adana, Turkey. After he got his B.S. degree as a chemical engineer in the Chemical Engineering Department of Middle East Technical University (METU) in 2003, he continued to his master in the same department in the field of process simulation and control. After receiving his M.Sc. degree in 2005, he started his Ph.D. studies in the field of theoretical chemistry with a joint Ph.D. program (bi-promotion) between Chemical Engineering Department of METU and Chemical Engineering and Chemistry Department of Eindhoven University of Technology (TU/e). During his Ph.D. studies he worked with Prof. Dr. Rutger A. van Santen (TU/e) and Prof. Dr. Işık Önal (METU) in the field of surface chemistry and heterogeneous catalysis. His Ph.D. project was the “Computational Study of Ethylene Epoxidation”. The most important results of his Ph.D. research are described within this thesis.

LIST OF PUBLICATIONS

1. Erdogan, R., O. Ozbek, and I. Onal, A periodic DFT study of water and ammonia adsorption on anatase TiO₂ (001) slab. *Surface Science*, 2010. 604(11-12): p. 1029-1033.
2. Özbek, M.O., I. Önal, and R.A. van Santen, Ethylene Epoxidation Catalyzed by Silver Oxide. *ChemCatChem*, 2011. 3(1): p. 150-153.
3. Özbek, M.O., I. Önal, and R.A.v. Santen, Ethylene Epoxidation Catalyzed By Chlorine Promoted Silver Oxide. *Journal of Physics: Condensed Matter*, 2011. Accepted for publication.
4. Özbek, M.O., I. Önal, and R.A. v Santen, Why Silver Is The Unique Catalyst For Ethylene Epoxidation. *Journal of Catalysis*, 2011. submitted.

5. Özbek, M.O., I. Önal, and R.A. v Santen, Effect Of Surface And Oxygen Coverage On Ethylene Epoxidation. 2011, submitted.

6. Özbek, M.O., I. Önal, and R.A. v Santen, Ethylene Epoxidation Catalyzed By Chlorine Promoted silver oxide. 2011, to be submitted.